IAEA Nuclear Energy Series

No. NF-T-2.6

Post-irradiation Examination Techniques for Research Reactor Fuels

IAEA
International Atomic Energy Agency

IAEA NUCLEAR ENERGY SERIES PUBLICATIONS

STRUCTURE OF THE IAEA NUCLEAR ENERGY SERIES

Under the terms of Articles III.A.3 and VIII.C of its Statute, the IAEA is authorized to “foster the exchange of scientific and technical information on the peaceful uses of atomic energy”. The publications in the **IAEA Nuclear Energy Series** present good practices and advances in technology, as well as practical examples and experience in the areas of nuclear reactors, the nuclear fuel cycle, radioactive waste management and decommissioning, and on general issues relevant to nuclear energy. The **IAEA Nuclear Energy Series** is structured into four levels:

(1) The **Nuclear Energy Basic Principles** publication describes the rationale and vision for the peaceful uses of nuclear energy.
(2) **Nuclear Energy Series Objectives** publications describe what needs to be considered and the specific goals to be achieved in the subject areas at different stages of implementation.
(3) **Nuclear Energy Series Guides and Methodologies** provide high level guidance or methods on how to achieve the objectives related to the various topics and areas involving the peaceful uses of nuclear energy.
(4) **Nuclear Energy Series Technical Reports** provide additional, more detailed information on activities relating to topics explored in the **IAEA Nuclear Energy Series**.

Each publication undergoes internal peer review and is made available to Member States for comment prior to publication.

The IAEA Nuclear Energy Series publications are coded as follows: **NG** – nuclear energy general; **NR** – nuclear reactors (formerly **NP–** nuclear power); **NF** – nuclear fuel cycle; **NW** – radioactive waste management and decommissioning. In addition, the publications are available in English on the IAEA web site:

www.iaea.org/publications

For further information, please contact the IAEA at Vienna International Centre, PO Box 100, 1400 Vienna, Austria.

All users of the IAEA Nuclear Energy Series publications are invited to inform the IAEA of their experience for the purpose of ensuring that they continue to meet user needs. Information may be provided via the IAEA web site, by post, or by email to Official.Mail@iaea.org.

POST-IRRADIATION EXAMINATION TECHNIQUES FOR RESEARCH REACTOR FUELS

The following States are Members of the International Atomic Energy Agency:

AFGHANISTAN
ALBANIA
ALGERIA
ANGOLA
ANTIGUA AND BARBUDA
ARGENTINA
ARMENIA
AUSTRALIA
AUSTRIA
AZERBAIJAN
BAHAMAS
BAHRAIN
BANGLADESH
BARBADOS
BELARUS
BELGIUM
BELIZE
BENIN
BOLIVIA, PLURINATIONAL STATE OF
BOSNIA AND HERZEGOVINA
BOTSWANA
BRAZIL
BRUNEI DARUSSALAM
BULGARIA
BURKINA FASO
BURUNDI
CAMBODIA
CAMEROON
CANADA
CENTRAL AFRICAN REPUBLIC
CHAD
CHILE
CHINA
COLOMBIA
COMOROS
CONGO
COSTA RICA
CÔTE D'IVOIRE
CROATIA
CUBA
CYPRUS
CZECH REPUBLIC
DEMOCRATIC REPUBLIC OF THE CONGO
DENMARK
DJIBOUTI
DOMINICA
DOMINICAN REPUBLIC
ECUADOR
EGYPT
EL SALVADOR
ERITREA
ESTONIA
ESWATINI
ETHIOPIA
FIJI
FINLAND
FRANCE
GABON
GEORGIA
GERMANY
GHANA
GREECE
GRENADA
GUATEMALA
GUYANA
HAITI
HOLY SEE
HONDURAS
HUNGARY
ICELAND
INDIA
INDONESIA
IRAN, ISLAMIC REPUBLIC OF
IRAQ
IRELAND
ISRAEL
ITALY
JAMAICA
JAPAN
JORDAN
KAZAKHSTAN
KENYA
KOREA, REPUBLIC OF
KUWAIT
KYRGYZSTAN
LAO PEOPLE'S DEMOCRATIC REPUBLIC
LATVIA
LEBANON
LESOTHO
LIBERIA
LIBYA
LIECHTENSTEIN
LITHUANIA
LUXEMBOURG
MADAGASCAR
MALAWI
MALAYSIA
MALI
MALTA
MARSHALL ISLANDS
MAURITANIA
MAURITIUS
MEXICO
MONACO
MONGOLIA
MONTENEGRO
MOROCCO
MOZAMBIQUE
MYANMAR
NAMIBIA
NEPAL
NETHERLANDS
NEW ZEALAND
NICARAGUA
NIGER
NIGERIA
NORTH MACEDONIA
NORWAY
OMAN
PAKISTAN
PALAU
PANAMA
PAPUA NEW GUINEA
PARAGUAY
PERU
PHILIPPINES
POLAND
PORTUGAL
QATAR
REPUBLIC OF MOLDOVA
ROMANIA
RUSSIAN FEDERATION
RWANDA
SAINT KITTS AND NEVIS
SAINT LUCIA
SAINT VINCENT AND THE GRENADINES
SAMOA
SAN MARINO
SAUDI ARABIA
SENEGAL
SERBIA
SEYCHELLES
SIERRA LEONE
SINGAPORE
SLOVAKIA
SLOVENIA
SOUTH AFRICA
SPAIN
SRI LANKA
SUDAN
SWEDEN
SWITZERLAND
SYRIAN ARAB REPUBLIC
TAJIKISTAN
THAILAND
TOGO
TONGA
TRINIDAD AND TOBAGO
TUNISIA
TÜRKİYE
TURKMENISTAN
UGANDA
UKRAINE
UNITED ARAB EMIRATES
UNITED KINGDOM OF GREAT BRITAIN AND NORTHERN IRELAND
UNITED REPUBLIC OF TANZANIA
UNITED STATES OF AMERICA
URUGUAY
UZBEKISTAN
VANUATU
VENEZUELA, BOLIVARIAN REPUBLIC OF
VIET NAM
YEMEN
ZAMBIA
ZIMBABWE

The Agency's Statute was approved on 23 October 1956 by the Conference on the Statute of the IAEA held at United Nations Headquarters, New York; it entered into force on 29 July 1957. The Headquarters of the Agency are situated in Vienna. Its principal objective is "to accelerate and enlarge the contribution of atomic energy to peace, health and prosperity throughout the world".

IAEA NUCLEAR ENERGY SERIES No. NF-T-2.6

POST-IRRADIATION EXAMINATION TECHNIQUES FOR RESEARCH REACTOR FUELS

INTERNATIONAL ATOMIC ENERGY AGENCY
VIENNA, 2023

COPYRIGHT NOTICE

Marketing and Sales Unit, Publishing Section
International Atomic Energy Agency
Vienna International Centre
PO Box 100
1400 Vienna, Austria
fax: +43 1 26007 22529
tel.: +43 1 2600 22417
email: sales.publications@iaea.org
www.iaea.org/publications

Printed by the IAEA in Austria
April 2023
STI/PUB/1934

IAEA Library Cataloguing in Publication Data

Names: International Atomic Energy Agency.
Title: Post-irradiation examination techniques for research reactor fuels / International Atomic Energy Agency.
Description: Vienna : International Atomic Energy Agency, 2023. | Series: IAEA nuclear energy series, ISSN 1995–7807 ; no. NF-T-2.6 | Includes bibliographical references.
Identifiers: IAEAL 21-01462 | ISBN 978–92–0–101821–2 (paperback : alk. paper) | ISBN 978–92–0–101921–9 (pdf) | ISBN 978–92–0–102021–5 (epub)
Subjects: LCSH: Nuclear fuels. | Irradiation — Examination. | Nuclear reactors.
Classification: UDC 621.039.59 | STI/PUB/1934

FOREWORD

The IAEA's statutory role is to "seek to accelerate and enlarge the contribution of atomic energy to peace, health and prosperity throughout the world". Among other functions, the IAEA is authorized to "foster the exchange of scientific and technical information on peaceful uses of atomic energy". One way this is achieved is through a range of technical publications including the IAEA Nuclear Energy Series.

The IAEA Nuclear Energy Series comprises publications designed to further the use of nuclear technologies in support of sustainable development, to advance nuclear science and technology, catalyse innovation and build capacity to support the existing and expanded use of nuclear power and nuclear science applications. The publications include information covering all policy, technological and management aspects of the definition and implementation of activities involving the peaceful use of nuclear technology.

The IAEA safety standards establish fundamental principles, requirements and recommendations to ensure nuclear safety and serve as a global reference for protecting people and the environment from harmful effects of ionizing radiation.

When IAEA Nuclear Energy Series publications address safety, it is ensured that the IAEA safety standards are referred to as the current boundary conditions for the application of nuclear technology.

While research reactors have been operating for decades, new fuels for research reactors are undergoing substantial development and testing. The suitability of a new fuel for use in a research reactor can be assessed by determining the effects of irradiation on the fuel. Using post-irradiation examination (PIE) techniques, fuel samples are analysed in hot cells or with specialized equipment. PIE techniques can also be applied to driver fuel to determine whether fuel assemblies irradiated in a reactor core are suitable for further use. This publication provides information on the PIE techniques applied in the development of research reactor fuels, the equipment used and examples of the results obtained.

The IAEA wishes to thank all participants in the consultants meetings for their assistance with the drafting and preparation of this publication. The IAEA is particularly grateful to J. Noirot (France), A. Leenaers (Belgium) and D. Keiser (United States of America) for their contributions. The IAEA officer responsible for this publication was F. Marshall of the Division of Nuclear Fuel Cycle and Waste Technology.

EDITORIAL NOTE

This publication has been edited by the editorial staff of the IAEA to the extent considered necessary for the reader's assistance. It does not address questions of responsibility, legal or otherwise, for acts or omissions on the part of any person.

Although great care has been taken to maintain the accuracy of information contained in this publication, neither the IAEA nor its Member States assume any responsibility for consequences which may arise from its use.

Guidance provided here, describing good practices, represents expert opinion but does not constitute recommendations made on the basis of a consensus of Member States.

The use of particular designations of countries or territories does not imply any judgement by the publisher, the IAEA, as to the legal status of such countries or territories, of their authorities and institutions or of the delimitation of their boundaries.

The mention of names of specific companies or products (whether or not indicated as registered) does not imply any intention to infringe proprietary rights, nor should it be construed as an endorsement or recommendation on the part of the IAEA.

The IAEA has no responsibility for the persistence or accuracy of URLs for external or third party Internet web sites referred to in this book and does not guarantee that any content on such web sites is, or will remain, accurate or appropriate.

CONTENTS

1. INTRODUCTION

This publication provides information on the various post-irradiation examination (PIE) techniques used to investigate the in-pile behaviour and microstructural evolution of research reactor fuel. PIE techniques are used in the development of nuclear reactor fuel and components and in the evaluation of their operational performance. The techniques are presented from the perspective of irradiated research reactor fuel, but they may be applied to broader areas of nuclear material research.

1.1. BACKGROUND

PIE of irradiated research reactor fuel is performed using both destructive and non-destructive techniques. Most PIE is carried out in hot cells, although some specific non-destructive PIE is performed underwater in the pools adjacent to the reactors. PIE is used to achieve the following:

(a) Determine if an individual research reactor fuel assembly failed during service in the reactor and identify the nature and cause of fuel failure;
(b) Provide relevant information on the irradiation behaviour of new fuel systems under development or for their qualification;
(c) Provide information to be considered in licence extension applications or other regulatory qualifications;
(d) Evaluate the irradiation performance of lead test assemblies when changing fuel systems, geometry or manufacturer;
(e) Provide input to benchmark fuel behaviour codes;
(f) Provide key feedback to fuel designers, fuel fabricators, reactor operators and regulators on the irradiation behaviour of a particular research reactor fuel;
(g) Provide input to standards for irradiated material examinations.

PIE is an indispensable step in the selection of new or improved research reactor fuel materials, in the characterization and understanding of the in-core behaviour of research reactor fuel materials, in support of the qualification of new research reactor fuel, and in the interpretation of research reactor fuel safety tests.

1.2. OBJECTIVE

The objective of this publication is to disseminate information on the use of PIE techniques to advance knowledge of the irradiation behaviour of research reactor fuels. It discusses the destructive and non-destructive PIE techniques used to study the irradiation impact of research reactor fuels with increasing uranium densities under the extreme flux conditions typical of research reactor operations. Much of the work presented here was generated by research and development on new low enriched uranium (LEU) research reactor fuels. The PIE facilities and services of a selection of nuclear research centres are identified for reference in this publication.

Guidance provided here, describing good practices, represents expert opinion but does not constitute recommendations made on the basis of a consensus of Member States.

1.3. SCOPE

This publication introduces PIE concepts and techniques to readers who are not directly involved in the PIE of research reactor fuel. It presents the research reactor fuel materials (in plate and rod type fuels), the history of research reactor fuel development and the phenomena that drive research reactor fuel behaviour during irradiation. It describes a typical PIE process, starting from intercycle inspections in the reactor pool or channel and proceeding to hot cell PIE techniques. Hot cell PIE techniques are subdivided into non-destructive and destructive testing techniques. For each PIE technique, the technique is introduced, examples of results are provided, and advantages and drawbacks are considered. The suitability of the technique to understanding fuel irradiation behaviour is also discussed.

The PIE techniques considered in this publication focus on fuels for general purpose research reactors. The approaches are nevertheless valid for fuel systems used in some demonstration reactors (e.g. high temperature gas cooled reactors) or single purpose reactors (e.g. the Transient Reactor Test Facility). These techniques can also be applied to power fuel development for Generation IV nuclear power reactor systems (including fast neutron reactors and those using novel coolants, such as sodium, lead and molten salts), where displacement damage (displacement per atom) and operating temperatures are even more severe than in current designs.

This publication primarily provides information on the practice of research reactor PIE and the interpretation of PIE data for four user groups:

(1) Nuclear professionals seeking a background publication on PIE to enhance their knowledge and education;
(2) Organizations interested in research reactor fuel performance under normal and accident operating conditions, such as fuel developers, research reactor operating organizations, fuel manufacturers, regulatory bodies and their technical support organizations, hot cell laboratory management and staff, budget managers, and policy makers;
(3) Operating organizations of existing PIE facilities, and those who are considering enhancements to broaden their service offering;
(4) Users or potential users of PIE services with specific questions about specialized PIE facilities or equipment.

1.4. STRUCTURE

Following the introductory section, Section 2 provides a brief introduction to research reactor fuels. Section 3 presents a description of the main irradiation phenomena that have an impact on the fuel. Section 4 describes the examination processes and techniques applied to research reactor fuels prior to irradiation. Section 5 provides information on the necessary infrastructure and approach for the implementation of PIE campaigns. The examination processes and techniques applied to research reactor fuels during intercycle poolside examinations are described in Section 6. The examination processes and techniques applied to research reactor fuels in hot cell facilities after irradiation are presented in Section 7 (non-destructive PIE techniques applied to the whole fuel assembly) and Section 8 (destructive PIE techniques applied to samples cut from the fuel elements), respectively. In Section 9, a number of specialized characterization techniques are introduced. Section 10 provides conclusions.

2. RESEARCH REACTORS AND THEIR FUELS

2.1. GENERAL PROPERTIES OF RESEARCH REACTOR FUELS

Research reactors provide a source of neutrons for use in applications such as training and education, production of radioisotopes, material testing and characterization, transmutation, activation or other irradiation services [1].

In general, research reactors operate close to atmospheric pressure and at relatively low temperatures (typically with a fuel temperature of less than 200–250°C and a water temperature of less than 50°C, compared with a fuel temperature of 1000–1500°C in 350°C water for power reactors). Although many designs exist, most research reactors have a pool type design where the reactor core, consisting of the fuel assemblies, control rods and empty channels for experiments, sits in a pool of water. Water is the typical coolant and moderator, while graphite or beryllium acts as a neutron reflector.

A research reactor has a much smaller core than a power reactor and therefore needs far less fuel. On the other hand, research reactor fuel generally operates at much higher power densities (typically up to 2000–2500 W/g U, compared with 20–50 W/g U in power reactors) to generate the desired high neutron fluxes, and therefore requires higher uranium enrichment. This higher power density pushes the constituent materials of the fuel matrix and cladding to their limits, resulting in phenomena that PIE techniques are designed to study.

Nuclear fuels are designed to dissipate the decay heat generated by nuclear fission, generally through a large cooling surface and a high thermal conductivity of both the fuel and cladding. Most research reactors use some form of metallic or intermetallic fuel (high thermal conductivity) and the highest power reactors use these in plate form (to have a large cooling surface). The lower power research reactors use fuel pins or rods. Another characteristic of research reactor fuels (plates and rods) is the absence of a plenum (i.e. an open volume initially filled with helium gas in light water reactor fuels). This is present in power reactor fuels to accommodate fission gases released in the fuel. As fission gas quantities are lower in research reactor fuels, gaps are not necessary to achieve high thermal conductivity. However, if fission gas does become mobile, it usually collects in large bubbles, eventually causing plate pillowing, an excessive local swelling of the plate. PIE techniques are used to measure plate pillowing during the development and testing of research reactor fuels.

Many research reactor fuel types are in use, and most are either plate (flat or curved, or in tubes) or rod type fuels. Initially, many research reactors were designed to operate with high enriched uranium (HEU) fuel, but more recently countries have converted research reactor cores to LEU fuel (^{235}U is limited to less than 20%) to improve security and reduce proliferation risks. To compensate for the higher amounts of ^{238}U in the fuel required to achieve <20% of ^{235}U, LEU fuels have to accommodate higher overall uranium densities (g U/cm^3). The first substantial design change was the introduction of higher density uranium silicide (U_3Si_2–Al) fuels in the early 1990s, which led to the conversion of many reactors. However, several of the higher power research reactors require a new approach to fuel design to enable conversion from HEU to LEU fuels. This requirement has pushed fuel design to new limits and increased the need for PIE techniques. Many of the examples provided in this publication to demonstrate the PIE techniques are drawn from recent research reactor fuel development efforts.

2.2. PLATE TYPE FUELS

Aluminium clad fuel plates are among the oldest types of fuel element ever developed. Initially they consisted of a ‘fuel meat’ of uranium–aluminium (U–Al) alloy, contained in an aluminium alloy ‘envelope’. Many were replaced in the 1960s by dispersion fuels in which uranium oxides or U–Al intermetallic phases are dispersed in a pure aluminium matrix. The most frequently used oxides are U_3O_8

and UO_2. The U–Al intermetallic phases used are referred to as UAl_x. Since the 1980s, the UAl_x material has generally been replaced with U_3Si_2.

U_3Si_2 by itself is insufficient to allow a conversion of the highest power density research reactors from HEU to LEU based fuels. Therefore, recent developments have focused on the uranium–molybdenum (U–Mo) alloy system. In addition to a dispersion version of this fuel type, a monolithic version is also being developed, in which the aluminium matrix material is not present and instead a foil of U–Mo alloy is pressed between two cladding plates. This achieves maximum uranium loading. The production process does not involve compacting and hot rolling, but rather foil rolling and subsequently hot isostatic pressing to create fuel–clad bonding. Variations in the process exist and the production method is still under development.

The processes used for fabricating the fuel plates are essentially the same for the different plate type fuels. They consist of fuel constituent preparation, plate fabrication and cladding, plate inspection, plate forming (bending), and finally mounting of the plates and structural components into a fuel assembly. Typically, the fuel constituent preparation consists of mixing pure aluminium powder with a powder of a uranium based compound such as UAl_x. This homogeneous mixture is pressed into a compact with very high pressure to maximize the density. All plate fabrication procedures use the hot rolling technique. The major components are two flat covers and a frame of the same width and length, with a cavity that fits the compact. Hot rolling a billet of this type bonds all contact surfaces and sizes the plate.

Aluminium alloys used in fuel cladding include Al1100 for low power applications; aluminium–magnesium (Al–Mg), typically used in European research reactors; aluminium–magnesium–silicon (Al–Mg–Si) in reactors in the United States of America (usually Al6061) and Russian reactors; and aluminium–magnesium–iron–nickel (Al–Mg–Fe–Ni) in the newest European reactors.

Plate inspections usually examine fuel meat location, density and homogeneity (using X ray techniques); fuel to clad bonding and minimum clad thickness (by ultrasonic testing or destructively by bend testing and metallography); and blister testing (by heat treatment of the plates). Finally, the plates are formed and assembled in the fuel assembly geometry, which is reactor specific. Figure 1 [2] shows different fuel plate shapes.

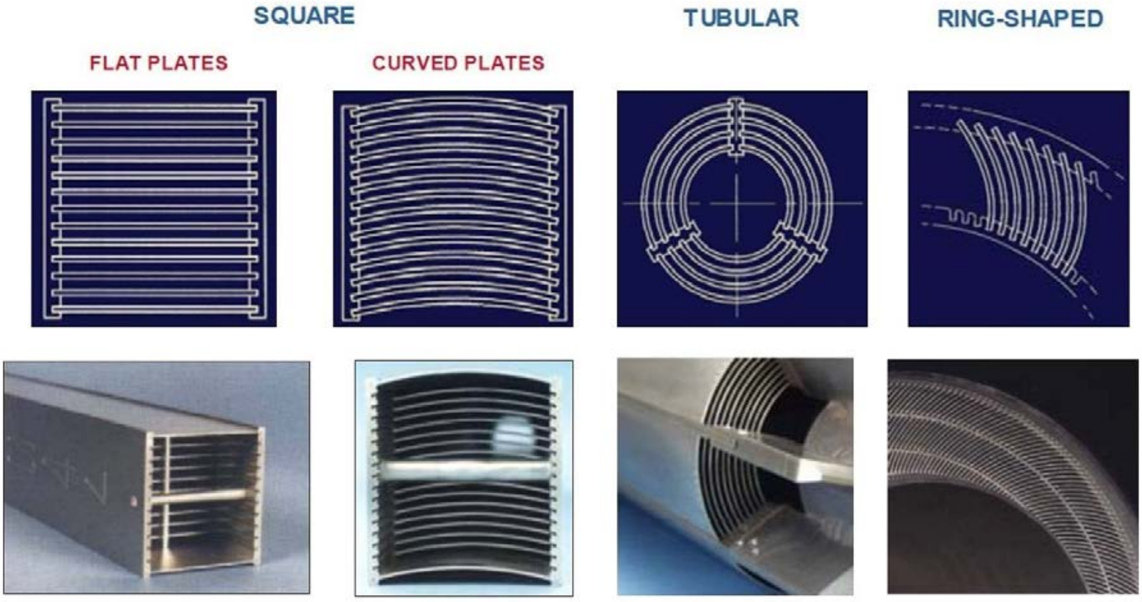

FIG. 1. Fuel plate and subassembly examples [2]. (Courtesy of Framatome.)

2.3. ROD AND TUBE TYPE FUELS

A large number of research reactors with pin type fuels have been developed, initially in the Russian Federation and Canada, and later adapted by the Republic of Korea and China. A typical example is provided by the SLOWPOKE reactors developed by Atomic Energy of Canada Limited (AECL). The SLOWPOKE reactors originally used HEU in the form of U–Al alloy with aluminium cladding until a LEU design was commissioned using CERMET UO_2 dispersion fuel.

Typically, rod type fuels for research reactors are manufactured by extrusion. In most cases, coextrusion of fuel dispersion in the aluminium matrix and the cladding is performed. The extruded pin is then further machined and end caps are welded to seal the pin. To increase the cooling surface, fins are often incorporated on the fuel pin surface, which is easily achieved by the extrusion process.

Research reactors with fuel rods generally operate at lower powers than plate fuelled research reactors. Fuel rods have a lower volumetric loading of uranium than plates and operate at higher temperatures because of the lower cooling surface to volume ratio.

The extrusion process is also used to manufacture tubes, a common fuel type in research reactors of Russian design. Tubes behave similarly to plates and can sustain higher powers because of their seamless design and large cooling surface. Their disadvantages are that it is more difficult to achieve high uranium loadings and that there is generally less control over the minimum cladding thickness.

3. GENERAL DESCRIPTION OF RESEARCH REACTOR FUEL PHENOMENA

When a research reactor fuel element is irradiated, several microstructural and physico-chemical changes occur that affect fuel performance. The phenomena specified below occur in most research reactor fuel systems. The fuel–matrix interaction only occurs in dispersion fuels. For other fuels, such an interaction phenomenon is limited to the fuel–cladding interface (if such an interface exists).

The principal phenomena to be observed are listed below [3] (see also Fig. 2):

(a) Corrosion of the cladding by the cooling water. The development of corrosion depends heavily on water pH, temperature, specific conductivity and the cladding material. A corrosion layer serves as a thermal barrier, causing the fuel itself to run hotter.
(b) The physical and chemical impacts of fission products. Fission products, typically solid and gaseous atoms, affect fuel properties such as melting temperature and thermal conductivity, and also cause swelling.
(c) Fuel–matrix interaction layer formation, between the matrix and fuel kernels in dispersion fuel. This is a result of the intermixing or intermingling of fission product ions and is influenced by a combination of physical and irradiation parameters, such as phases formed, additives in the matrix and fuel kernel, burnup and operating temperature. Interaction layer formation only leads to limited swelling.
(d) Amorphization. This occurs when a material loses all crystalline structure and becomes random or consists solely of short range order. Amorphization can occur when irradiations are conducted at low temperatures, where the diffusion of point defects, such as vacancies and interstitial atoms, is low and point defects cannot recombine to annihilate or form clusters such as precipitates or bubbles, or reach sinks, such as pores and grain boundaries. The defect concentration continues to increase in the material until the ordered crystalline structure is entirely consumed, leaving only a short ordering of crystalline structure. Amorphization in metal systems is often referred to as metallic glass formation.

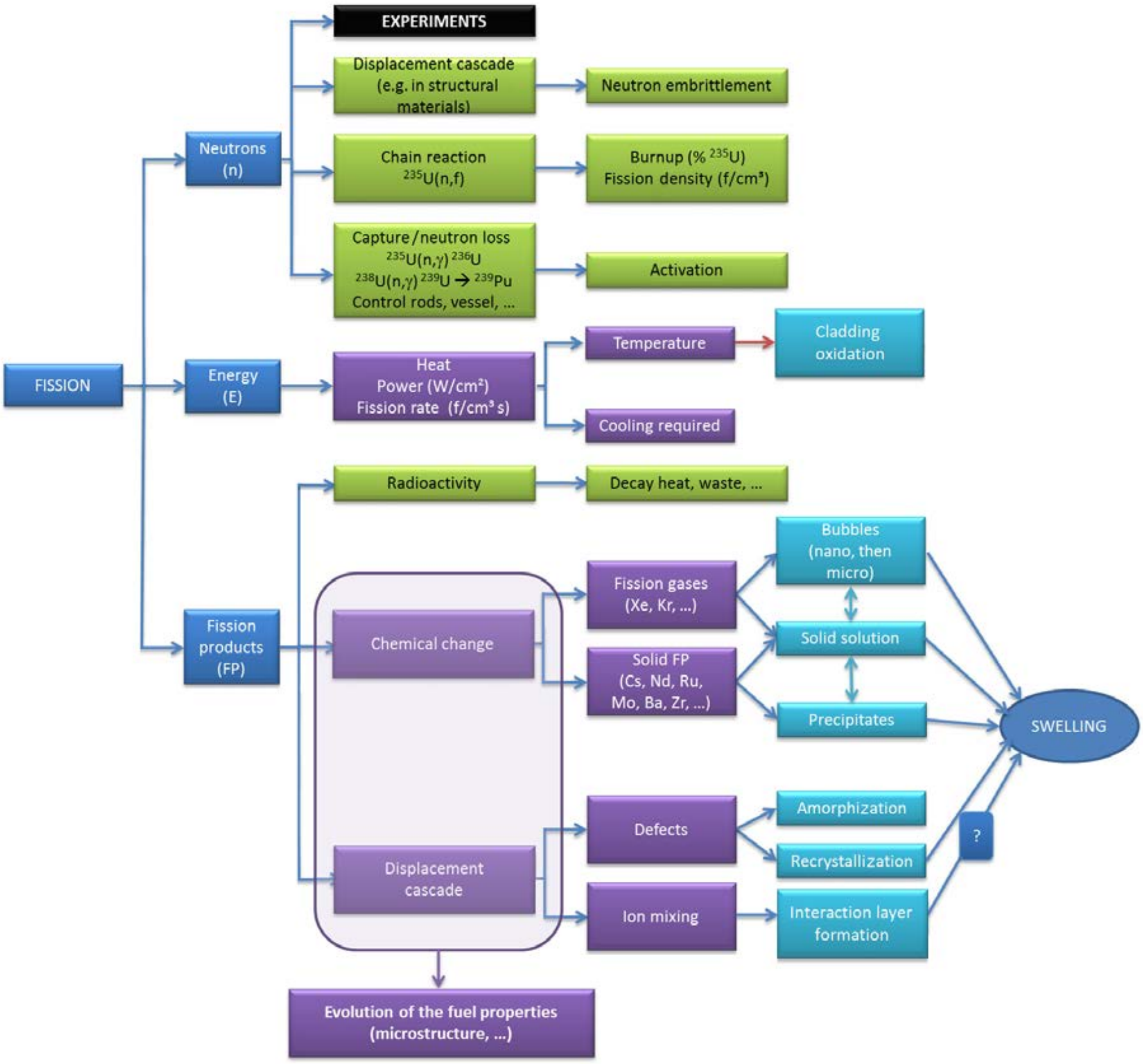

FIG. 2. Summary of the most important phenomena occurring as a consequence of a nuclear fission event. (Adapted from Ref. [2] with permission from SCK•CEN.)

(e) Restructuring. Irradiation induced grain refinement (also referred to as irradiation induced recrystallization) is a general phenomenon observed in a variety of crystalline nuclear fuel types, for example, UO_2, U_3O_8 and U–Mo. Restructuring results in sub-μm sized grains that accelerate fission gas swelling because of the combination of short diffusion distances, increased grain boundary area per unit volume and greater intergranular bubble growth rates as compared with that in the grain interior [4]. Recrystallization is not a direct cause of swelling but can lead to swelling through the release of overpressurized nanobubbles.

(f) Fuel swelling in dispersion fuel resulting from the combination of fission product accumulation and fuel microstructural changes. Two types of swelling may be identified. Solid fission product induced swelling is caused by the volume difference between the original uranium atom and the solid fission products that reside in the fuel compound lattice. Fission gas bubble induced swelling relates to factors such as recrystallization, fuel composition, fuel type, fabrication process (e.g. pre-irradiation voids may increase in size during irradiation) and fission rate [5].

(g) Creep. There are two types of irradiation creep: radiation induced and radiation enhanced creep. Both arise primarily because of vacancies: radiation produced vacancies can be large enough to induce creep. At high temperatures, thermal creep is enhanced by radiation. Creep depends on diffusion, so if the vacancy concentration increases, there is more diffusion and creep accelerates.

The phenomena with the highest impact on fuel structure and behaviour are those resulting from the fission products, as these are the phenomena that alter the fuel and cause its microstructure and properties to evolve with the accumulation of fissions (burnup) [2]. The remainder of this publication focuses on these phenomena and the PIE techniques used to explore their causes in order to gain a better understanding of fuel behaviour under irradiation conditions.

4. PRE-IRRADIATION CHARACTERIZATIONS

To understand the irradiation induced changes to the microstructure or other characteristics of the fuel and to ensure that the fuel elements meet the specifications of the reactor, pre-irradiation examinations of research reactor fuel are required. For fuel under development, additional detailed examination of the microstructure of the unirradiated fuel is performed using the same techniques as for the PIE. This enables a controlled comparison of the samples to identify the irradiation effects.

During fabrication, a rigorous quality assurance programme is applied to the fuel plates, rods and full fuel assemblies. The two pre-irradiation inspections that are the most important for comparing and understanding the PIE results are the following:

(1) X ray radiography: a high exposure radiograph is taken to measure the dimensions and shape of the fuel meat and its position within the plate and to identify stray particles (fuel particles outside the fuel meat zone). The homogeneity of the uranium distribution is checked via a second lower exposure radiograph.
(2) Ultrasound: an immersion ultrasound technique is employed to detect the non-bond regions and minimum cladding thickness.

4.1. RADIOGRAPHY

In the preliminary stages of pre-irradiation testing, the test specimens are characterized using a series of radiographic examinations. For fresh fuel, conventional X ray radiography is used prior to fuel plate or rod irradiation. In the process of radiography, X rays are passed through the test specimens. Depending on the mass absorption coefficient of the target materials, differing intensities of the X rays pass through the fuel plate sample and onto a radiographic film. To ensure accurate results, the film used for radiography is a fine grain, high contrast, double emulsion type of X ray film, equivalent to the film grade often used in industry [6]. After the X rays have passed through the target fuel plates, areas on the film darken. The most intense or least attenuated signals produce the darkest areas. In this way, the intensities of the X rays that pass through the plate samples can be observed and certain properties of the material can be ascertained.

More recently, digital radiography is the method used to capture the radiograph instead of traditional film. Digital radiography is expected to make the radiographic process more efficient and cost effective by eliminating the need for new film for each radiograph and allowing scans to be saved in a more versatile digital format.

The two most useful properties that can be determined using radiography are the location of the fuel in the plate relative to the aluminium cladding and the density throughout the sample. This density is used to determine the local thickness of the fuel meat and the local U–Mo loading over the whole fuel plate.

4.1.1. Fuel location radiography

Fuel location radiographs can determine whether the fuel meat contained within the aluminium cladding has shifted or if a fuel particle is out of place or has broken off from the fuel meat. For these types of radiographs, a lower intensity X ray beam is passed through the fuel sample, creating a much lighter image on the film. Because the area containing the aluminium cladding has minimal absorptive qualities, this area on the film is much darker than the area containing the dense fuel meat. Consequently, the location of the fuel meat can be clearly differentiated from the aluminium cladding, as shown in Fig. 3, where the cladding is the dark grey area and the fuel meat is within the lighter white area.

Fuel location radiographs are inspected visually using an overlay template of the fuel plate drawing that includes a precise location of the fuel plate boundary [7]. Comparing the overlay template and the fuel plate radiograph ensures that the fuel meat is in the proper position. From these radiographs, fuel particles outside the established fuel boundary can be identified and the final shearing locations can be determined [6]. Rejection may be necessary if the fuel meat has shifted significantly.

4.1.2. Density radiography

Density radiographs are obtained by passing much higher intensity X ray beams through the fuel plates and onto a film. This higher intensity beam produces a significantly darker image on the film than the radiographs used for fuel location radiography, as can be seen in Fig. 4 [7]. After the radiographic image is developed on the film, a densitometer is used to take readings of the film based on a density standard. This standard, along with the fuel plate identification and the orientation or step numbers, is generally included on the film [8]. The densitometer operates by passing light through the film in areas over the regions of the sample containing the fuel meat. A detector senses the relative lightness and darkness of the film and assigns a value between 1.0 and 4.0 from the density standard. A lighter area on the film implies a higher density point of the fuel plate.

The density of the fuel meat and its thickness are correlated to premeasured density standard thicknesses based on image darkness [7]. This correlation can also be applied to many of the densitometer measurements from the zone containing the fuel. With this information, an equivalent thickness of the

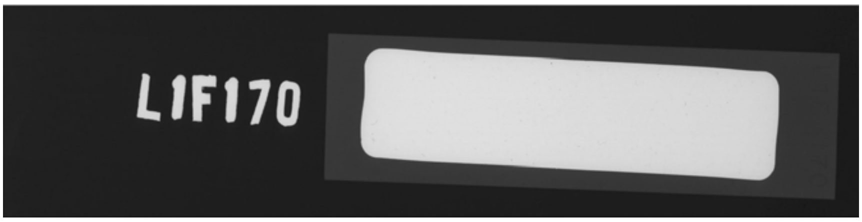

FIG. 3. Fuel location radiograph. (Courtesy of INL.)

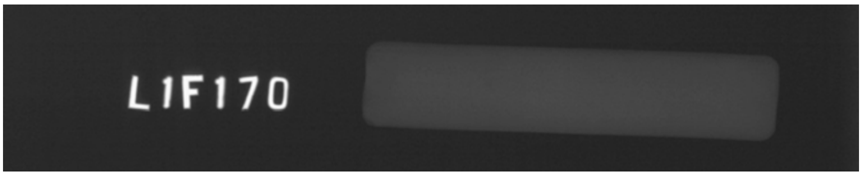

FIG. 4. Fuel density radiograph. (Courtesy of INL.)

fuel meat can then be calculated using the U–Mo mass absorption coefficient standard. The accuracy of this method has been demonstrated by a comparison of the calculated thickness of the fuel plates with micrometre thickness measurements conducted on surrogate foils, with an average difference being found of around 11.4 µm between the two measurement types [9].

The radiographic technique for performing density measurements and determining the thickness correlation of the samples is also useful for determining fuel loading based on the data obtained from thickness calculations. Using the nominal fuel area and thickness from the correlated density data to calculate fuel loading, neutronic and thermal analyses can be conducted on the fuel plates to determine how the fuel will behave when irradiated [8]. In cases where fuel loading is found to be above the desirable limit, 'hot spots' and unwarranted power peaking may occur during irradiation, leading to local regions of unacceptable thermohydraulic conditions. Thermal modelling is used to determine these loading specifications and ensure that these hot spots do not occur [7]. Therefore, the data obtained from the density radiographs are essential for helping to ensure that fuel elements meet approved specifications.

4.2. ULTRASONIC TESTING

Two critical parameters are identified by ultrasonic signals: debonds (locally delaminated regions, if they exist) and minclad (minimum cladding thickness). These criteria are part of the fuel specification.

The technique of ultrasonic testing on the fuel plates makes use of mechanical waves with a higher frequency and shorter wavelength than typical sound waves. A piezoelectric emitter passes ultrasonic waves through a target. A piezoelectric transducer then receives a signal through which the properties of the target are determined. As ultrasonic waves pass through media of different densities, their speed depends on the medium's impedance as well as the ability of the wave to be reflected, scattered or absorbed [7]. This creates a temporary deformation in the transducer, leading to a voltage change that is equivalent to the strength of the reflected or attenuated ultrasonic wave. This voltage change can then be measured and the relative strength of the reflected or attenuated ultrasonic signal can be determined. At Idaho National Laboratory (INL), ultrasonic testing scan experiments are conducted underwater with both the transducer and experimental fuel plate fully submersed in a specialized water tank, as ultrasonic testing waves travel more easily through a liquid medium than through air. The ultrasonic waves that are used for debond scans operate at a frequency of 15 MHz as opposed to the 40 MHz frequency used for the minclad scans. This difference in frequencies between the debond and minclad scans allows for signal differentiation. Both transducer systems may therefore operate in tandem and do not interfere with each other [7]. The transducer configuration for ultrasonic testing scans is shown in Fig. 5 [7].

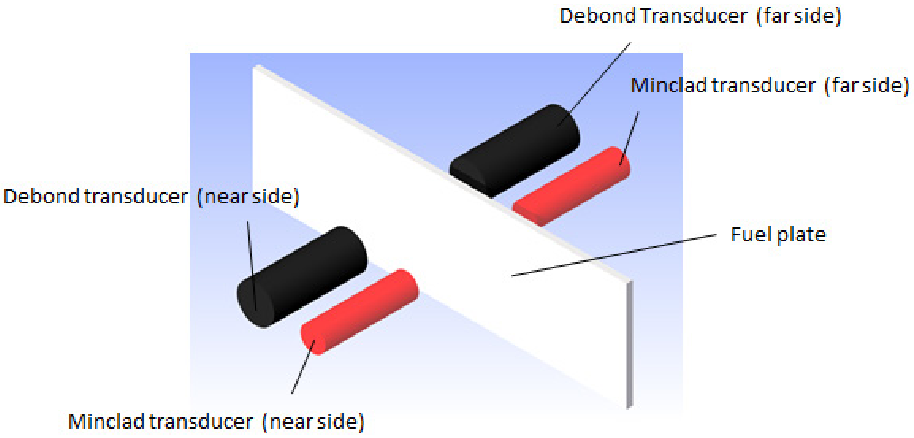

FIG. 5. Ultrasonic testing transducer configuration. (Adapted from Ref. [7] with permission from INL.)

4.2.1. Debond ultrasonic testing scans

Debond ultrasonic testing scans detect areas containing manufactured voids or abnormalities in the fuel plates. These scans use lower frequency ultrasonic waves transmitted ‘through’ the plate to a second receiving transducer on the opposite side [6]. If one of these ‘through’ transmissions is interrupted by a significant void in the fuel plate, a disruption in the ultrasonic signal occurs. This disruption in the ultrasonic signal can cause a subsequent disruption in voltage across the receiving transducer that can be clearly observed on a plot of the piezoelectric voltage. A plot showing a void disruption voltage change in the piezoelectric transducer versus the time since the ultrasonic wave was emitted for an area containing a debond can be seen in Fig. 6 (a) [10], along with an image created of the fuel plate locating the area of the debond.

For the debond scan transducer, the beam size is approximately 0.25 mm in diameter with scan and step increments of approximately 0.08 mm. With such a small step size in relation to the beam diameter, an overscan greater than 300% is necessary, which ensures that no area of the fuel plate is overlooked [8]. Because this method makes use of through transmission, the measurements obtained from this examination are based purely on the attenuation of the ultrasonic signal. However, errors due to the geometry of the fuel plate may occur that can scatter the signal to produce inaccuracies in the data, such as edge effects. Edge effects occur when the ultrasonic beam is dispersed, reflected or attenuated in some way. This indicates a boundary between the edges of the fuel meat material and the aluminium cladding [6]. Figure 6 (b) [10] shows a signal plot of the edge effect and the location along the fuel meat edge at which it occurs. Other inaccuracies may also arise from signal scattering owing to defects in the surface of the cladding that can be mistakenly classified as debonds [7].

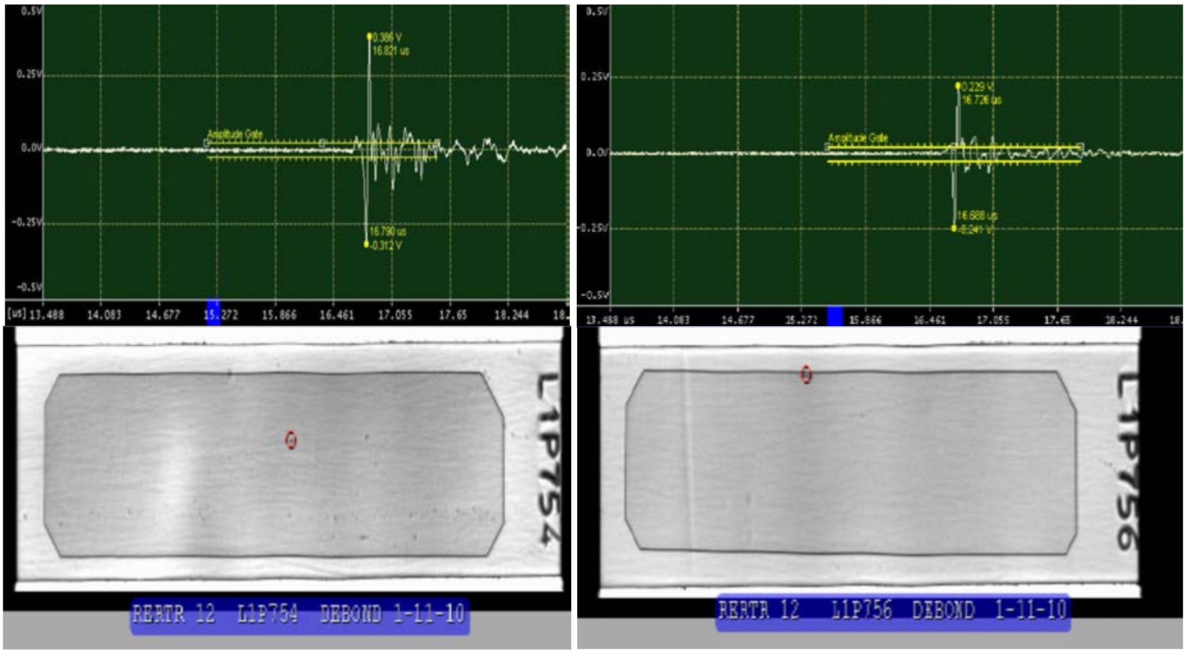

(a) (b)

FIG. 6. (a) Ultrasonic testing scan signal and image of debond. Sensor at locations indicated by the red dots on the plate. (b) Sensor at edge illustrating edge effect. (Reproduced from Ref. [10] with permission from INL.)

4.2.2. Minclad thickness ultrasonic testing scans

Minimum cladding (minclad) thickness testing is essential to decrease the likelihood of a cladding breach. Rather than utilizing through transmission, minclad ultrasonic testing uses a technique known as pulse echo mode. Pulse echo mode emits brief ultrasonic signals from each of the transducers at high frequencies (approximately 40 MHz). These same transducers then receive the reflections (or echoes) of these signals to produce an amplitude versus time waveform for the received reflections [7]. The signal is most strongly reflected back to the transducer when these ultrasonic pulses encounter a boundary or interface between two different media, which can be distinctly observed in the waveform signal. In the case of the fuel plates, each side has two interfaces. The first interface is between the background medium, the water and the cladding material. The second interface occurs between the cladding material and the fuel meat. The time interval taken for the transducer to receive each of these interface reflections can be measured and plotted to create an A-scan. Figure 7 [11] shows a simplified schematic diagram of an ultrasonic testing deep focus beam and the reflected signals from the edges of the fuel plate as well as the reflected signal from a fuel meat boundary indication or flaw that can be picked up by the transducer.

With the data from the A-scan, the cladding thickness can be calculated using time of flight, which is the time necessary for a signal to travel a certain distance through a specific medium [7]. By knowing the time of flight for ultrasonic waves through aluminium, the thickness of the aluminium cladding can easily be calculated using the time interval between the boundary reflections. These calculations can provide the location of the fuel boundary and the thickness of the cladding. By compiling a number of the individual A-scan 'slices', a rendering of the entire plate can be created at any given depth from the surface of the fuel plate [7]. This compilation is known as a C-scan.

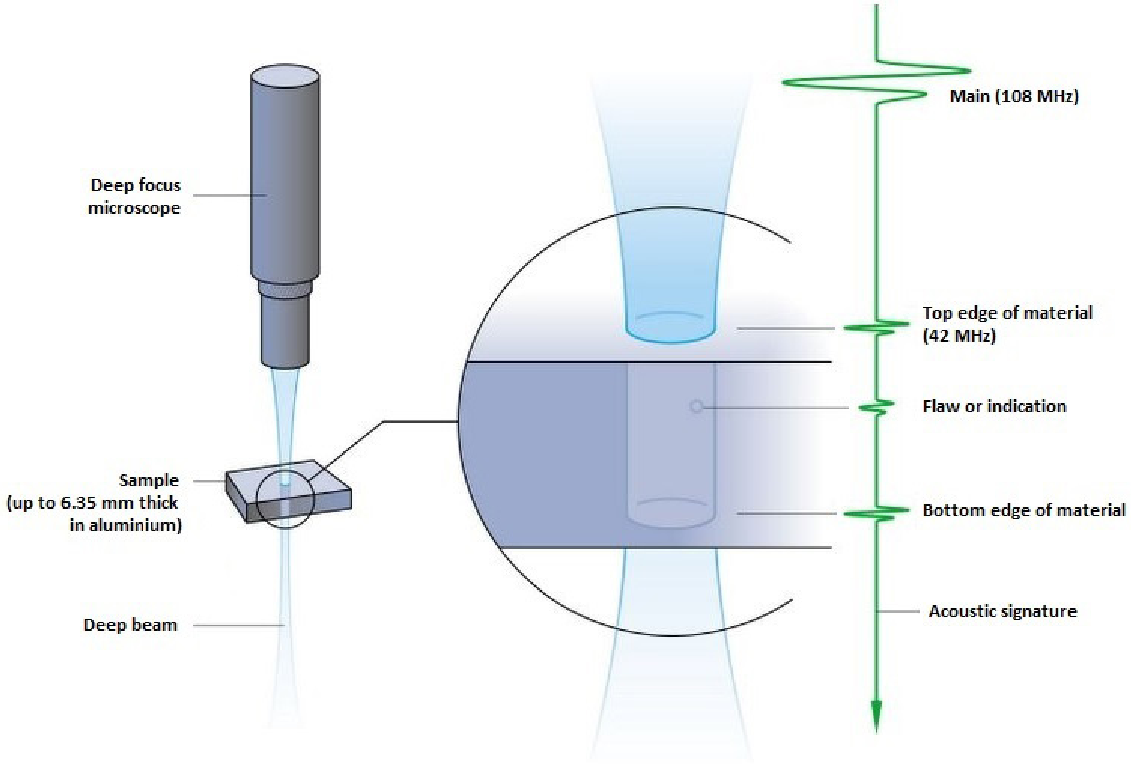

FIG. 7. Schematic diagram of an ultrasonic testing deep focus beam and reflected signals from material boundaries. (Adapted from Ref. [11] with permission from INL.)

A strong advantage of the minclad ultrasonic testing examination method is the fact that the measured data do not depend on the transducer distance from the actual fuel plate. This is because the reflection from the surface interface provides a clear indication of where the outer edge of the fuel plate is. For this reason, it is not necessary for the fuel plate to be perpendicular to the ultrasonic signal emitted by the transducer when determining cladding thickness. However, scattering issues may be created if the fuel plate is too severely misaligned with the transducer beam [7]. For minclad ultrasonic testing scans, the size of this beam is slightly smaller than that used to detect debonds, with a total beam diameter in the range of 0.15–0.20 mm and a step size of approximately 0.08 mm, resulting in an overscan of ~250% [8]. This is sufficient to ensure that the entire fuel plate is examined thoroughly.

5. INFRASTRUCTURE AND APPROACH FOR POST-IRRADIATION EXAMINATIONS

PIEs of fuels (except for those performed in the reactor pool or canal) require special infrastructure to handle the highly radioactive fuel plates or rods. These facilities are commonly described as hot laboratories and house a number of hot cells.[1] A hot cell is a shielded area providing protection against radiation which is equipped with an alpha particle tight containment (biological shielding) in which contaminating materials such as fuel can be handled. The highly radioactive materials in the cells are handled by remote operation, using telemanipulators, also known as master–slave manipulators. Most PIE equipment is custom designed and constructed by the hot laboratory engineers specifically for their laboratory. Furthermore, as electronics and optical components do not survive the high radiation fields present in the hot cells, they are therefore avoided or replaced with radiation-hardened alternatives (e.g. magnetic systems instead of optical), placed outside the shielded area and connected with cables, or locally shielded within the hot cell.

PIE techniques are generally divided into two categories: poolside PIE techniques and hot cell PIE techniques. The latter are further subdivided into non-destructive testing (NDT) and destructive testing. Typical PIE campaigns follow the timeline shown below:

(1) Poolside fuel or experiment inspections between irradiation cycles and after irradiation;
(2) Dismantling of experiment or fuel assembly;
(3) Non-destructive examinations in the hot cell;
(4) Development of the sampling plan based on neutronics and NDT results;
(5) Sampling and sample preparation;
(6) Destructive examinations in the hot cell;
(7) More advanced PIE techniques, including sample miniaturization, for the conduct of PIE outside of the hot cell environment.

In some cases, the PIE campaigns do not follow this sequence and steps are skipped or interrupted once the necessary information is obtained.

Poolside PIE techniques are generally applied between irradiation cycles, and irradiation continues afterwards if no unsuitable conditions are detected. PIE helps to assess whether the irradiation is proceeding as expected or if unexpected conditions are present. The inspections are performed underwater, in the reactor pool or the canal. They can include visual inspection with underwater cameras, dimensional checks (plate thickness, rod diameter, interplate spacing), wet sipping tests (detection of fission product release) and sometimes gamma scanning. Once the poolside measurements have been completed, the irradiation can be resumed, or the assembly is transported to the hot cell facility to be dismantled for further PIE.

---

[1] An overview of hot cell facilities around the world can be found at https://infcis.iaea.org/

In the case of NDT, physical measurements are performed to detect dimensional changes (i.e. thickness, length, diameter), corrosion layer thicknesses, cladding defect detection and gamma spectrometric measurements. In some cases, special techniques, such as neutron radiography or immersion density on full fuel plates or rods, are also applied. These NDT results are also used to identify the area of highest interest on the irradiated fuel (e.g. highest burnup location, defect location, abnormal behaviour) for further investigation.

Alternatively, to meet research programme objectives, a sampling plan may be drawn up to extract appropriate samples from the fuel plate or rod for destructive analyses. Optimizing the cost of a research programme sometimes means reducing the number of samples required for destructive examination by using non-destructive examination techniques to understand the fuel element characteristics.

The sampling plan indicates the exact location at which different samples will be taken for different purposes. After extraction of the samples, typically by cutting but sometimes by punching, the samples are prepared for analysis. Careful handling at this stage is crucial to avoid the introduction of artefacts.

An important subfield of destructive analyses relates to sample miniaturization to reduce the radiation fields of the samples. A popular technique, whereby miniature samples are machined to a few hundred square micrometres and to a thickness of only a few nanometres, is the focused ion beam (FIB) system. The FIB system can be used to obtain samples for site specific transmission electron microscopy (TEM) and/or atom probe tomography (APT) sample preparation. This strategy allows for analysis using instruments with limited radiological shielding.

Thin foils (for TEM) or needles can be milled out of the sample using a high energy gallium (Ga^+) ion beam. Localized sampling can be important in fuels that are heterogeneous at the micrometre level, such as dispersion fuels.

Although FIB offers advantages over conventional mechanical and chemical TEM sample preparation, it also has the drawback of high energy operation (i.e. formation of a defected, amorphous and/or implanted surface layer). The influence of sample preparation ought to be considered in the evaluation of all PIE results. To avoid false conclusions, a rigorous validation process, using multiple techniques, needs to be applied to challenge the sample preparation method.

Destructive analyses generally use microscopy techniques to examine the micro- and nanostructure, spectroscopic techniques to determine local chemical compositions, diffraction techniques to determine the crystal structure on a local or more global level, and radiochemical techniques to determine irradiation parameters such as radiochemical burnup. In some cases, destructive techniques are also used to investigate thermal parameters (e.g. thermal diffusivity, thermal conductivity), mechanical properties or more advanced properties.

PIE results obtained using multiple techniques need to be compared to provide a reliable explanation for the observed properties. A meaningful assessment of the results requires a thorough understanding of PIE techniques. Artefacts introduced during sample preparation, calibration errors, human errors, defective equipment, etc. are very common in all material analyses, including in the nuclear field. Once reliable results are obtained, the data have to be processed to become useful for modelling or fuel development.

6. INTERCYCLE POOLSIDE EXAMINATIONS

Before hot cell examinations are possible, several months of cooling are often required to reduce the radiation and decay heat levels to acceptable values for material transfer and to within hot cell limits. However, intercycle poolside examinations may be undertaken to monitor certain changes in the fuel elements during reactor operation. Poolside examinations can even be performed in-between irradiation cycles to follow the evolution of the fuel plate, rod or assembly properties from cycle to cycle. Examples of these examinations are in-canal visual examination, thickness and interplate space measurements, gamma scanning, and sipping or soaking tests.

6.1. IN-CANAL VISUAL EXAMINATION

The visual examination of fuel and test capsules, using underwater radiation resistant cameras, is conducted in the reactor pool or canal prior to irradiation, between irradiation cycles and after irradiation to detect changes in the fuel or capsule configuration. In-canal visual examination also establishes the condition of the fuel and capsules prior to shipment, for comparison with their condition after receipt at the hot cell. Using photographs, a comparison of the pre-irradiation, mid-cycle, in-canal and in-cell conditions of the fuel is possible. Recognizing the variability of imaging equipment and lighting at these different stages, best efforts are made to develop a method to normalize image quality in order to allow more quantitative comparisons. These examinations are performed to detect blisters, plate pillowing, buckling, warping, corrosion or twisting. Any one of these characteristics can be indicative of a loss in mechanical integrity or geometric stability of the fuel plate. Data from visual examination can be used to determine the priorities for subsequent examinations.

6.2. THICKNESS AND INTERPLATE SPACE MEASUREMENTS

Different systems to measure the evolution of fuel plate thickness between irradiation cycles have been developed. Typically, contact methods or ultrasonic methods are used. These are described below using examples of devices that have been constructed and employed.

The evolution of fuel plate thickness with burnup is a crucial parameter in the qualification of research reactor fuel, since the cooling gaps between fuel plates in research reactor fuel assemblies are typically narrow. If fuel plate swelling reduces these cooling gaps too much, coolant flow decreases, leading to temperature increases for the cladding. Aluminium alloys generally undergo rapid corrosion once temperatures exceed ~180°C [12]. In addition to normal swelling effects, these measurements can detect the presence of ‘pillowing’ (Fig. 8), where swelling no longer evolves quasi-linearly with burnup, but develops much more quickly. The detection of pillowing can lead to a decision to interrupt the irradiation campaign.

6.2.1. Contact probe thickness measurements

Contact probe thickness measurements have been used for the IRIS irradiation programme in the French Alternative Energies and Atomic Energy Commission (CEA) OSIRIS reactor. The IRIS experiment involves the irradiation of between one and four fuel plates in the OSIRIS core. The IRIS irradiation device (see Fig. 9) has the same geometry as the OSIRIS U_3Si_2 standard fuel element. It is cooled by the water of the reactor core cooling system and can be loaded with four plates, either fuel or

FIG. 8. Photograph of a slice cut from a flat fuel plate showing the deformed or pillowed area. (Reproduced from Ref. [2] with permission from SCK•CEN.)

FIG. 9. *IRIS irradiation device. (Reproduced from Ref. [13] with permission from CEA.)*

inert plates, separated by inert aluminium alloy plates. The dimensions of the experimental plates are 641.9 mm × 73.3 mm × 1.27 mm. The IRIS device consists of an aluminium alloy body which is connected to an upper assembly, preventing the plates from sliding out as the water flows upwards [13, 14].

Between two consecutive irradiation cycles, each plate is transferred, one after the other, into the IRIS measurement bench to monitor thickness profiles. If the observed swelling and the accumulated burnup comply with authorized safety criteria, the plate can be returned to the irradiation box to continue the planned testing.

The contact probe thickness measurement device is underwater and is composed of a frame to hold the plate to be tested, a displacement system to select a position to measure on the plate's surface and sensors to measure the local thickness at this position. Figure 10 shows a photograph and schematic diagram of the IRIS underwater plate thickness measurement device.

The plate is inserted vertically into an aluminium frame. The opening is then closed with a cap to prevent movement of the plate during the measurement sequence.

A displacement system allows sensors to move in the horizontal and vertical directions. The displacement is operated by two stepper motors, one per direction, located in a watertight chamber. Limit switches determine the actual dimensions of the plate. Their service range is approximately 710 mm vertically and 65 mm horizontally. The position is obtained by counting the number of steps covered by the motor from a reference point.

A pair of linear variable differential transformer (LVDT) sensors, mounted on each opposite side of the plate, measure a representative voltage of the local thickness. Because of vibrations from the motors, a delay is introduced to make sure the plate is steady before recording the measurement.

An aluminium wedge (standard gauge block) is positioned at the lowest part of the device, and the plate makes contact with it. At the beginning and the end of a measurement sequence, sensors run along the wedge to reset the position reference point and calibrate the LVDT sensors. For that purpose, a hole acts as a position mark. In addition, the wedge consists of two steps, the thicknesses of which are respectively lower (1.3 mm) and higher (1.9 mm) than the expected plate thickness. These enable

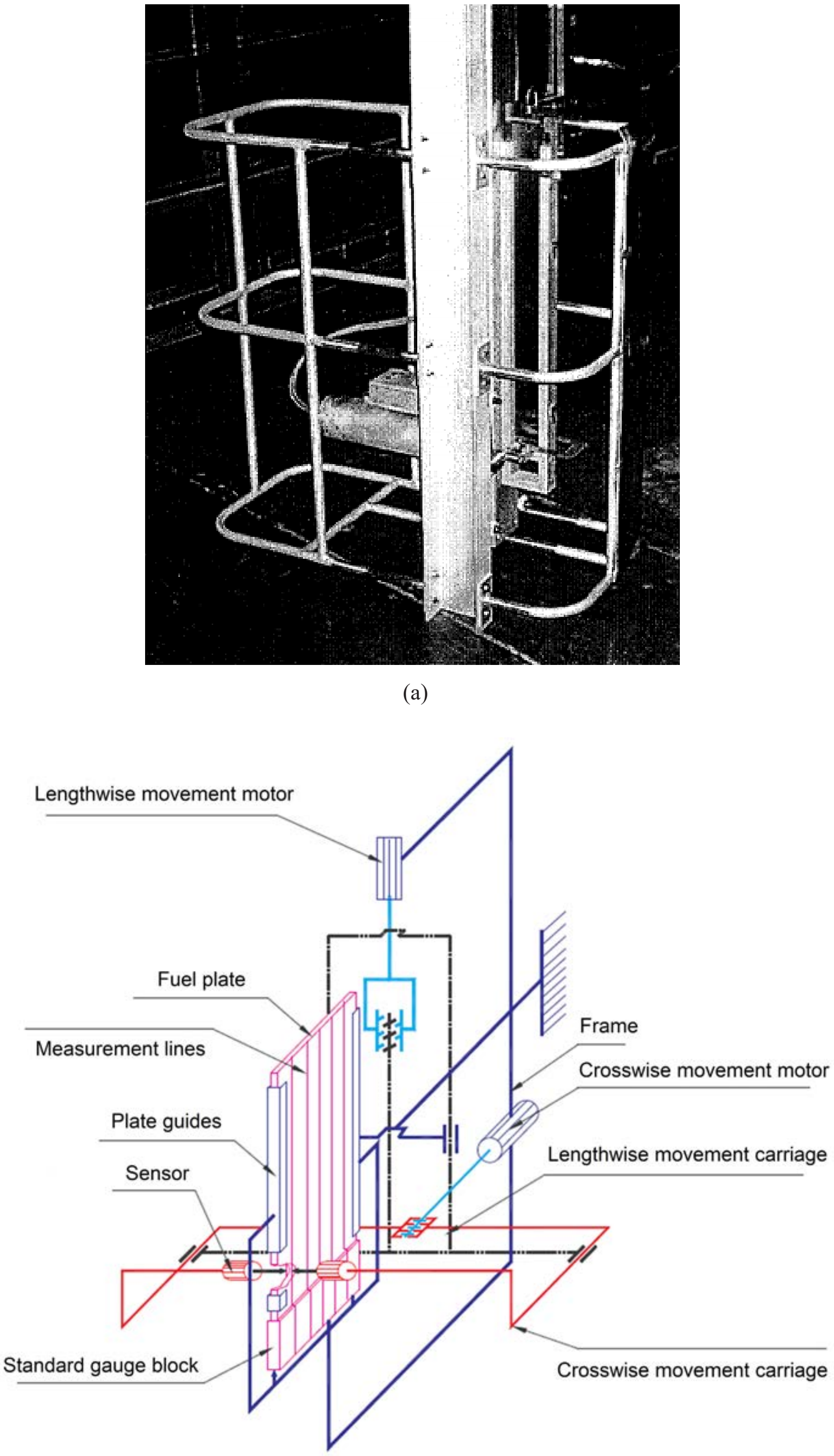

(a)

(b)

FIG. 10. The IRIS underwater plate thickness measurement device. (a) Image of the device immersed in the pool. (b) Schematic principle of the measurement. (Adapted from Refs [13, 14] with permission from CEA.)

calibration of the LVDT sensors in the useful thickness range through a linear relation between thickness and voltage reading.

The quality of measurement is validated using a calibration plate, prepared with three calibrated notches, which is inserted into the IRIS bench at the beginning and at the end of the measurement campaign.

The usual measurement programme consists of scanning the plate along five vertical lines distributed equally over the width of the plate. A horizontal line is also scanned corresponding to the maximum flux plane of the reactor (Fig. 11) [15]. The selected step along each line is usually between 0.5 mm and a few millimetres. To ensure consistency in thickness measurements, the same scanning lines are used throughout measurement campaigns (Fig. 12). This method enables detection of the areas showing the onset of swelling. A 3-D rendering with a finer mesh can be performed in a window centred on areas where swelling is suspected (Fig. 13), providing a better characterization of peak location and swelling rate change. These measurements allow a direct comparison of the swelling observed for various plates. Figure 14 shows the results for plates from the IRIS irradiations.

The contact probe thickness measurement system has the following advantages:

(a) A cooling period is not necessary after irradiation, enabling plate examination between two consecutive irradiation cycles.
(b) Measurements are performed on full scale plates.

Its drawbacks are the following:

(a) The system only allows for the monitoring of a single plate, which is removed from an irradiation box, or a fuel assembly.
(b) The repeated mechanical contact of sensors on the plate may distort the visual appearance of the plate, namely through the appearance of discoloration lines.
(c) In cases of plate deformation, the positioning of the plate is less accurate, and it can be impossible to insert the plate within the support. Additionally, plate deformations can prevent accurate operation of the measurement device.
(d) In cases of cladding failure, measurement is not possible.

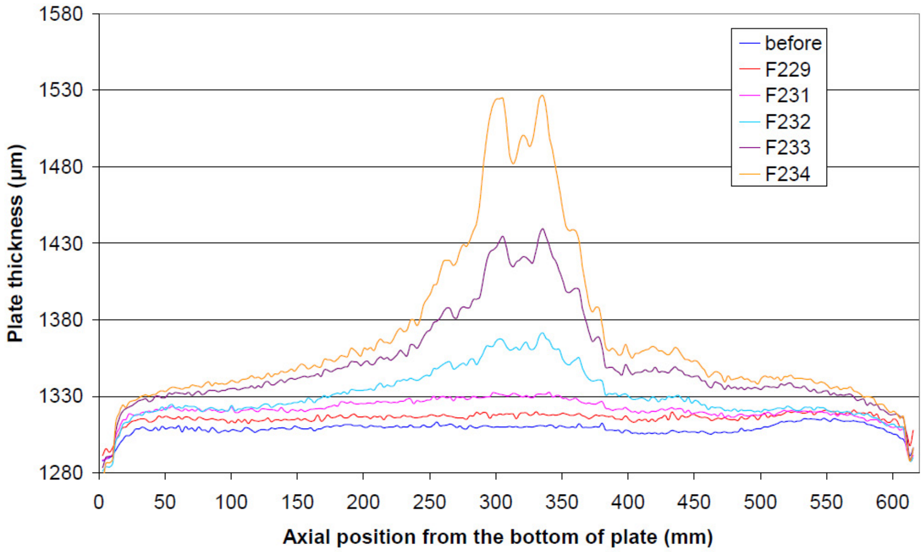

FIG. 11. Thickness measurements along the maximum flux plane before irradiation and after each one of the six cycles (F229 to F234) of one of the plates of IRIS 4 irradiation. The measurements after the second cycle (F230) are not available due to technical problems. (Reproduced from Ref. [15] with permission from CEA.)

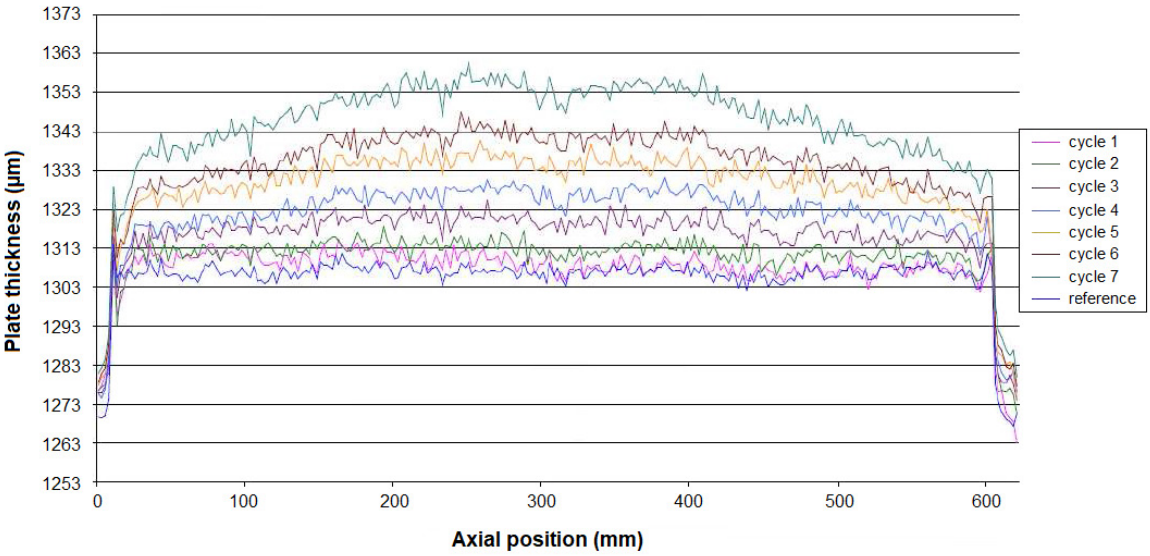

FIG. 12. IRIS 1 irradiation thickness measurement along the length of a plate, before irradiation (blue curve, designated as 'reference') and after each one of the seven irradiation cycles. It shows a gradual increase of plate thickness with increasing burnup. (Adapted from Ref. [13] with permission from CEA.)

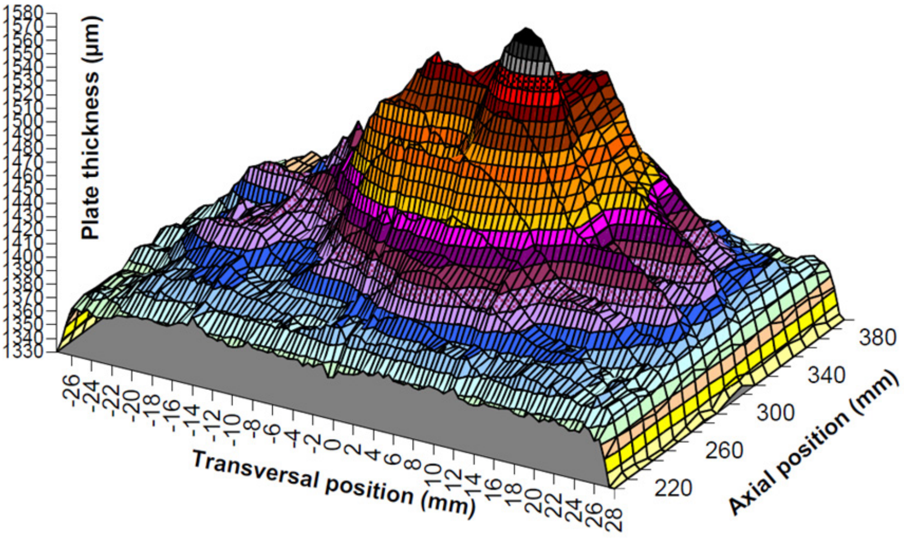

FIG. 13. Detailed thickness measurements for an area where severe swelling (pillowing) was detected. (Reproduced from Ref. [15] with permission from CEA.)

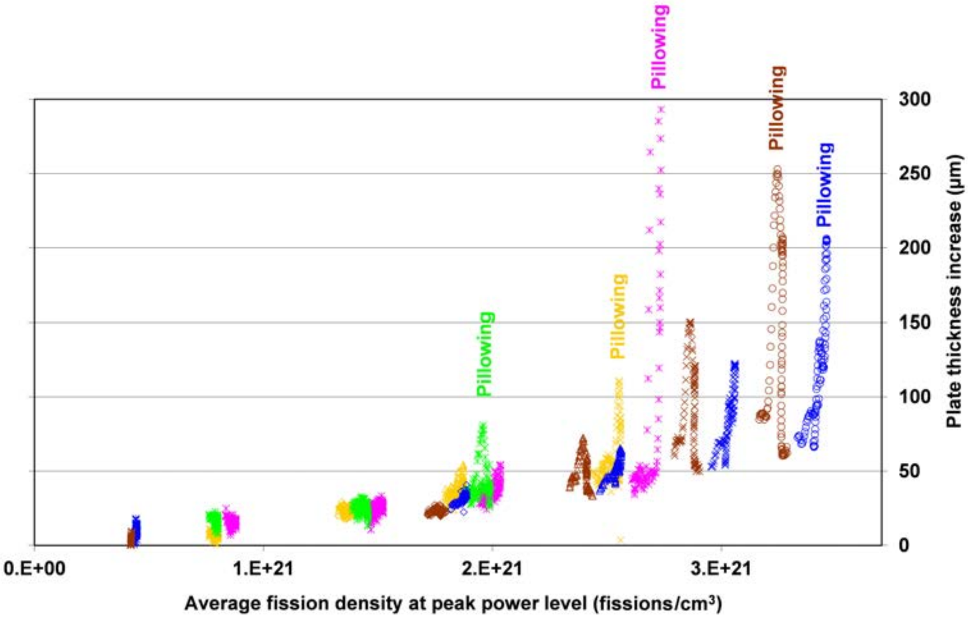

FIG. 14. IRIS 2 and IRIS 4 plates: increasing thickness as a function of the average fission density at the maximum flux plane. (Adapted from Ref. [15] with permission from CEA.)

6.2.2. Ultrasonic measurements

Ultrasonic evaluations are used at different stages of fuel life: during fuel fabrication, as a final qualification inspection prior to placement in the reactor, and to measure plate expansion and debond growth between reactor irradiation cycles.

As an example, interim reactor cycle inspections are performed in situ at INL's Advanced Test Reactor (ATR) canal on the ATR Full-size plate In center flux trap Position (AFIP) fuel plates prior to reactor insertion and again after each reactor cycle.

The in-canal ultrasonic inspection device (shown in Fig. 15) was developed at INL specifically for the inspection of research reactor fuel plates. This inspection allows for the geometric evolution of the plate to be measured throughout the life cycle of the experiment. For the AFIP-1 experiment [16], measurements were performed four times (prior to irradiation and after the first, second and third irradiation cycles). The device consists of two detectors [17] located on opposite sides of the plate that generate and monitor the response of ultrasonic signals sent towards the plates. The detectors are mounted on a rail system that moves in the *x*–*y* plane, which allows positioning over any location on the plates. This system is used to examine the fuel plates on an extremely fine grid, where measurements are taken at 80 µm intervals in the *x* and *y* directions such that around 5 million data points are collected on each plate.

The signals can be used to identify the presence of large voids in the fuel that are typically a precursor to blister formation and subsequent loss of fission product encapsulation, as well as the distance from the detector to the surface of the plate. This second set of data is used to evaluate the general shape and local thickness of the plate.

The results of the thickness measurements performed on AFIP-1 fuel plates after each cycle of irradiation can be found in Ref. [16]. A series of 'debond scans' based on through transmission of the ultrasonic signal were taken before irradiation and after each irradiation cycle to track the evolution of any macroscopic porosity during irradiation. Thickness scans were also performed on each plate to evaluate the general geometry of the fuel plates and fuel plate swelling. Before each scan, the device is calibrated using a known standard. To enable a quantitative analysis, the thickness measurements need to be reset to zero. The reason is that the decay heat from the plate gives rise to local water temperature variations,

FIG. 15. ATR in-canal ultrasonic inspection system. (Courtesy of INL.)

which lead to small drifts in measurement values. These small changes alter the speed of sound in the water. The time of flight used for calibration purposes therefore needs to be corrected, to allow a direct comparison of plate thickness between different cycles of irradiation.

6.3. GAMMA SCANNING

Gamma scanning can detect the presence of nuclides of varying half-lives. Measurements made shortly after irradiation capture nuclides with shorter half-lives, which give information on the power distribution during the last part of the recent irradiation. Measurements made later in the hot cell after a cooling period detect nuclides with longer half-lives, which provide an integral of the activity over the entire irradiation and therefore a better picture of the burnup distribution.

For plate type fuels, poolside gamma spectrometry examinations are mainly used for the following reasons:

(a) Validating the neutronic calculations for each irradiation cycle;
(b) Relating the plate swelling and the recent local powers or the local burnup;
(c) Evaluating the integrated fission densities.

Many of the fission product nuclides are gamma emitters, typically in the high energy range, above 10 keV. These gamma rays are emitted in connection with α and β decays in the transitions between excited states of the radioisotope nucleus. For each radioisotope, the transitions are very specific so that the gamma rays emitted have well defined energies or wavelengths. Gamma rays emitted by nuclear fuel elements can be measured using a high purity germanium (HPGe) crystal, cooled to liquid nitrogen temperatures associated with a high tension system, and an electronic chain including amplifiers and a multichannel analyser. The role of the multichannel analyser is to differentiate the interactions in the HPGe crystal according to their energy, producing a spectrum. Using a collimation system, it is possible, for a given period of time, to measure the gamma rays emitted by a sample. In the case of nuclear fuel rods or pins, the collimation is often a slit, perpendicular to the rod, allowing the measurement of a slice of the rod. Successive translations of the rod in front of the slit, with steps in the range of the slit thickness, generate complete relative axial profiles of the studied isotopes along the rod. In the case of fuel plates, the slit geometry is not appropriate for the collimation system. However, using a more isotropic collimation and a horizontal and vertical scanning of the plate, a map of each studied radioisotope can be produced. Using calibration sources, these measurements can be quantitative.

In the OSIRIS facility, the spectrometer bench is submerged in the reactor pool (Fig. 16). This enables the rapid and flexible transfer of the plates to be scanned. The table supporting the plates is moved vertically and horizontally by stepping motors. The cooling and acquisition times are optimized according to the nuclides of interest. Averaged power distributions over irradiation durations are usually given by measuring the beta decays of, for example, ^{132}Te to ^{132}I ($t_{1/2}$ = 3.2 days), ^{131}Te to ^{131}I ($t_{1/2}$ = 25 minutes), ^{140}Ba to ^{140}La ($t_{1/2}$ = 12.8 days) and ^{95}Zr to ^{95}Nb ($t_{1/2}$ = 64 days), whereas ^{137}Cs, with its half-life of 30.17 years, is more representative of the burnup, or of the total fission activity from the start of the irradiation [13]. Figure 17 shows an example of the relative power distribution over an entire fuel plate obtained from ^{95}Zr–Nb. Figure 18 shows a detail along a transverse section of a plate, for a long period isotope and a short period one. Both examples show higher burnup and power on one side of the plate. Figure 18 illustrates the gradual flattening of the power profile with increasing burnup.

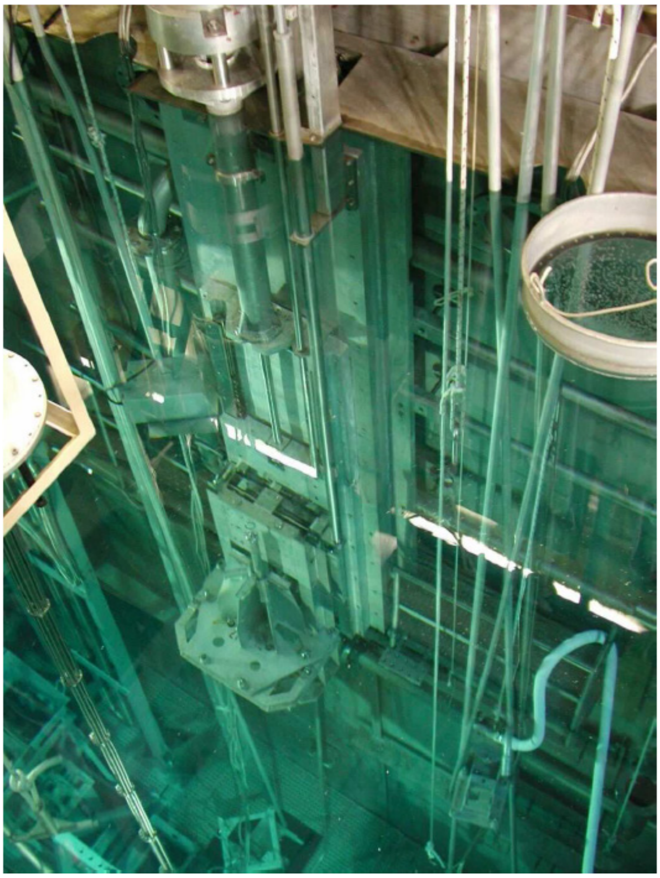

FIG. 16. Poolside gamma scanning device in OSIRIS. (Reproduced from Ref. [13] with permission from CEA.)

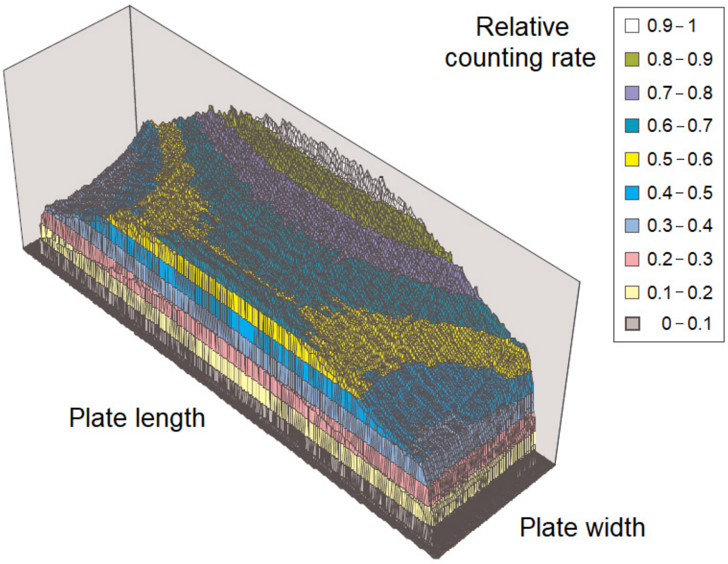

FIG. 17. Relative power distribution over the surface of a fuel plate deduced from poolside gamma scanning. (Adapted from Ref. [13] with permission from CEA.)

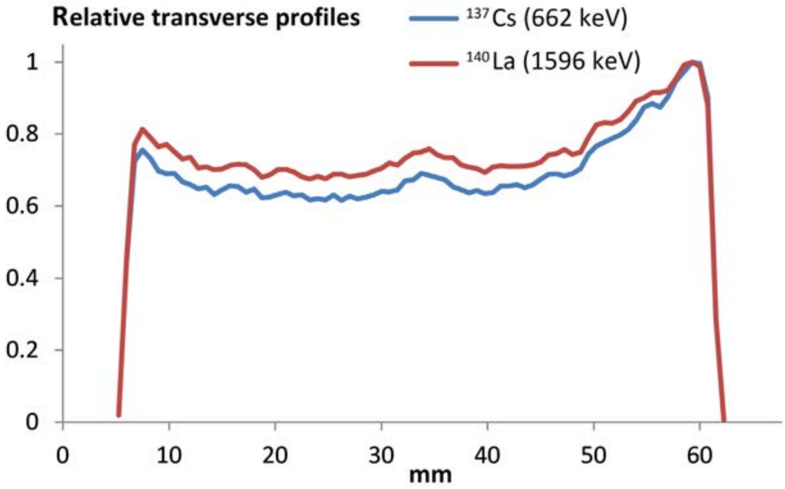

FIG. 18. Relative transverse gamma profiles on an irradiated fuel plate. Examples for a long period radioisotope, ^{137}Cs, and for a short period one, ^{140}La. (Courtesy of CEA.)

6.4. SIPPING OR SOAKING TESTS

During reactor operation, the reactor coolant is monitored continuously to detect fuel failure. Ultimately, it is important that the root cause of a failure is identified so that corrective actions can be taken in the operation, design, manufacturing or development of a fuel. Of interest is the time that a fuel element failed, the location in the core of the defective fuel element and the cause of the failure. Eventually, it has to be decided whether the defective fuel element needs to be discharged.

Sipping or soaking is the most common technique used to locate fuel failures in both power reactor fuels and research reactor fuels [18]. To identify a fuel rod failure, it is necessary to detect the fission product activity released through defects during sipping. For that purpose, the fuel element is put in an isolated container and regular sampling of the container atmosphere (e.g. water, vacuum) is performed to detect any contamination with radioactive fission products. Xenon and krypton are fission gases that are detected, while caesium and iodine are detected in water samples. Various versions of sipping have been employed to detect leaking fuel assemblies, and they depend on the details of the configuration and system and the physical phenomena responsible for fission product release (i.e. application of vacuum, heat, elevation). The different techniques are known as vacuum sipping, wet sipping, and in-mast or telescope sipping.

The results of a sipping test performed on an irradiated plate type fuel that had failed in the Open Pool Australian Lightwater (OPAL) reactor are reported in Ref. [19]. To conduct the test, a sipping assembly was manufactured at the Australian Nuclear Science and Technology Organisation (ANSTO) and placed in the service pool of the OPAL reactor. In the sipping assembly, a fuel element was encased with a fixed volume of water and isolated from the reactor pool. To circulate a volume of water through the element, one hose was attached to the top of the assembly, and one was attached at the bottom. An electric powered centrifugal pump was located at the reactor pool side to circulate the water. If a failure was present in a fuel element, radioactive fission products would be released into the circulating water. After a period of time, there would be a significant increase in the concentration of the radioactive components. To monitor the release of fission products, two methods were employed using gamma spectroscopy: an external method and an in situ one. The external method required the collection of sipping water samples and their measurement using two HPGe detectors. The in situ method employed scintillator detectors in the circulating water. The sipping of each fuel element took 120 mins, excluding the time taken to load an element into the sipping assembly.

7. NON-DESTRUCTIVE POST-IRRADIATION EXAMINATIONS

Before the destructive sampling of an irradiated fuel element, non-destructive analyses in the hot cell may provide information on its irradiation behaviour, complementing information obtained by poolside examinations. Non-destructive analysis generates a more global view of the state of the fuel element, whereas destructive techniques focus on the details of specific locations in the fuel element. In this way, NDT results can help to guide the sampling and identify the locations that are likely to yield the most important information. NDT typically starts with a visual examination that can identify locations where the behaviour differs from expectation (e.g. discolorations, deposits, ruptures, gross deformations).

The non-destructive assessment is based on different dimensional metrologies to evaluate the evolution of the element geometry under irradiation. Because swelling is an essential aspect of fuel behaviour, such non-destructive measurements can be very informative. Metrology also involves an assessment of the oxidation and corrosion of the cladding material. In addition to metrology, gamma spectrometry can assess burnup distributions and in some cases fission gas release in a quantitative way without sampling. Radiography techniques, using either X rays or neutrons, allow a view of the inside of the fuel elements without destroying them.

7.1. VISUAL EXAMINATION

A visual examination of fuel elements brought into the hot cell is generally the first non-destructive test performed. By examining the pattern of oxidations, inferred by colour changes, it is possible to gather first impressions of the fuel element behaviour. Deformations or deposits found on the cladding are the first indications of potential problems. These observations guide subsequent measurements by indicating where more attention is needed.

The difference in colours, resulting from the different levels in oxidation, is clearly visible in Fig. 19 [20].

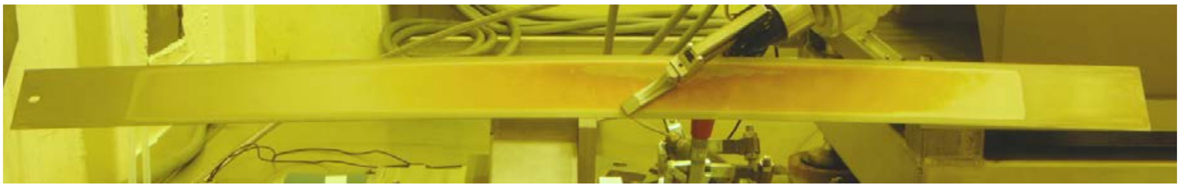

(a)

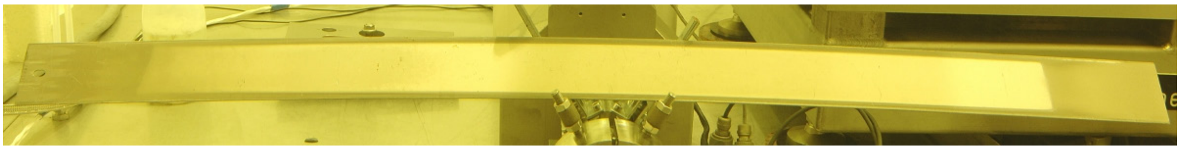

(b)

FIG. 19. Example of visual examination of two sister fuel plates that were irradiated at two different power levels. (Courtesy of SCK•CEN.)

7.2. THICKNESS, DIAMETER AND OXIDE THICKNESS MEASUREMENTS

With swelling being one of the major phenomena occurring in research reactor fuels, particularly where high power densities and narrow cooling channels are used, the accurate prediction of the swelling behaviour of a fuel is important. A plenum is an air space provided between the fuel and cladding where gaseous fission products can accumulate without causing swelling. While power reactor fuels are generally designed with a plenum, many research reactor fuels are not. Thus, in research reactors, dimensional changes in the fuel are often a direct function of the local fission density or burnup. For a fuel to be qualified, potential swelling needs to be demonstrated to be predictable, gradual and limited. Different metrologies can be applied to measure swelling during PIE of a test fuel. One of the most commonly applied methods uses two opposed probes, typically LVDTs or probes based on a magnetic ruler. Ceramic thickness reference samples can be used to calibrate the probes. For accurate measurements of fuel swelling, measurements need to be corrected to take into account oxide formation, which increases plate thickness unrelated to fuel swelling. An example of an implementation of such measurements in a hot cell is given below in the description of the Bench fOr Non-destructive Analyses of Plate And Rod Type fuel Elements (BONAPARTE) [21].

The BONAPARTE was designed for the non-destructive analysis of irradiated research reactor fuel plates, in curved or flat geometry, and fuel pins. The measurement bench consists of two components: a modular fuel plate clamping system enables plate rotation (for fuel rods and curved fuel plates), and a modular measurement head enables motorized movements in x and y directions (the latter is solely used in the case of flat fuel plates). The measurement head on the bench holds probes for measurements of plate thickness and oxide thickness. In addition, the measurement head can also house a video camera for visual inspection of the fuel plate. Oxide thickness measurements are based on the eddy current principle and can be performed simultaneously on both sides of the fuel plate. Calibration is performed using certified Mylar foils or, alternatively, a well characterized oxidized surface of cladding material. Plate thickness measurements are performed using two opposed, customized Sony Magnescale contact probes, whose measurement principle is based on a magnetic ruler. Ceramic thickness reference samples are used for probe calibration.

Detailed metrology allows a full 2-D mapping of local fuel plate and oxide thicknesses. The local fuel plate thickness increase (swelling), corrected for oxide formation, may be correlated with the local burnup or fission density derived from neutronic calculations or from quantitation gamma spectrometry. This correlation can be visualized in a contour plot, as shown in Fig. 20.

By averaging measurements taken at locations with similar burnups, a plot can be generated of the fuel plate thickness increase as a function of burnup. Figure 21 is derived from the 2-D plot in Fig. 20.

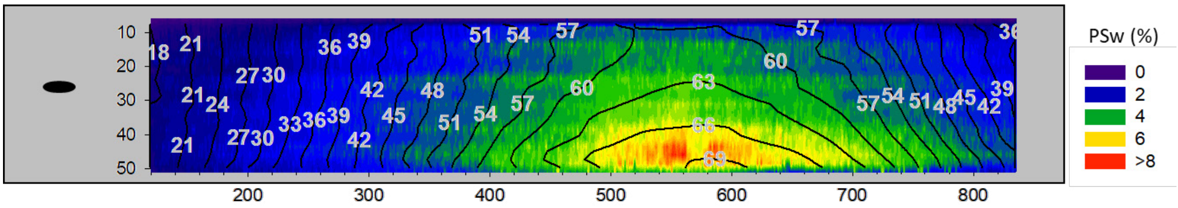

FIG. 20. Corrected plate swelling map with the calculated burnup distribution superimposed. (Reproduced from Ref. [2] with permission from SCK•CEN.)

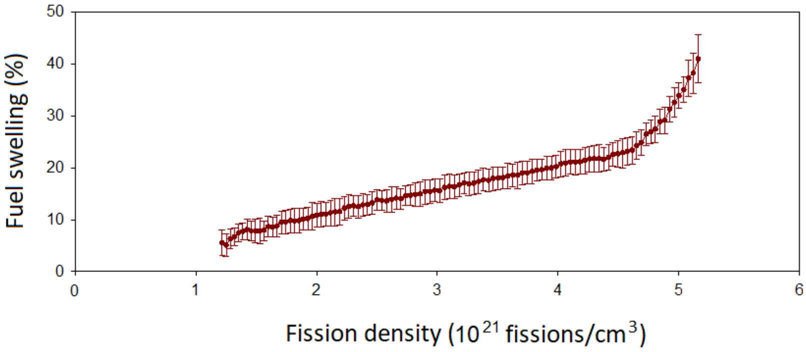

FIG. 21. Measured fuel swelling profile of the fuel plate shown in Fig. 20, averaged at locations with similar burnup and plotted as a function of the fission density, including the 1σ spread of the datapoints. (Adapted from Ref. [2] with permission from SCK•CEN.)

7.3. NEUTRON RADIOGRAPHY

Neutron radiography is a powerful non-destructive material examination technique applied extensively on irradiated fuel [22, 23]. Neutron radiography is used to obtain macro information on the sample or to decide where to perform further examinations and which methods to employ. Information obtained from neutron radiography is normally complemented with information obtained using other non-destructive methods (e.g. gamma scanning and eddy current techniques) to decide what additional examinations are necessary and where to perform further destructive examination of the fuel.

The principle of image formation in neutron radiography is based on the attenuation of a collimated thermal neutron beam transmitted through the sample (see Figs 22 [24] and 23 (left) [25]). The degree of attenuation is measured by detecting the intensity of the neutron beam transmitted through the sample. The method relies on the buildup of radioactivity in the activation foil produced by neutron absorption.

The high attenuation of neutrons in hydrogen-containing materials, with a high penetration for heavy metals, makes neutron radiography a complementary technique to X ray imaging with a spatial resolution of 40–50 μm. Unlike X rays and γ rays, neutron radiography relies on the interaction of a neutron beam with the nucleus of the material through which it passes.

The pattern of radioactivity is transferred to the X ray film by placing the activated metal foil in close contact with it. The X ray film is then blackened by the β and γ radiation, and thereafter developed using a standard photographic technique, as shown in Fig. 23 (right) [25].

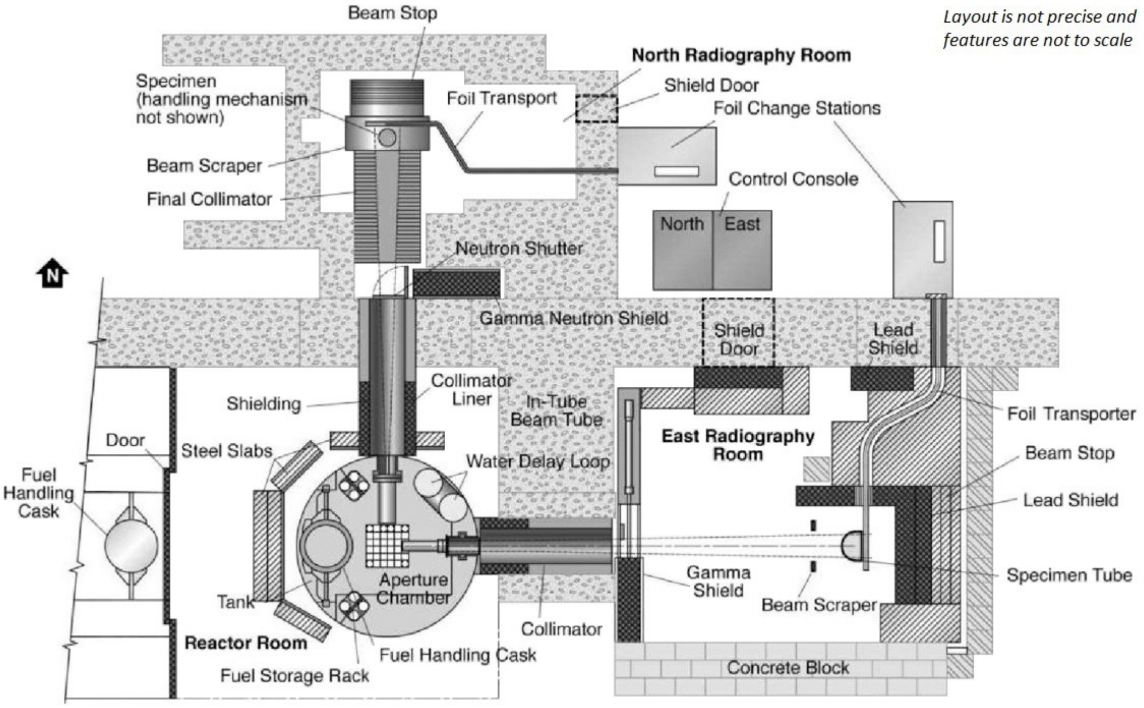

FIG. 22. Floor plan layout of the NRAD neutron radiography system with two neutron beamlines at INL. (Adapted from Ref. [24] with permission.)

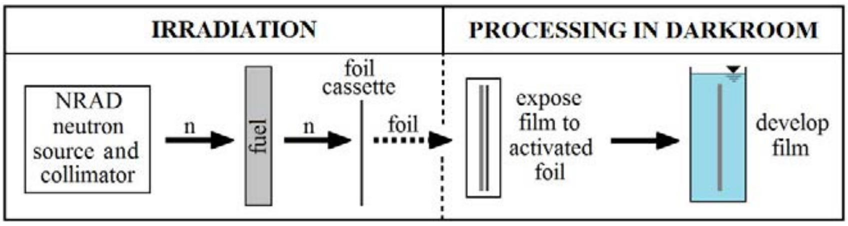

FIG. 23. Schematic diagram of the indirect neutron radiography process. (Adapted from Ref. [25] with permission from INL.)

7.3.1. Neutron radiography of fuel plates

For irradiated research reactor fuel plates, neutron radiography can be employed to evaluate the integrity of the fuel and the fuel density, and to determine whether cracking or fuel relocation has occurred. Figure 24 shows where fuel relocation was observed in an irradiated U–Mo monolithic fuel plate.

Radiographs can also show the visible expansion of the cladding, or ‘pillowing’ [24]; this is identifiable by visual examination of a sample fuel plate and is confirmed by neutron radiography. A thermal neutron radiograph reveals fuel relocations in the pillowed region and in other regions of the fuel plate. Radiographs of fuel plates can also be used to extract thickness profile data and other desired information that can be correlated to fission density.

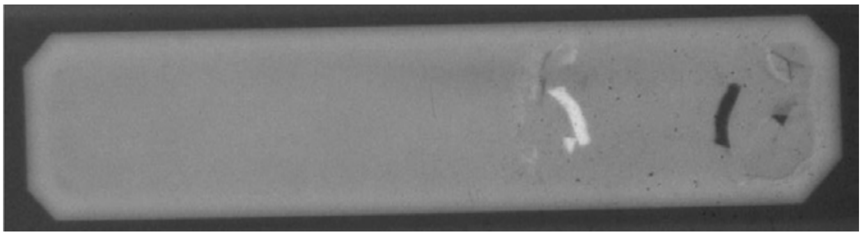

FIG. 24. Image of an irradiated U–Mo monolithic fuel plate (2.5 cm × 10 cm) showing where a piece of the fuel foil has been displaced. The image provides no information about the state of the bonding between the fuel and cladding. (Courtesy of INL.)

7.3.2. 3-D tomography

Computed tomographic reconstructions of a fuel element can be analysed to assess its post-irradiation geometric condition; specific information can include geometric defects such as bowing, twisting, plate buckling and cracks [25]. Neutron tomography typically requires a set of images taken over 180° of a specimen in increments as small as 1°. These images can be produced using the activation transfer technique (see Fig. 23). Increasing the neutron beam flux typically decreases the time required to produce an image if a digital system is used, compared with a process needing additional processing after exposure. An excessively long exposure time can make tomographic reconstruction prohibitively expensive.

Advanced neutron detector systems and tomographic reconstruction techniques, such as neutron computed radiography and microchannel plate detectors, may reduce the time and cost of acquiring images for neutron computed tomography. These systems enable tomographic reconstruction techniques that require a relatively small set of radiographs. The detector systems need to have low sensitivity or total insensitivity to gamma radiation. Figure 25 shows a tomographic reconstruction for recently irradiated AFIP-7 curved fuel plates. No evidence of defects (e.g. cracks, buckling) can be observed.

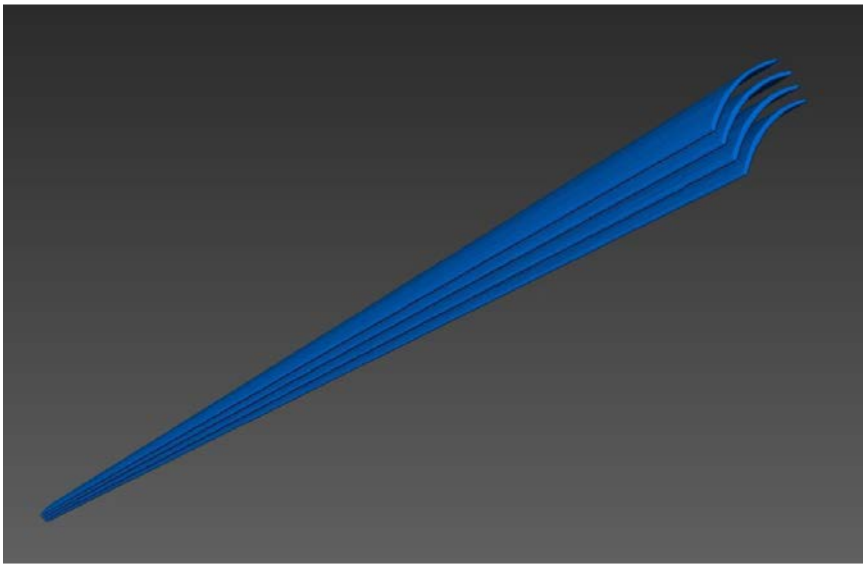

FIG. 25. Tomographic reconstruction images of AFIP-7 curved fuel plates irradiated in the ATR. (Courtesy of INL.)

7.4. GAMMA SCANNING

Many hot laboratories operate a gamma scanning set-up, which is often only equipped for fuel rods located in a hot cell. Such a set-up typically has a collimation system leading to a HPGe detector located outside the hot cell. The fuel rod is scanned over the collimator using a measurement and positioning bench inside the hot cell. A modified version of such a set-up is used for measurements on fuel plates.

To perform gamma spectrometry for fuel plates, a clamping device can be attached to the existing positioning bench. A typical example is given in Fig. 26. The fuel plate is loaded into a cassette to permit lateral displacement of the plate. The longitudinal displacement is assured by the positioning bench itself.

The gamma measurement installation can be used for both gross gamma measurements and quantitative gamma spectrometry measurements. For both gross gamma and gamma spectrometry measurements, the measuring bench is centred at the axis of the fuel element at a fixed distance above a cell collimator. The cell collimator consists of a set of lead shielded heavy tungsten alloy inserts with different slit sizes, which allow selection of the appropriate slit for each measurement, depending mainly on the fuel rod activity and requested axial spatial resolution. Located below the cell collimator, the gamma measurement device comprises an out of cell detector collimator, an intrinsic HPGe detector, a gamma spectrometry amplifier, an analogue–digital converter and a computer equipped with a multichannel analyser acquisition system. A technical design of the geometrical set-up is given in Fig. 27.

7.4.1. Gross gamma and gamma spectrometry measurements of fuel rods

Measurements of the gross gamma axial distribution of fission products show the gross gamma count rate distribution in the fuel pellet stack and pellet interfaces. This can provide details of the irradiation behaviour, such as fission product migration and dimensional changes of the fuel stack, resulting from fuel density evolution.

Quantitative gamma spectrometry, which is taken at discrete points along the fuel rod length, shows the discrete axial distribution of the most important gamma emitting radionuclides. Calibrated with appropriate standards, it allows an assessment of burnup distribution over the fuel rod.

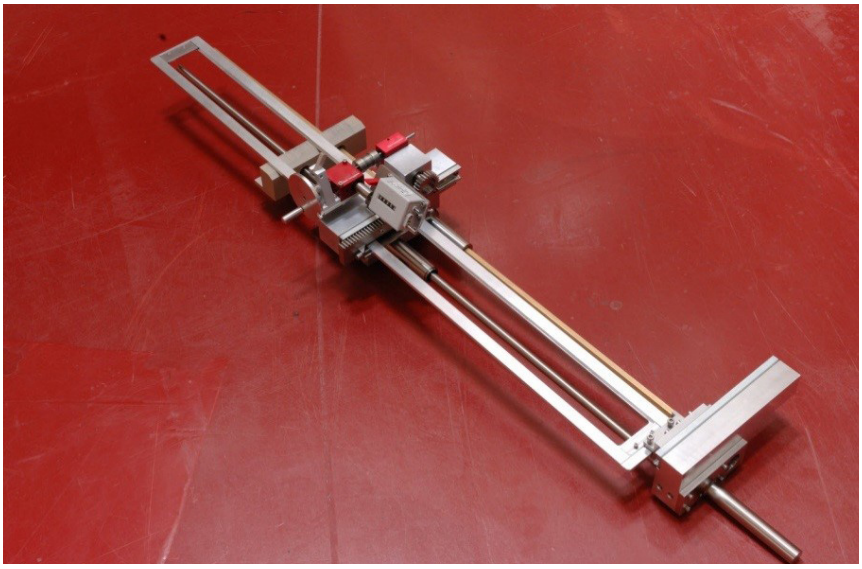

FIG. 26. Plate clamping device for gamma spectrometry. (Courtesy of SCK•CEN.)

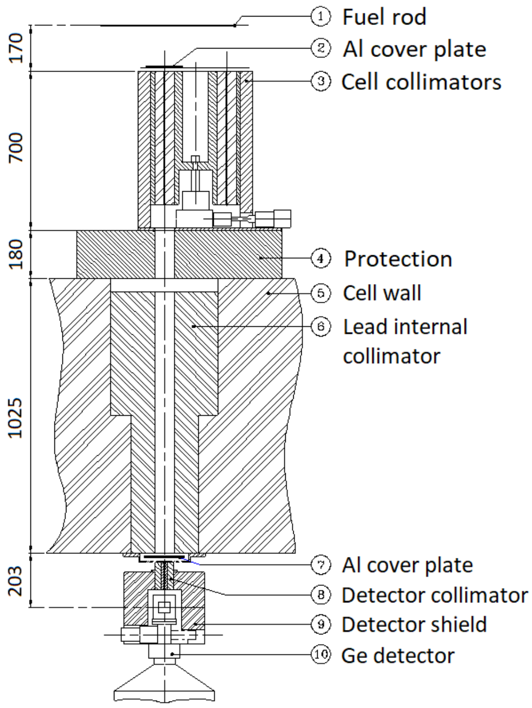

FIG. 27. Schematic representation of the gamma spectrometry collimation system. (Courtesy of SCK•CEN.)

The gamma spectrometry results, calculated from ^{137}Cs, for each fuel rod are reported as follows:

(a) Total number of fissions and average fissions per unit length and axial distribution along the fuel stack;
(b) Burnup expressed in average fissions per initial metal atom and its axial distribution along the fuel stack (pellet based fuels);
(c) Burnup expressed in average energy per mass unit of heavy metal (GWd/tHM) and its axial distribution along the fuel stack.

7.4.2. Gross gamma and gamma spectrometry measurements of fuel plates

The gross gamma count rate distribution over the fuel meat provides a general view of irradiation behaviour, such as burnup and power distribution, fission product migration and dimensional changes of the fuel plates.

Quantitative gamma spectrometry, taken at discrete points over the fuel meat, shows the 2-D distribution (mapping) of the most important gamma emitting radionuclides. Calibrated with an appropriate standard, it allows a quantitative assessment of the local burnup.

7.5. IMMERSION DENSITY ON MINIPLATES

Immersion density measurements on individual plates provide average plate swelling values for specific operating conditions and burnup. Immersion density measurements are corrected for cladding and oxide thickness to provide average fuel swelling over a plate in a quantitative manner. The wet and dry weights of each plate are recorded in addition to any calculated values.

Immersion density measurements were made at INL using selected irradiated fuel plates. These were performed using the in-cell Mettler Toledo PR-503 balance equipped with the associated commercially available density kit. This consisted of a glass container filled with deionized water, three drops of Synopharm solution for the reduction of gas bubbles, and a fixture to hold the test specimen. The scale was calibrated by INL calibration services using certified weight standards according to accepted procedures.

Each test plate is first weighed dry and then immersed into the fluid and weighed again while submerged. The results of each measurement are recorded, along with the temperature of the fluid. Using the dry weight, the submerged weight and the temperature corrected density of the fluid, the volume of the sample can be calculated using Eq. (1):

$$\text{volume}_{\text{sample}} = \frac{\text{weight}_{\text{dry}} - \text{weight}_{\text{submerged}}}{\rho_{\text{fluid}}} \tag{1}$$

Fuel swelling is calculated using the volume data from Eq. (1) and the pre-irradiation volume data. These values are used to determine the volumetric change in the fuel plate specimen.

8. DESTRUCTIVE POST-IRRADIATION EXAMINATION TECHNIQUES AND APPLICATIONS

At the end of the non-destructive examinations, it is important to introduce a hold point to determine if all the necessary data obtainable by non-destructive means have been captured and are reliable. Once the plate or rod is cut, further non-destructive evaluations are rarely possible.

As a next step, a sampling plan is drawn up based on the non-destructive examination results. The locations of the samples for destructive PIE techniques are marked in relation to the local irradiation conditions or observed phenomena and are clearly referenced with respect to a fixed point on the object. Reserve samples with similar characteristics need to be provided to accommodate potential problems during sample preparation. The sampling process generates significant waste and hot cell contamination, so each plate or rod needs to be sampled thoroughly in a single pass.

8.1. GUIDELINES FOR SAMPLING AND SAMPLE PREPARATION

Appropriate sampling and sample preparation techniques are vital to ensure that results from microanalysis are reliable. Artefacts (i.e. physical modifications accidentally introduced during sampling or sample preparation) are often not recognized as such and erroneously become interpreted as part of the fuel microstructure. The introduction of cracks, porosity, discolorations, surface modifications, or other artificial effects during sample preparation complicate both the qualitative and quantitative interpretation of results significantly.

8.1.1. Sample production

Microscopy and microanalysis require the cutting of samples from selected sites on the fuel elements. Given temperature and flux gradients during irradiation, one location is never fully representative of the whole fuel element. The intensity of gamma emitting isotopes, and particularly ^{137}Cs, is used to assess the burnup distribution and to select sample positions accordingly.

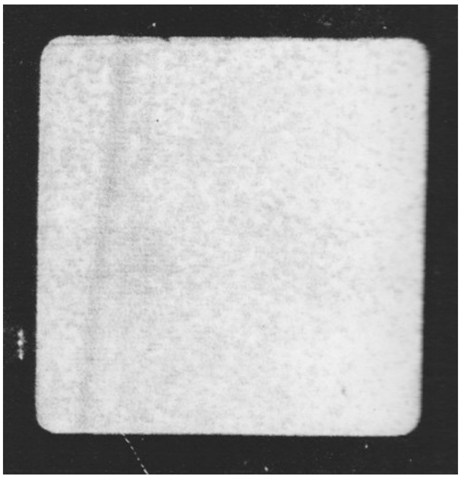

(a)

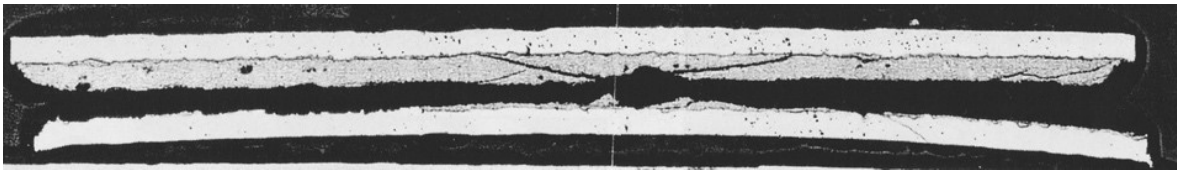

(b)

FIG. 28. (a) Example of a sample obtained using a square 16 mm × 16 mm punch system. (b) Meat brittleness at room temperature led to a rupture during sampling. (Courtesy of CEA.)

The typical maximum length of a sample is a few centimetres for optical microscopy and less than 2 cm for microanalyses involving, for example, electron probe microanalysers. It is important to do the following:

(a) Label the samples;
(b) Keep track of the original location of the sample within the fuel element;
(c) Keep track of the original orientation of the sample within the fuel element and relative to the rest of the subassembly.

Various systems have been used for cutting samples, taking the geometry of the fuel into account. For fuels with a rod or pin geometry and a hard ceramic fuel in a metallic cladding, the most common sampling tool is a circular diamond blade saw to cut sections. In this case, the sample top–down and azimuthal orientation may be tracked by making a mark with a saw.

For thin fuel plates, it might seem possible to punch out samples. However, with the successive layers of the meat and the cladding, this method sometimes leads to a rupture within the thickness of the sample. Figure 28 shows an example of such a sample obtained with a square 16 mm × 16 mm punch system.

Hole saws (or crown saws) are also used to cut circular samples. This can put stress on the rim of the samples, resulting in cracks in the fuel meat. However, the remainder of the sample can still be examined. This is illustrated in Fig. 29, which shows two views of a sample cut with a hole saw (diameter 15.4 mm): (a) surface on the marked side, and (b) rim of the disc optical macroscopy after polishing along a diameter, showing a sampling induced crack in the fuel meat limited to the periphery. The surface shown here is the marked side. The comparison of these ink marks with the full plate images after marking maintains the orientation until the sample is embedded for polishing (see Section 8.1.2 for sample preparation). The plate rolling traces at the surface of the sample also indicate the original orientation.

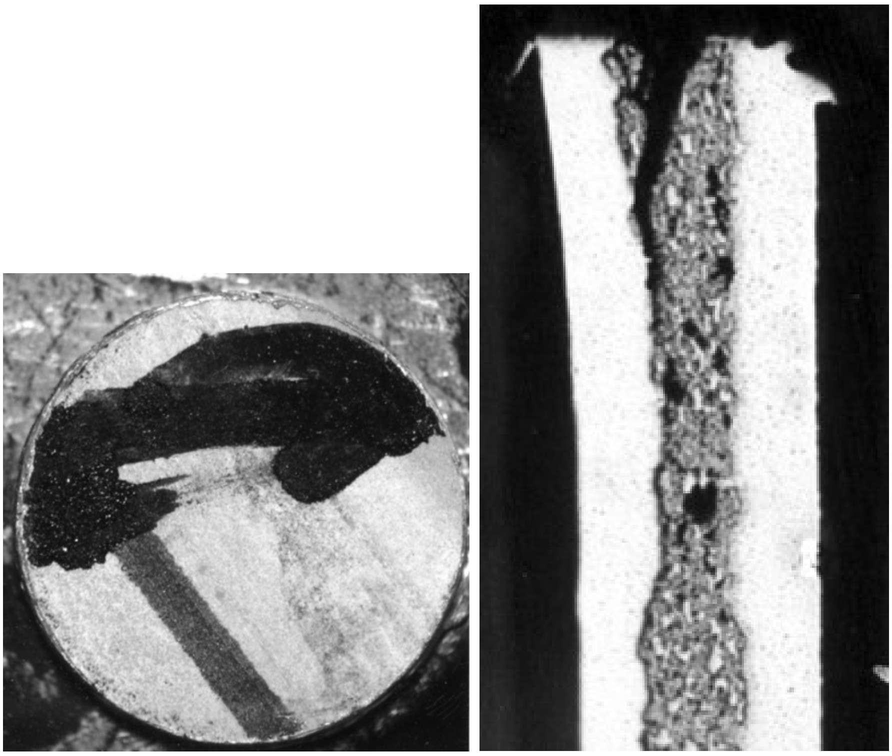

(a) (b)

FIG. 29. Circular sample cut with a hole saw. (a) Global view after sampling. (b) Edge of the sample; macrograph after embedding and polishing, showing fuel cracking resulting from the cutting method. (Courtesy of CEA.)

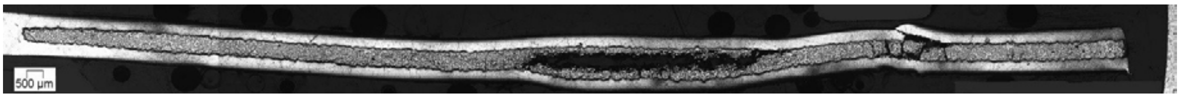

FIG. 30. Optical macrograph of a 4 cm long sample, bent during the cutting process to remove the other side of the whole plate width strip. (Courtesy of CEA.)

When using a typical diamond blade saw, a specially designed rig holds an entire fuel plate (either flat or curved) on both sides of the saw to allow translation perpendicular to the saw cutting plane. Strips can then be cut again in the other direction, forming small rectangular samples. This method leads to good results, generally without edge effects. Care needs to be taken when handling the strips in the hot cell to avoid damage that could affect the analysis. Figure 30 shows pillowing in the central part of the macrograph caused by irradiation, which had previously been detected by thickness measurements. However, the general bending and the fractures on the right side of the figure were caused by manipulation error with the saw during the cutting process. Qualitatively, it shows the brittleness of the irradiated U–Mo dispersion meat at room temperature. This sample was embedded and examined in spite of its obvious damage, because it contained a pillowing area that had been previously detected by thickness measurements on the whole plate. This pillowing area is visible in the central part of the macrograph.

8.1.2. Sample preparation

Light microscopy, electron probe microanalysis (EPMA), secondary ion mass spectrometry (SIMS) and part of the scanning electron microscope examinations require polished samples, as smooth as possible and with a mirror finish. These PIE techniques are discussed in further detail in Sections 8.2–8.4.

It is important to impregnate highly porous materials with resin before polishing. This helps to prevent grit, polishing media or etchant being trapped in the pores. It also preserves the open structure of the material.

The basic steps for this sample preparation are mounting the specimens into a holder that can be handled without damaging the specimen, grinding, polishing to enable clear views of the fuel material structures, and then possibly etching to reveal surface structures. The following sections describe these steps and compare different techniques.

8.1.2.1. Sample mounting

The specimens need to be mounted into a holder to enable them to be handled in the hot cell; this can also minimize damage to the specimen during hot cell investigations [26]. However, it is also important that the mounting material used does not affect the specimen as a result of chemical reaction or mechanical stresses. The mounting material needs to adhere well to the specimen. If the specimen is to be electropolished or examined using a scanning electron microscope, an electron probe microanalyser or a secondary ion mass spectrometer (i.e. procedures where a charged beam is involved), care needs to be taken not to allow charges to accumulate in the sample, as this would disturb the examination. Since most fuels exhibit an electrical conductivity that is high enough to prevent charge accumulation, it is usually sufficient for the mounting and the balance of the sample holder to be electrically conducting.

Specimens are usually mounted at around 200°C in a press, in either a thermosetting plastic (e.g. phenolic resin) or a thermosoftening plastic (e.g. acrylic resin). Cold mounting can be done using epoxy, acrylic or polyester resin, if hot mounting is likely to alter the structure of the specimen. Metallic alloys with a low melting point, such as tin–bismuth (Sn–Bi) alloys, are also used.

For the embedding in epoxy, a primary vacuum is used to enable the epoxy to penetrate cracks and open pores. For the embedding in a low melting point alloy, a primary vacuum is also used, in conjunction with heating of the alloy before its introduction into the sample embedding ring. A return to room pressure while the alloy is still liquid enhances its penetration in cracks and open pores.

The diameter of a mounted specimen is usually twice its thickness and the edges of the mounted specimen are slightly rounded to minimize the damage to grinding and polishing discs (see Fig. 31). Table 1 lists different sample mounting materials and specifies the advantages and disadvantages of each.

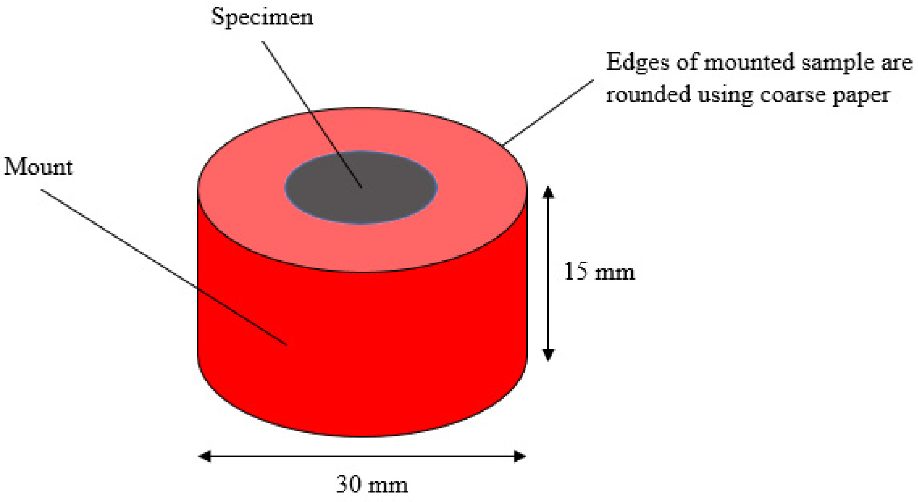

FIG. 31. Diagram of a mounted specimen (dimensions can differ).

TABLE 1. COMPARISON OF SAMPLE MOUNTING MATERIALS

Sample mounting material	Advantage	Disadvantage	Electrically conductive/ need for coating	Polishing/ smearing	Storage/ radiation effect	Impregnation	Removal
Epoxy	Simultaneous cold mounting and impregnation	Needs	− −	+	− −	++	−
Hot pressed resin	Immediately ready for polishing; Easy for remote handling	Temperature; Pressure	++	++	++	−	− −
Alloy Sn–Bi	Immediately ready for polishing	Temperature	++	+	++	+	+
Micarta	Immediately ready for polishing	No specimen contact (gap) leading to problems in polishing and conductivity; Machining required	− −	++	+	− −	++

Note:

− − The sample mounting material is very poorly suited for the activity.
− The sample mounting material works poorly for the activity.
\+ The sample mounting material works well for the activity.
++ The sample mounting material is very well suited for the activity.

For this mounting step, the main issue with plate type research reactor fuels is the need to hold the very thin sample in such a position that the cross-section of the fuel plate can be observed before the mounting. This can be achieved by using a clamping system for the sample (see Fig. 32).

For examinations of larger surfaces, the sample is mounted with the plate surfaces parallel to the polishing plane. Special attention needs to be paid to stop grinding and polishing when the observation plane is within the meat. An example of a polished sample is given in Fig. 33.

8.1.2.2. Grinding

Grinding can remove surface layers that may have been damaged by cutting [26]. The mounted specimens are ground with rotating abrasive paper discs, flushed with a suitable coolant to remove debris and heat. The paper coarseness is indicated by a number, for example the number of grains of silicon carbide per square inch. This means that 180 grit paper is coarser than 1200 grit paper.

Grinding is performed in several stages, using a finer paper for each successive stage. Each grinding stage removes the scratches made by the previous coarser paper. Between each stage, the specimen is washed with soapy water to prevent contamination from coarser grit present on its surface. Typically,

FIG. 32. Mounting of a piece of a flat research reactor plate using a stainless steel clamp. (Courtesy of SCK•CEN.)

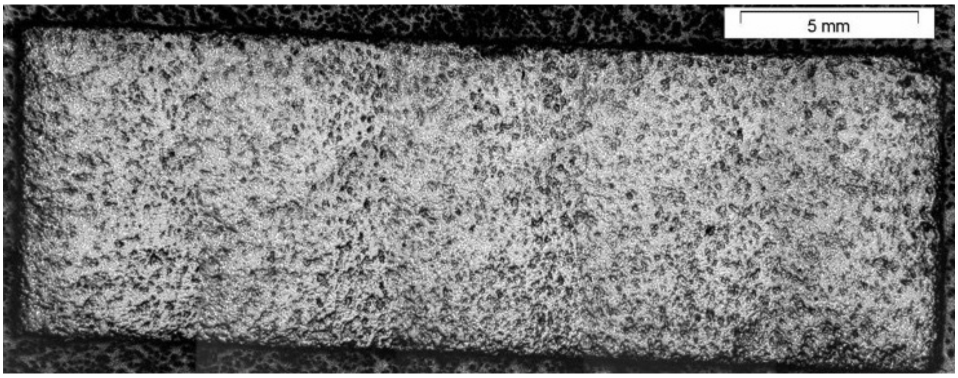

FIG. 33. Macrograph of a 25.7 mm × 8.2 mm U–Mo/Al dispersion fuel sample, flat polished to obtain a large surface of fuel meat for X ray diffraction. (Courtesy of CEA.)

1200 grit paper is the finest grade of grit paper used. When all grinding stages are completed, the specimen is washed, possibly in an ultrasonic bath, and then allowed to dry.

Figure 34 shows a grinding and polishing device used in a hot cell. The series of photographs in Fig. 35 shows the progression of a copper specimen when ground with progressively finer grit paper.

8.1.2.3. Polishing

Polishing is performed using discs covered with soft cloth impregnated with abrasive diamond particles and an oil based lubricant [26]. Two different particle grades are used: a coarser polish (e.g. with diamond particles 6 µm in diameter that remove the scratches produced from the finest grinding stage) and a finer polish (e.g. with diamond particles 1 µm or 0.25 µm in diameter to produce a smooth surface). The polishing can be finished with a 0.04 µm colloidal silica suspension. It is important to wash the specimen between polishing steps to prevent contamination of the disc and to remove possible loose particles that could lead to scratching of the sample surface in the next step. Figure 36 shows the surface of the copper specimen after two polishing steps. At the end of the 1 µm polishing step, there are ideally no scratches, but it is difficult to completely remove all scratches.

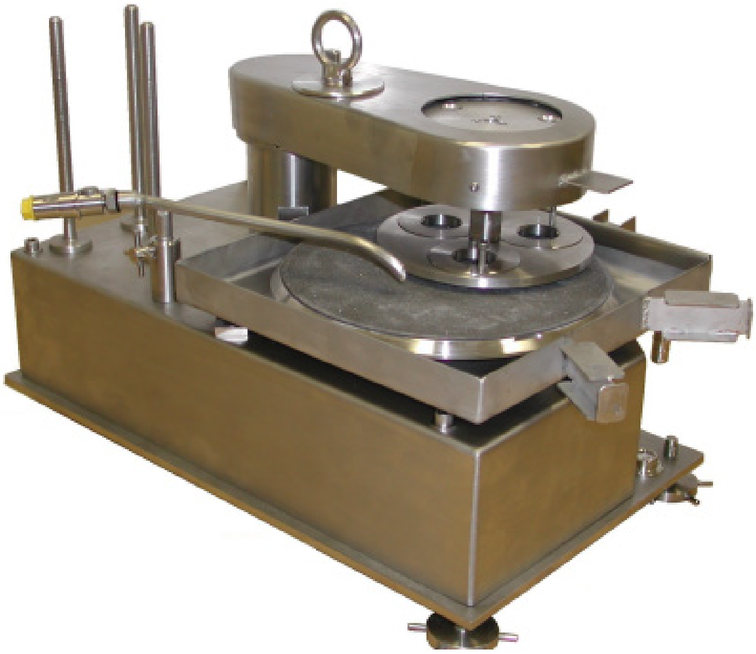

FIG. 34. Example of a polishing device used for grinding and polishing in a hot cell. (Courtesy of CEA.)

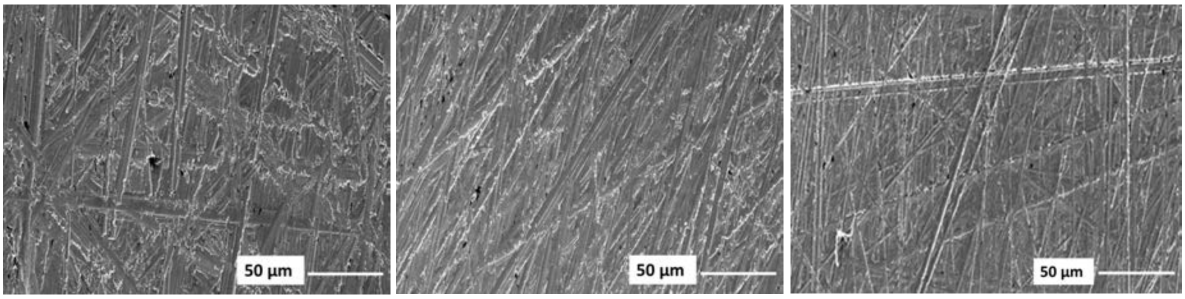

(a)
Stainless steel specimen ground
with 220 grit paper

(b)
Stainless steel specimen ground
with 500 grit paper

(c)
Stainless steel specimen ground
with 1200 grit paper

FIG. 35. Examples of the sample surface condition after the grinding steps. (Courtesy of SCK•CEN.)

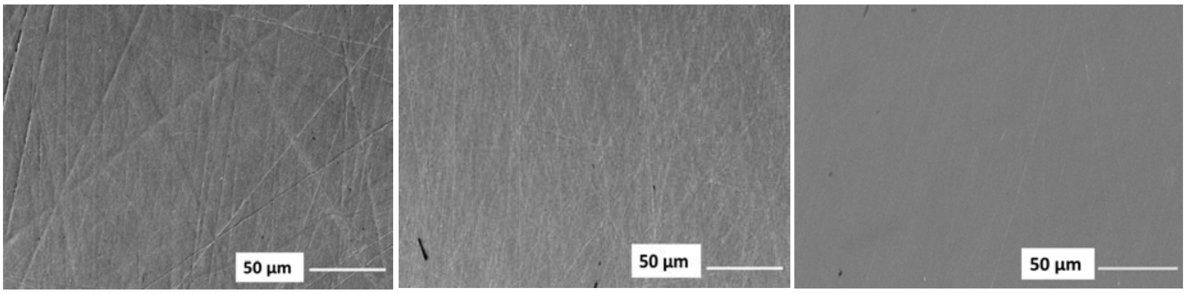

(a)
Stainless steel specimen polished
to 6 µm level

(b)
Stainless steel specimen polished
to 3 µm level

(c)
Stainless steel specimen polished
to 1 µm level

FIG. 36. Examples of the sample surface condition after the grinding steps. (Courtesy of SCK•CEN.)

Mechanical polishing usually leaves a layer of disturbed material on the surface of the specimen. Debris can become embedded in the surface and plastic deformation may exist below the surface of the specimen. However, electropolishing or chemical polishing can be used to remove this.

In cases of non-conductive specimens or if a non-conductive material has been used for mounting, coating the surface of the sample after polishing with a thin conductive layer of carbon, preferred for quantitative EPMA, or with a metal such as gold, is generally sufficient for preventing charge accumulation.

8.1.2.4. Etching

Depending on the features that need to be revealed, the specimen is etched using a specific reagent. Reference etchants can be found in Refs [27, 28]. Exposing the polished surface to an etching reagent can reveal the microstructure (e.g. grain boundaries, hydrides, precipitates) of a sample so that it can be examined with optical microscopy.

In multiphase alloys, etching creates contrast between different regions (see Fig. 37). Crystallographic orientation, the phases present and the local material response to the etchant affect the etching rate. Thus, contrast may arise from either differences in topography or changes in reflectivity, revealing different specimen features. Typically, etchants preferentially affect high energy sites, such as boundaries and defects, in all specimens.

Etching may create small pits on the surface, caused by localized chemical attack. The pits typically do not represent specimen microstructure features. They may occur in regions of high local disorder, for example, where there is a high dislocation concentration.

If the etching time is too long, the surface pits can grow, obscuring the main features to be observed. If this occurs, grinding off the poorly etched surface layer and then repolishing and etching is recommended. However, it is important to note which features are being investigated. Repeatedly grinding a very thin specimen may leave nothing to see.

A way of revealing phase distributions is by using etching techniques to attack one of the phases and increase the contrast with the other phases. One of the challenges in this process is to identify the most appropriate etchant and etching parameters, which often depend on the burnup of the sample. The use of etchants is mostly a trial and error process, often requiring multiple repolishing steps, and is generally performed after all other analyses have been completed to retain the same surface for other microscopy techniques.

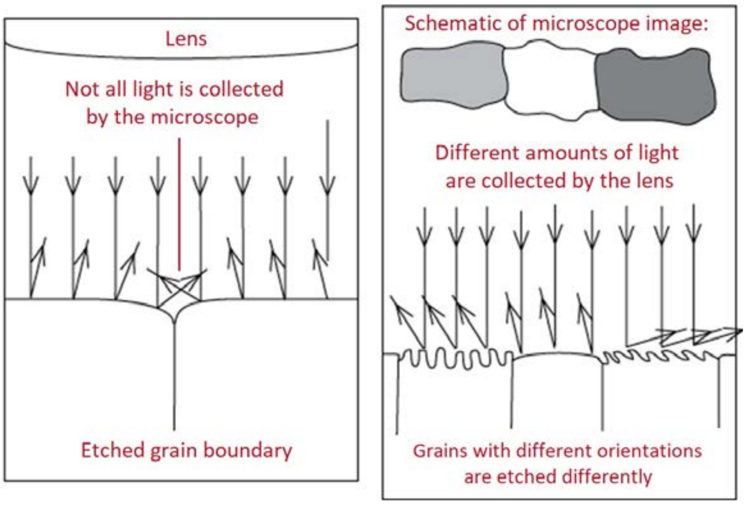

FIG. 37. Schematic view of the effect of etching on image formation in light microscopy. (Courtesy of SCK•CEN.)

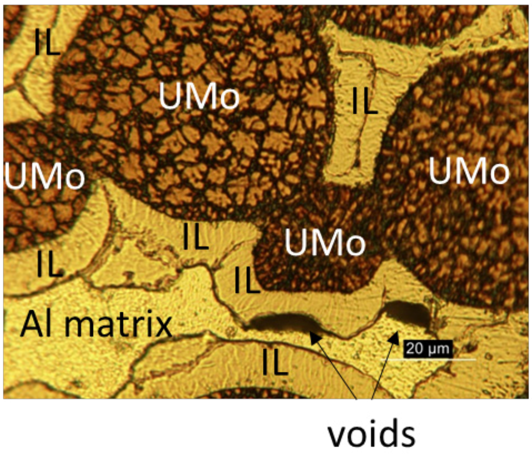

FIG. 38. Optical image of a U–Mo fuel particle in an irradiated fuel plate after etching (IL — interaction layer). (Adapted from Ref. [29] with permission from SCK•CEN.)

As an example, Fig. 38 depicts the optical image of a fuel particle in an irradiated U–7 wt% Mo dispersion fuel plate after etching. The formation of an interaction layer, surrounding the fuel particle, has occurred during irradiation [29].

8.2. OPTICAL METALLOGRAPHY

Optical metallography entails the examination of materials using visible light (i.e. optical microscopy) to provide a magnified image of their micro- and macrostructure. The optical microscopes installed in hot cell facilities are typically reflection optical microscopes. These are used for studying solid polished samples. Light rays, perpendicular to the specimen surface, pass through the system of condensing lenses and the shutters, up to a half-penetrating mirror. The light rays pass through the objective to the specimen surface, and are reflected off the surface of the specimen back to the objective, where they are gathered and focused, forming the primary image. This image is then projected to the magnifying system of the eyepiece or camera [30].

The observed contrast results from either an inherent difference in intensity, the light absorption wavelength characteristics of the phases present, or from the topography of the specimen. Preferential staining or attack of the surface by etching with a chemical reagent may also induce contrast.

Various microscopy systems have been used in hot cell facilities; several early configurations are described in Ref. [30]. Applications include the use of commercial remote microscopes as well as standard microscopes modified by users. Microscopes can be installed inside cells or inside a glovebox in a cell, with the image acquisition systems outside the cell. Technological improvements include motorization, which is replacing mechanical remote control systems, and digital cameras, which have replaced Polaroid films. In some facilities, the entire microscope has been set in the cell, including the digital camera. Figure 39 shows three examples of optical microscopes designed for use on irradiated fuels.

In the post-irradiation examination process, optical microscopy is sometimes the only destructive examination performed to complement the non-destructive examinations and obtain a general overview of the microstructure. It provides magnified views of the sample surfaces, thereby detailing features such as different phases (e.g. fuel, matrix, interaction layers) and pore or precipitate distribution. The optical microscope is often equipped with a hardness tester that can be used to measure microhardness.

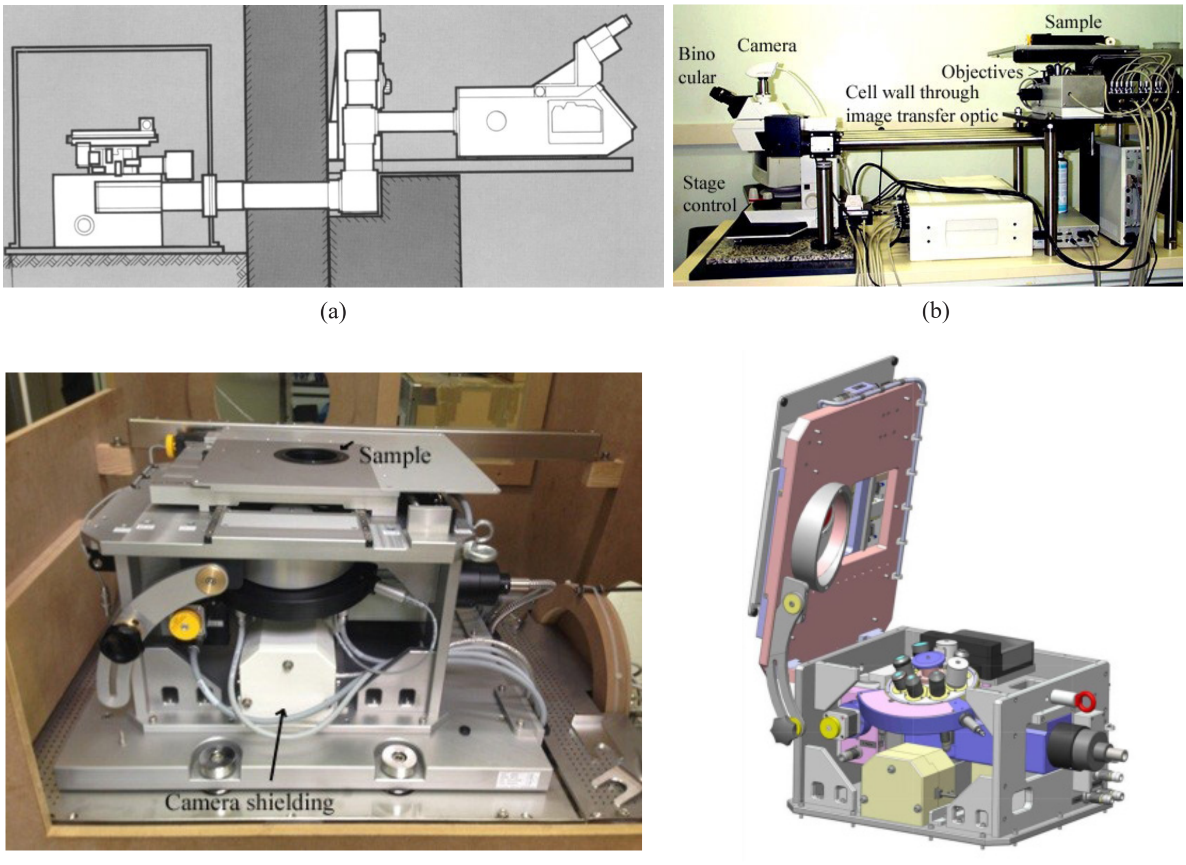

(a) (b)

(c)

FIG. 39. Examples of optical microscopes designed for use on irradiated fuels: (a) and (b) with through wall image and light transfer optic tubes; (c) with a built-in shielded camera. (Courtesy of CEA.)

The main advantages of optical metallography are the following:

(a) A relatively large field of view is possible at low magnification (15×), but with magnification spans of up to 1000×.
(b) It is relatively easy to use, and does not require a vacuum chamber.
(c) It shows stability with time in terms of size measurements. Periodic calibration using standard grids is necessary, however.
(d) The modern stage control systems offer high precision, allowing direct distance measurements at high optical magnification over the whole sample.

Limitations include the following:

(a) The observation of small features is limited by the maximum resolution.
(b) The limited depth of field (μm) prevents imaging inside pores. This can be used, by means of multi-image acquisition on the same area and the accuracy of the vertical axis stage control to reconstruct 3-D images of rough or sloped surfaces.
(c) Contrast depends on differences in reflectivity. If no difference exists, features cannot be resolved.
(d) It gives no spectroscopic data and therefore no chemical information.
(e) It requires a polished sample and therefore only yields 2-D information. This can be overcome by multi-polishing/imaging cycles and 3-D reconstruction, but this is a long process given the timescale for the manipulation processes.

For research reactor fuel PIE, transverse and longitudinal samples are sliced from archive fuel plates at different locations and prepared for optical microscopy. The analysis is performed to reveal the different phases and their distribution, plate swelling behaviour, fission gas bubbles and dimensional measurements, and to measure microhardness. The subsections below provide details on the information gained from the use of optical metallography.

8.2.1. Phase distribution

Phase distribution is studied based on morphological or reflectivity differences (matrix–interdiffusion layer–fuel and all extra phases). This implies pre-existing information on the expected phases, since no spectroscopy is involved in optical microscopy. This knowledge can come from EPMA measurements on sister samples or from previous microanalyses in similar programmes. Figure 40 shows an example of a ground U–Mo dispersion fuel with U–Mo particles, interaction layer and what remained of the aluminium matrix. The brightest surfaces are remnants of the aluminium matrix. The light grey surface surrounding the aluminium matrix is an interdiffusion layer. The medium grey surfaces with small dark spots are the U–Mo ground particles, and the small dark spots represent fission gas bubbles. This image also shows the presence of a darker phase around the particles. The optical microscope gives no information on the content of the interdiffusion layer or the dark phase. Image analysis yields information on the phase distribution. For example, in Fig. 40, the aluminium matrix only covers 5.8% of the surface. Figure 41 gives an example of main phase distribution deduced from optical micrographs of three irradiated samples and the non-irradiated reference. The changes in the interaction layer formation as a function of the examined field position can be seen in Fig. 41 (a). The increase in the interaction layer formation with increasing burnup can be seen in Fig. 41 (b).

8.2.2. Plate swelling behaviour

A good example of how optical microscopy can enhance understanding of phenomena detected during non-destructive examinations is plate pillowing (see Fig. 8). Figure 42 shows a low magnification overview and detailed images of an area surrounding a large pillow in an irradiated U–7 wt% Mo dispersion fuel [29]. Details show examples of the first cavities forming at the interfaces between the interaction layer and the aluminium matrix. These cavities have a lenticular shape, with a smaller curvature radius on the interaction layer side. Close to the pillow, these cavities interconnect. At the rim of the pillowing

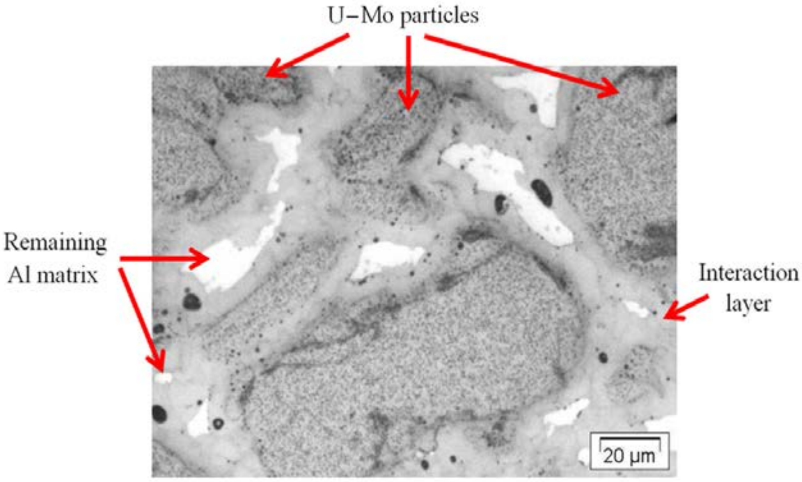

FIG. 40. Optical micrograph of U–Mo dispersion fuel, with ground U–Mo particles that display fission gas bubbles. The bright phase is the aluminium matrix and the intermediate contrast phase is the interaction layer. (Adapted from Ref. [31] with permission from CEA.)

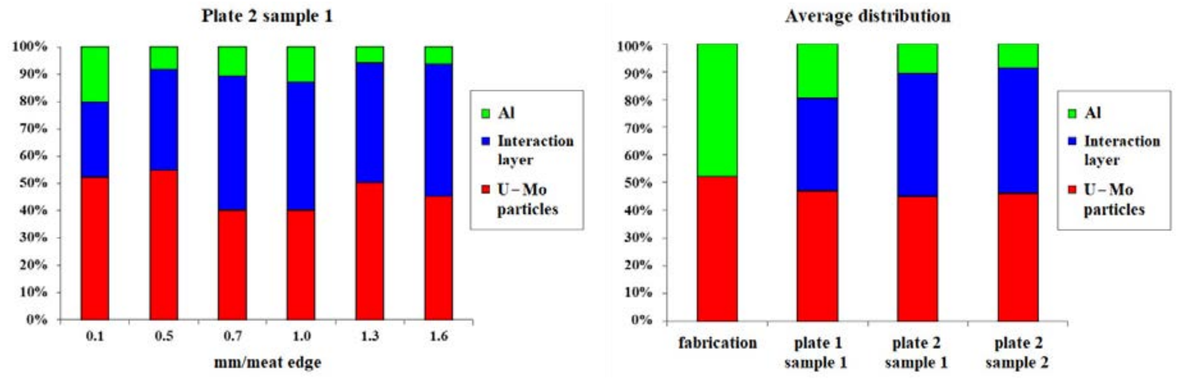

(a) (b)

FIG. 41. Optical microscopy image analysis of main phase distribution: (a) for one sample as a function of the distance to the meat edge; (b) for three samples from two plates and a non-irradiated reference sample. (Courtesy of CEA.)

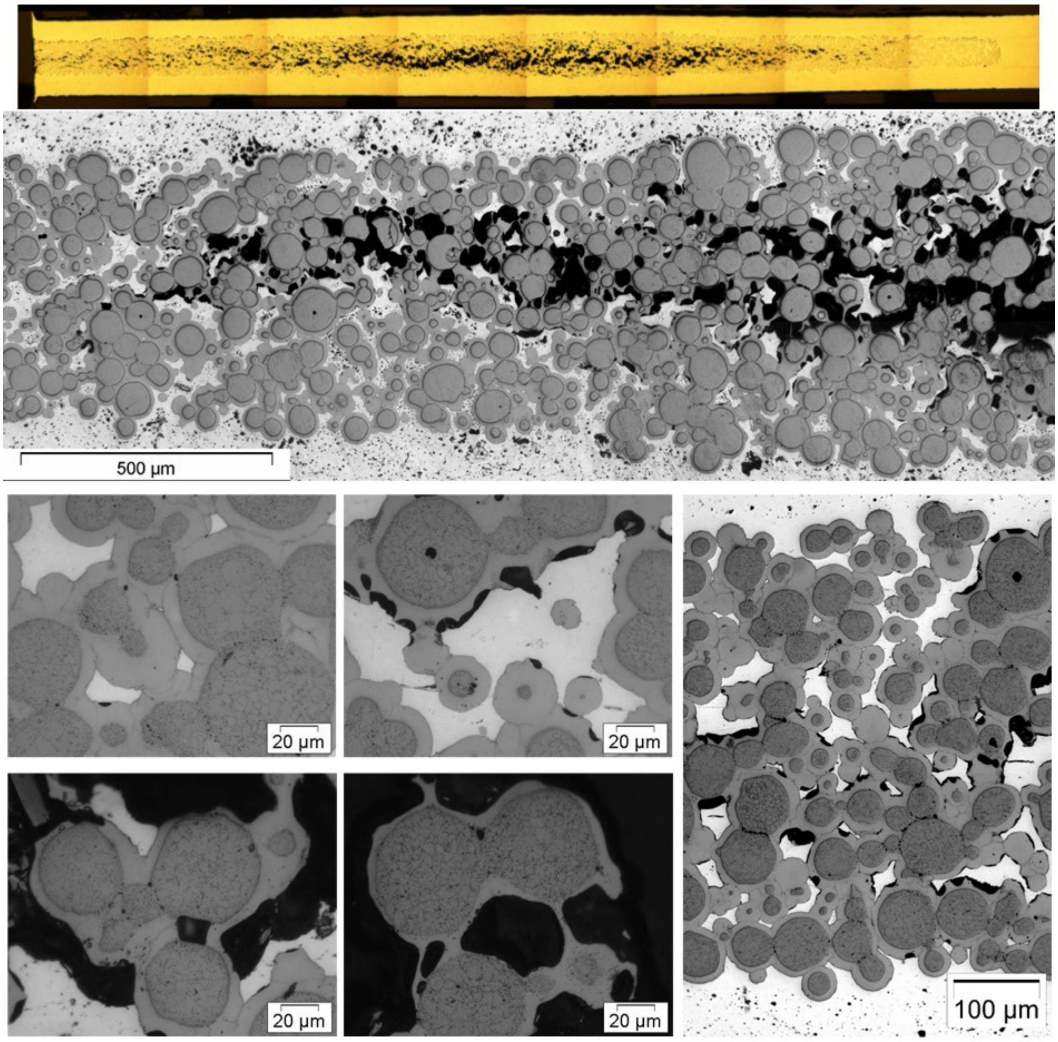

FIG. 42. Optical microscopy of polished samples of U–Mo dispersion fuels around pillowing areas at various magnifications. (Adapted from Ref. [29] with permission from SCK•CEN.)

and inside the pillowing area, the interaction layer exhibits plastic strain. Some of the observed irregular shaped porosities may be related to the extraction of material during polishing. This observation indicates decohesion of the matrix from the fuel. Furthermore, caution is needed when interpreting observed cracks. They could be the result of irradiation or an artefact from sample preparation (as shown in Fig. 30).

Figure 43 (a) shows, for the IRIS-2 plate [32], the presence of short but wide cracks that were probably not caused during preparation. Figure 43 (b) shows, for the same plate, cracks in what remains of the meat along the cladding in front of the main cavity of a pillowing area. These cracks were probably caused by plate manipulation before the cavity was filled with epoxy, but it is difficult to be certain. Figure 44 shows a string of large pores that formed in an irradiated U–10Mo monolithic fuel at the interface between the fuel and the zirconium diffusion barrier. Figure 45 gives another example of a U–Mo dispersion fuel, with the formation of interdiffusion layers and the presence of large pores or cavities at their interface with the unreacted aluminium matrix. Figure 46 is a collage of micrographs covering the whole thickness of a U_3Si_2 based fuel plate, with cladding and the meat [33]. Details within this area show the cladding oxide layer formed at the surface of the plate. Other details in the meat show the aluminium matrix, an interdiffusion layer and the presence of micrometric bubbles in the U_3Si_2.

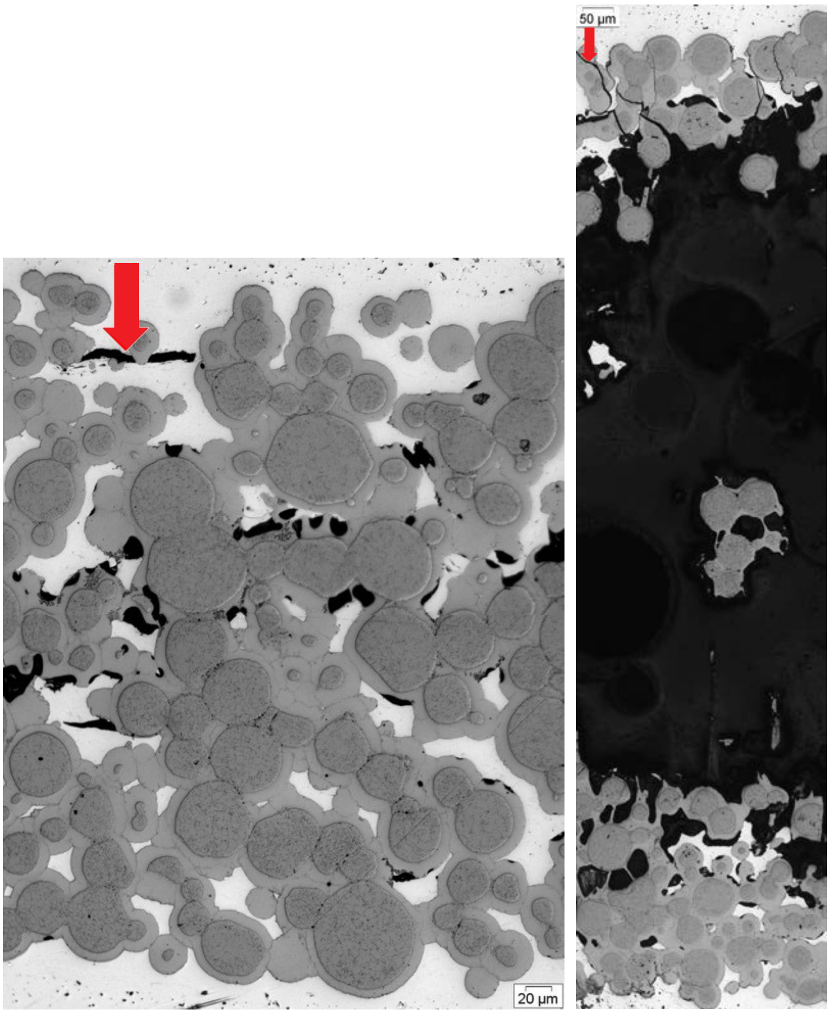

(a) (b)

FIG. 43. Optical microscopy of polished samples of U–Mo dispersion fuels around pillowing areas exhibiting two types of cracks: (a) short but wide cracks that were probably not caused during preparation; (b) cracks in what remains of the meat along the cladding in front of the main cavity of a pillowing area. (Courtesy of CEA.)

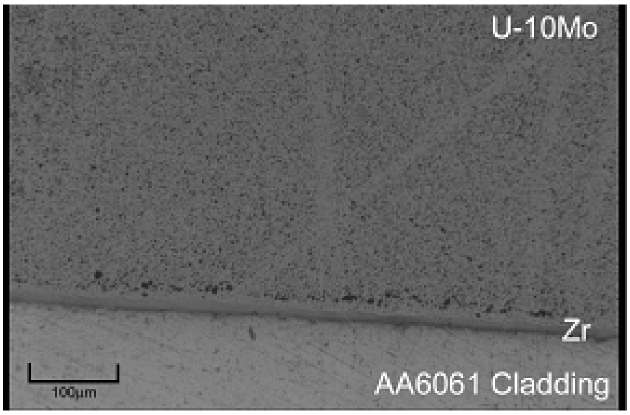

FIG. 44. Monolithic U–10Mo high burnup fuel at the fuel–zirconium diffusion barrier interface; optical microscopy image showing interconnected porosity in the fuel along this interface. (Courtesy of INL.)

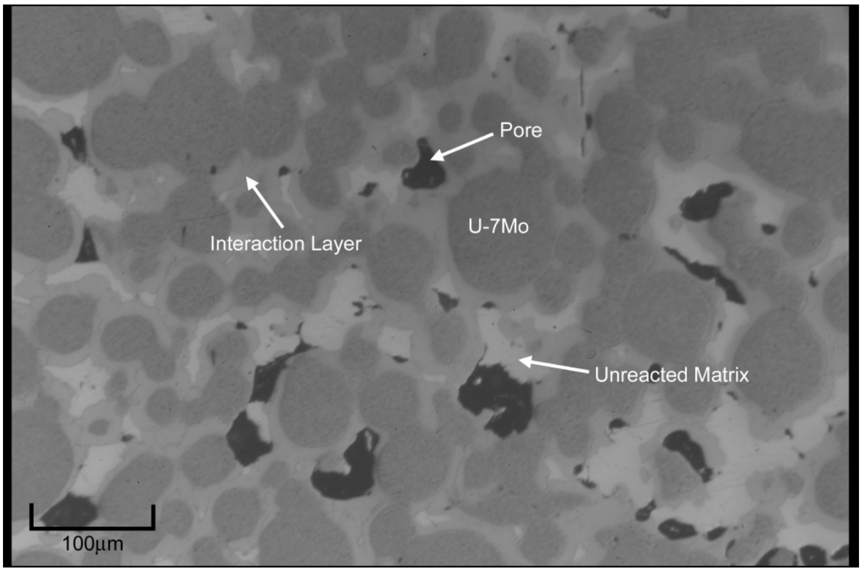

FIG. 45. AFIP-1 irradiated dispersion fuel optical micrograph showing interdiffusion layers and the presence of large pores. (Courtesy of INL.)

8.2.3. Fission gas bubbles

The size, morphology and spatial distribution of fission gas bubbles are of interest. Optical microscopy resolution limits this investigation to bubbles with a diameter greater than ~100 nm. Figure 47 shows an optical micrograph that reveals the microstructure of irradiated U–Mo dispersion fuel. In Fig. 47, the central region of the image is the U–Mo particle and the light grey region is the interdiffusion layer. Within the U–Mo particle, very small bubbles appear as dark regions in the image, but they are not distributed randomly; instead, they are located in the U–Mo cell boundaries. Image analysis can be used to obtain the pore and grain size distributions, and porosity, but better results can be obtained from scanning electron microscopy (see Section 8.3).

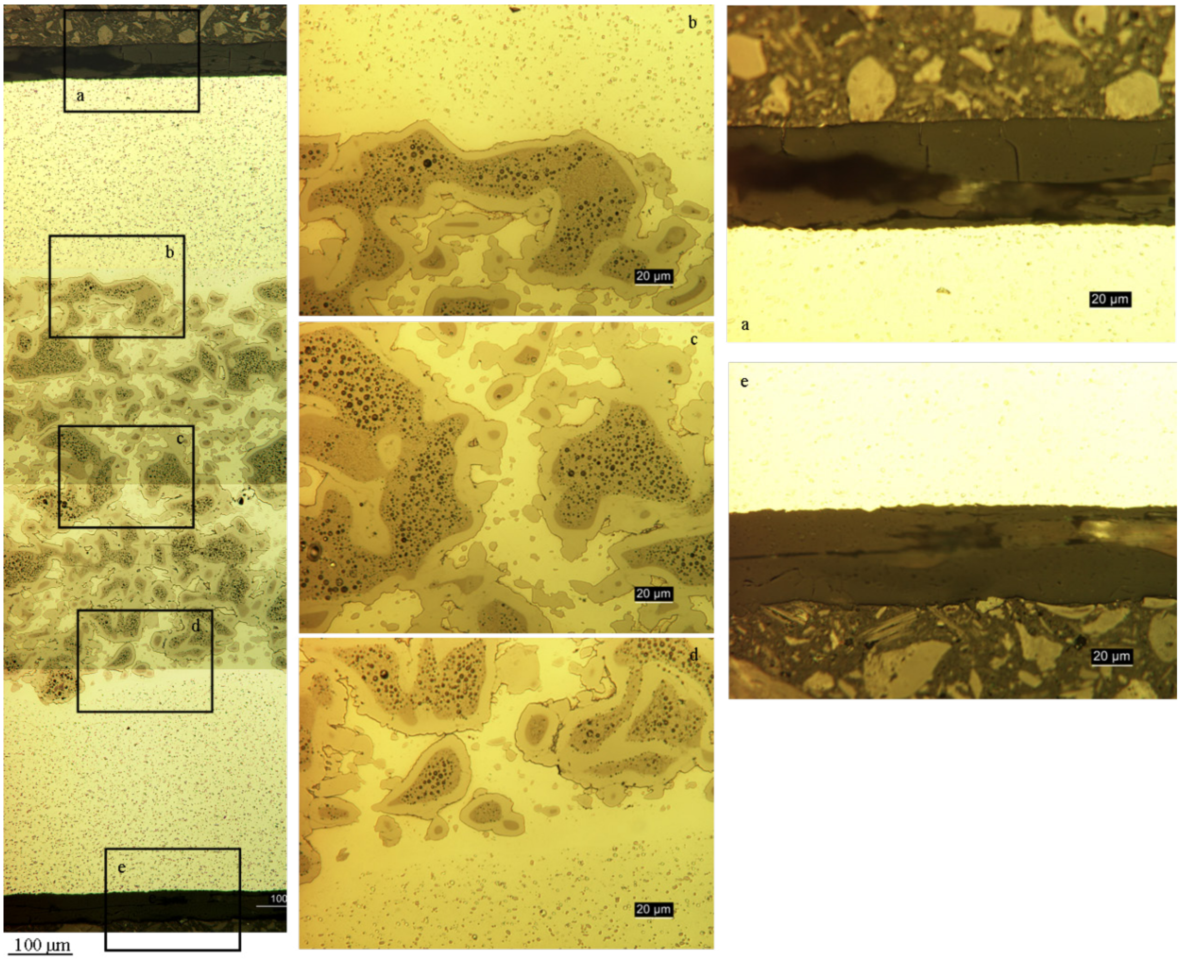

FIG. 46. Collage of micrographs showing the layers in the cladding, oxide layer and meat of a U_3Si_2 based fuel plate. (Adapted from Ref. [33] with permission from SCK•CEN.)

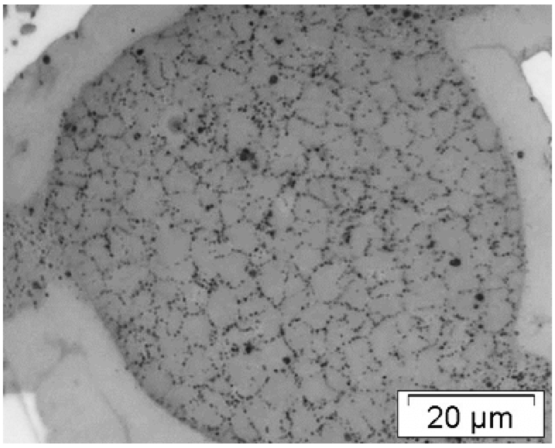

FIG. 47. Optical microscopy of typical microstructure details in U–Mo dispersion fuel. (Courtesy of CEA.)

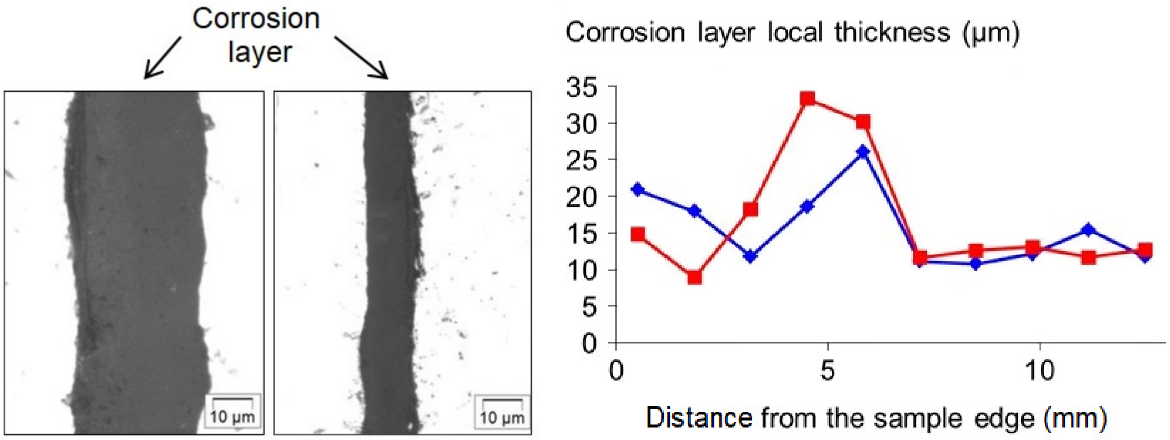

(a) (b)

FIG. 48. Local oxide layer thickness measurement. (a) Oxide layer optical microscopy examples. (b) Local measurement results along the sample surface on both sides of the plate (blue on one side and red on the other). These local measurements are average values obtained by image analysis of oxide layer thickness. (Courtesy of CEA.)

8.2.4. Local oxide layer thickness measurement

Optical metallography can be used to measure local oxide layer thickness. Measurements are typically made at multiple locations to obtain an average thickness. An example of local oxide layer thickness measurement is given in Fig. 48, which presents optical images of an oxide layer on two sides of a fuel plate, along with a plot of the results of the image analysis of the thickness of the oxide layer. The results of this type of measurement are similar to the non-destructive examination measurements at the same position. However, their resolution and accuracy are better than those of non-destructive examinations.

The quality of sample preparation can affect the results. For example, the sample position or polishing level during the embedding process can introduce uncertainties with this type of measurement. For example, for a plate, a slightly bent sample induces a slight overestimation of the thicknesses. In addition, the risk of spallation of the oxide layer during sample preparation needs to be minimized. The greatest risk of inducing spallation is during cutting, prior to epoxy embedding.

8.2.5. Local plate, cladding and fuel meat thickness measurements

Fuel swelling is best understood from measurements of local plate, cladding and fuel meat thicknesses obtained from the image analysis of generated optical micrographs. The results of these measurements have similar uncertainties to those found when measuring local oxide thickness. Higher magnification images are used to reduce the uncertainties. In the case of thicker sample measurements, such as the full plate thickness, the lowest level of uncertainty is usually reached using the highest magnification of the optical microscope and the high precision of the stage displacements, rather than using macrographs. An example of meat thickness measurement along a sample crossing a pillowing area is presented in Fig. 49.

8.2.6. Microhardness and toughness

Microhardness is measured to generate mechanical property information about various phases within the fuel system. These measurements can be made in hot cells using optical microscopes with a device such as the Vickers hardness testing machine. In a Vickers test, a diamond pyramid is pushed into the sample, perpendicular to its surface, with a known load. The local hardness of the material is

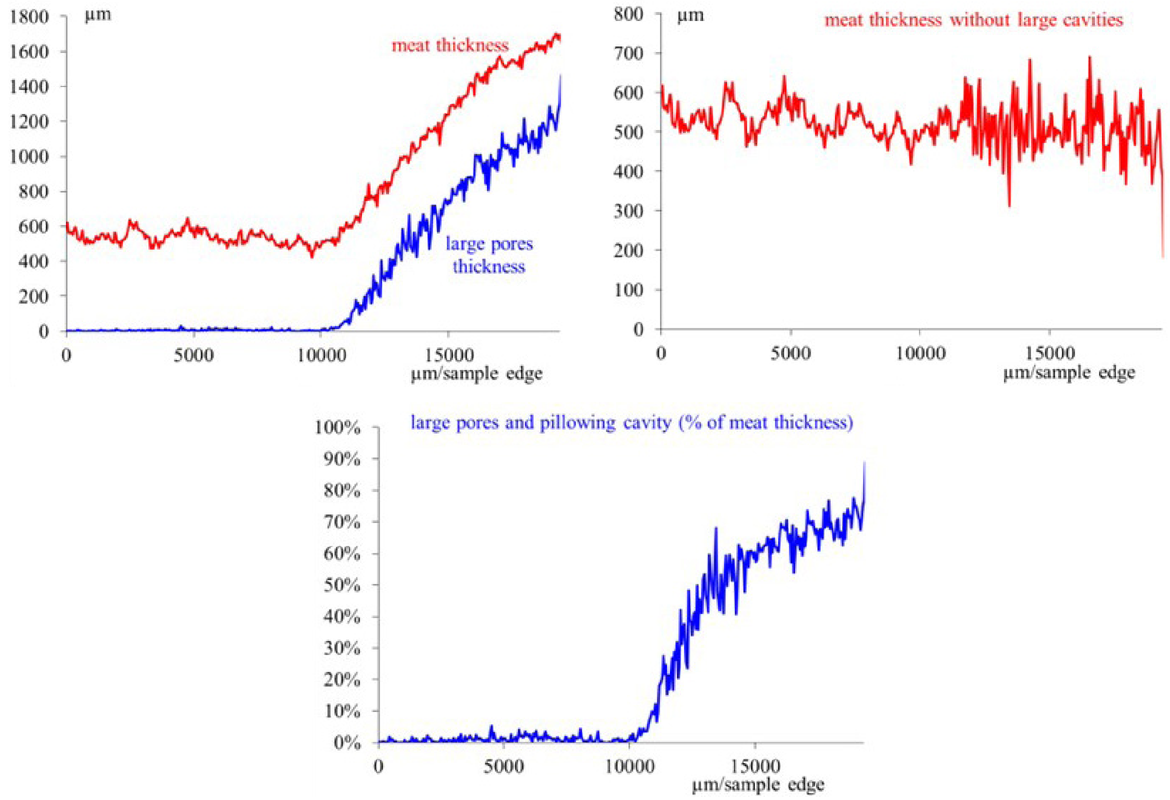

FIG. 49. Example of an optical microscopy image analysis. Meat thickness, interaction layer and aluminium matrix, and pillowing cavities for a U–Mo dispersion fuel sample. (Courtesy of CEA.)

determined by measuring the indentation left on the sample surface. The load needs to be adapted to the sample properties to obtain a measurable indentation. The sizes of the indentations are measured using an optical microscope.

In highly heterogeneous materials such as the microdispersed fuels, special care needs to be taken in the choice of the testing locations to involve only one phase. Figure 50 shows examples of indentations caused by Vickers tests in the cladding, in the aluminium matrix, in the interdiffusion layer and in a U–Mo particle of an irradiated U–Mo dispersion fuel. The loads, expressed in grams, have been adapted to the local hardness and to the geometry of each phase. For these four indentations, the corresponding hardness measurements, expressed in GPa, are shown in a graph, also presented in Fig. 50.

This technique can also be used for fracture toughness measurements. The toughness is deduced from the measurement of the cracks forming in the material at the corners of the indentations. No such measurement is possible with the examples in Fig. 50, as no cracking occurred.

8.3. SCANNING ELECTRON MICROSCOPY

Scanning electron microscopy (SEM) is used to conduct high magnification characterization of samples and to determine local compositions in the sample. With the SEM technique, an electron beam is focused on the surface of a sample generating secondary electrons, backscattered electrons (BSEs) and X rays.

The secondary electrons have low energy, providing high sensitivity for the sample topography and spatial resolution. The more energetic BSEs may escape from a greater depth within the sample, making them less resolved spatially (lower resolution) and less sensitive to the sample topography. However, the

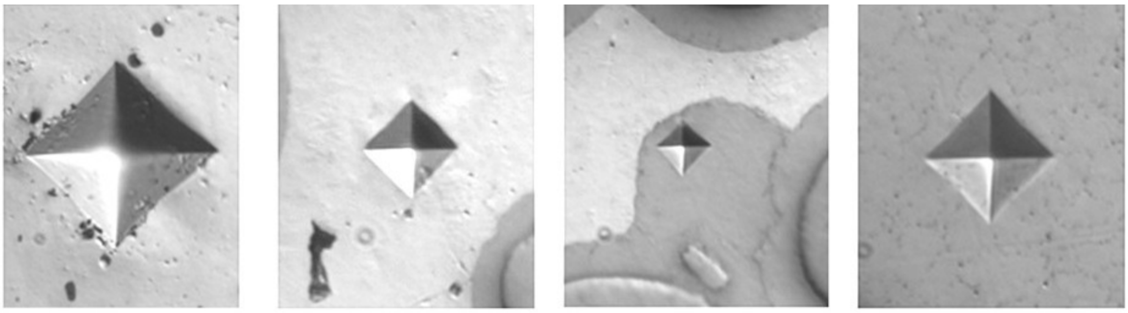

Cladding 50 g | Aluminium matrix 10 g | Interdiffusion layer 10 g | U–Mo particle 50 g

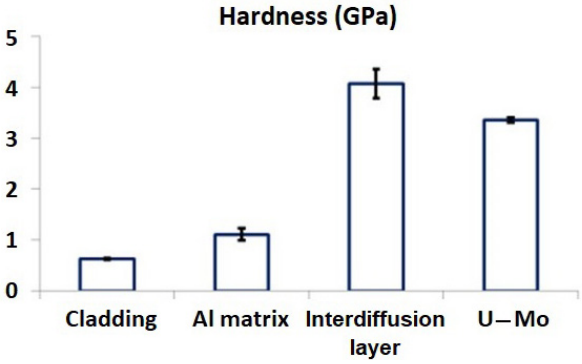

FIG. 50. Top: examples of Vickers indentations in the cladding, aluminium matrix, interdiffusion layer and U–Mo particle of a dispersion fuel. Bottom: graph of corresponding hardness measurements. (Courtesy of CEA.)

intensity of the BSE signal is defined by the mean atomic number of the material within the interaction volume, thereby providing information on the sample composition (density contrast).

Next to BSE and secondary electron signals, the primary electrons impinging on the sample have a probability of exciting characteristic X rays, which carry information on the elemental composition of the sample. Elements from atomic number 5 (boron) to 92 (uranium) can readily be detected in concentrations above 1000 ppm. The analysis of light elements, from atomic number 5 (boron) to 9 (fluorine), is more challenging owing to problems of a technical nature, instrument design and measurement procedure, or physical effects (e.g. low fluorescence yields, sample contamination). Detailed information on SEM and its applications can be found for example in Ref. [34].

A scanning electron microscope may also include shielding and micromanipulation devices for sample handling. Focused ion beam and micromanipulation also make SEM an efficient tool for defining samples for TEM (see Section 8.5).

Similar to optical microscopy, SEM analysis is also performed on transverse and longitudinal polished samples, as well as on fractured surfaces.

Different approaches have been used to adapt SEM for irradiated fuel examinations:

(a) The scanning electron microscope can be installed in a hot cell, possibly connected to a glovebox inside the cell (see Fig. 51) [35]. In these cases, relatively large samples may be examined.
(b) The adaptation to investigate radioactive material can be very limited, but in this case, smaller samples can be used to reduce the sample activity. This type of setting may include a glovebox.

SEM allows for microstructural analysis of the fuel plate at a higher magnification than optical microscopy, enabling the detection of smaller microstructural features, such as impurity phases, porosity,

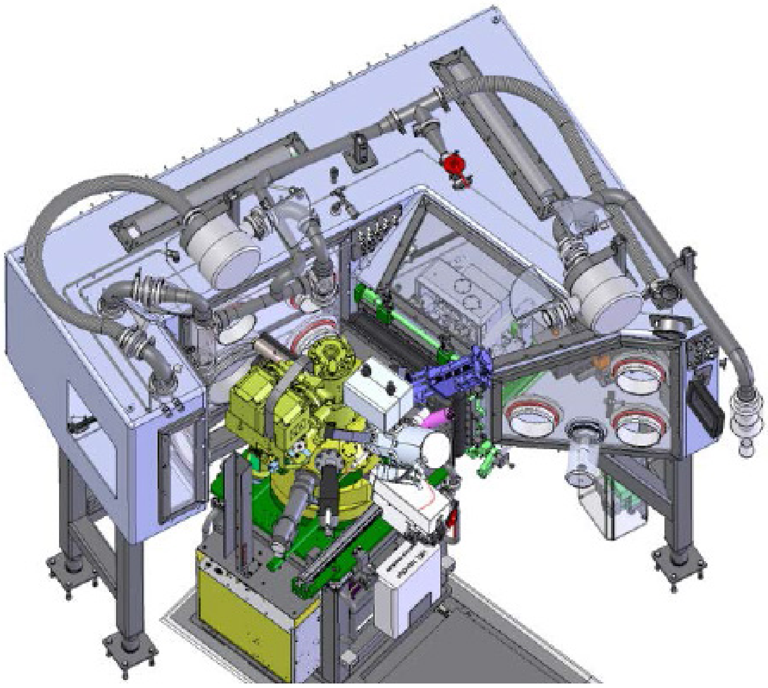

FIG. 51. Dual-beam scanning electron microscope setting (yellow), connected to a glovebox (blue), inside a hot cell. (Reproduced from Ref. [35] with permission from CEA.)

U–Mo alloy phases, cracks and debonds. These features need to be identified, since they can affect fuel performance. SEM images, and especially BSE images, are sensitive to differences in density, allowing the study of phase distribution.

Quantification of the characteristics of the imaged features can be performed through image analysis. Stitching images (manually or automatic) can be used to provide high resolution montages over large areas of the sample.

SEM analysis combined with energy dispersive spectroscopy (EDS) can reveal the chemical composition of the sample at specific locations in the microstructure. This capability is important for identifying chemical non-homogeneity in the material, for qualitative identification of phases and for identifying impurities. EDS can only be applied on non-radioactive or low radioactive specimens as the detector will become saturated (dead time 100%) when used in a high radiation field.

Depending on the material and how the sample has been prepared, surface coating can be necessary to prevent charge accumulation under the electron beam. Most fuels, however, have an electrical conductivity sufficient to avoid coating, provided that the embedding material is itself conductive.

BSE and secondary electron images are generated to examine the fuel microstructure, and spectrometers are employed to generate X ray distribution maps and line scans. Semiquantitative point to point compositional analyses determine the presence of various elements in the fuel, diffusion barrier, cladding and different interfaces. Phase composition analysis has to take the presence of a coating layer into account.

Electron microscopy is critical for examining samples beyond the capabilities of optical microscopy analysis, using high magnification imaging and determining compositions at various locations in a fuel plate. High magnification imaging in a scanning electron microscope can be an essential tool for the detection of cracking, porosity, impurity phases, U–Mo decomposition, etc.

The main advantages of the SEM technique are the following:

(a) Increased depth of field compared with optical microscopy, allowing the examination of fracture surfaces;
(b) Wide range of magnifications;
(c) Sensitivity to local density contrast (BSE);
(d) Speed and ease of use;
(e) Possibility to obtain relatively large samples of a few centimetres;
(f) Possibility to examine polished as well as fractured surfaces.

The SEM technique has one main limitation, in that EDS detectors are sensitive to radiation level (shielding can reduce the X ray signal). Wavelength dispersive spectroscopy (WDS) can be used as an alternative, but it can be relatively difficult to employ.

The subsections below provide details on the information obtained from the use of scanning electron microscopes.

8.3.1. Local oxide thickness layer measurement

Scanning electron microscope images of polished samples enable local oxide layer thickness measurements. The results of these measurements can be compared to those of NDT measurements. They are more accurate than NDT measurements, but they can only be performed at a few locations. Figure 52 shows a scanning electron microscope image that can be used for precise measurement of the thickness of the corrosion layer at the surface of the cladding.

8.3.2. Fission gas bubbles

Figure 53 shows BSE and secondary electron images of a fuel particle with fission gas bubbles similar to those shown in Fig. 40. The high magnifications reached with SEM (compared with optical microscopy) allow the application of image analysis techniques to establish 2-D size distribution histograms. These histograms show the different porosity distributions for different locations of the sample.

Figure 54 is a series of scanning electron microscope images showing the evolution of the fission gas bubbles with increasing burnup [36]. The images in Fig. 54 (sample 1) show that, at low burnup (2.1×10^{21} fissions/cm^3), fission bubbles start to appear on the cell boundaries. As the burnup increases, these bubbles become visibly larger, and at a burnup of ~3×10^{21} fissions/cm^3 (sample 2), some small subgrains also become visible on the boundaries. At larger fission densities, the recrystallization has proceeded inwards into the U–Mo grains and the fission gas bubbles have continued to increase in size. At a fission density of 4.5×10^{21} fissions/cm^3 (sample 6), the recrystallization has extended to the whole fuel volume. By comparing these images with those in Figs 40 and 47, it is apparent that the fission gas bubbles can be identified more effectively with higher magnification scanning electron microscope images.

Another approach for characterizing fission gas bubbles is to use samples with fractured surfaces. Figure 55 shows, for two similar locations of the same fuels, a fractured surface (a) and a polished surface (b), both obtained using the secondary electron detector. The images in Fig. 55 show the microstructure at increasing levels of burnup (1, 2 and 3). For the lowest burnup microstructure (1), the fission gas bubble formation in the grain boundary areas only produces a few bubbles in intragranular positions. For the intermediate burnup microstructure (2), small subgrains have formed along the main grain boundaries, which can only be detected on the fractured surface. For the highest burnup microstructure (3), recrystallization has progressed throughout the sample microstructure, resulting in widespread porosity.

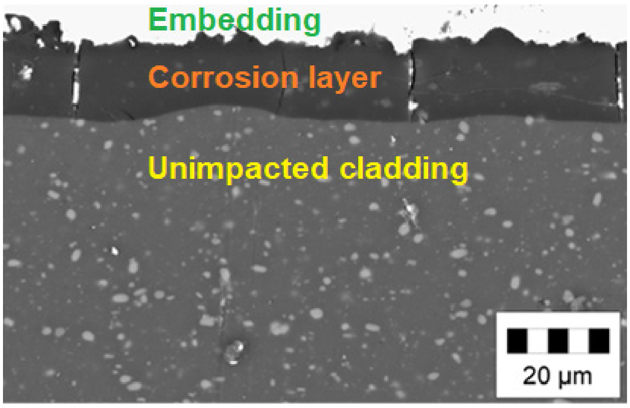

FIG. 52. Scanning electron microscope image of a corrosion layer. Brighter spots in the cladding are alloy precipitates. These precipitates are also visible in the corrosion layer, but their grey level is different from that of the precipitates in the unimpacted cladding, with their composition appearing to have been modified. (Courtesy of CEA.)

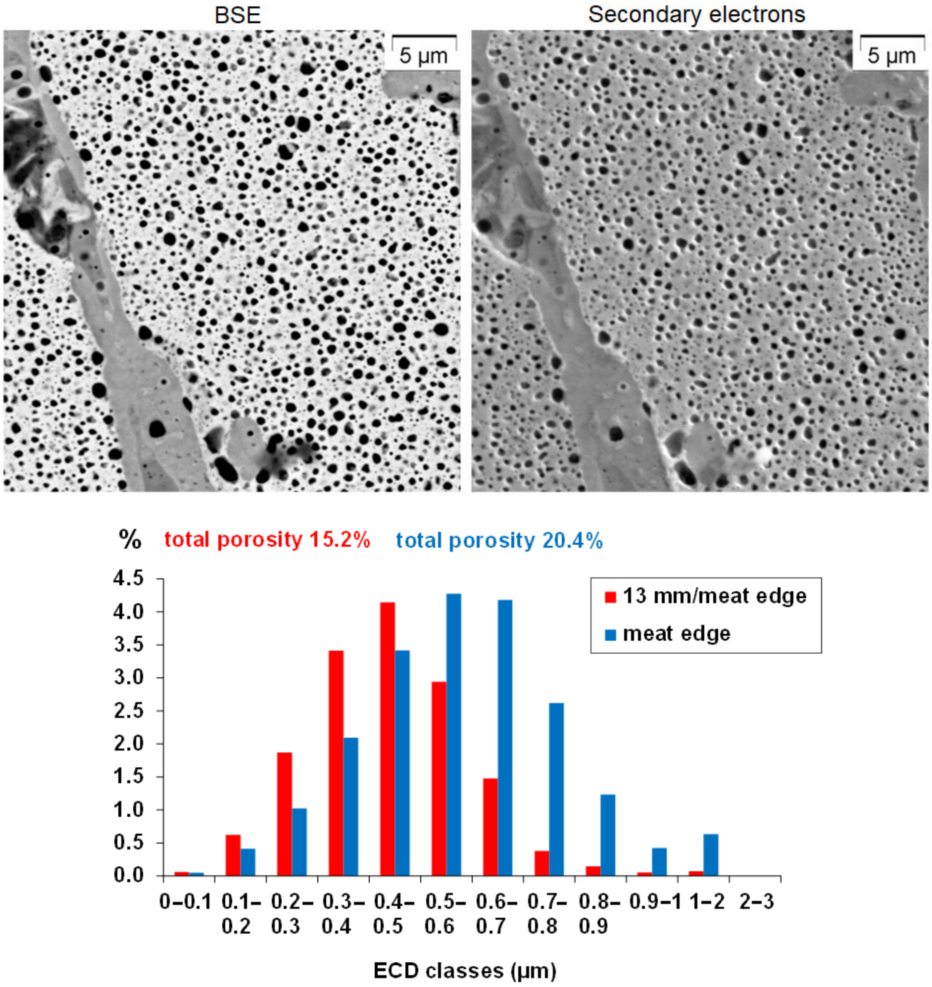

FIG. 53. Top: scanning electron microscope backscattered electron image (left) and secondary electron image (right) in a similar U–Mo particle to those of Fig. 40. Bottom: porosity size distribution at two different sample locations. (Top right: courtesy of J. Noirot (CEA). Top left and bottom adapted from Ref. [31] with permission from CEA.)

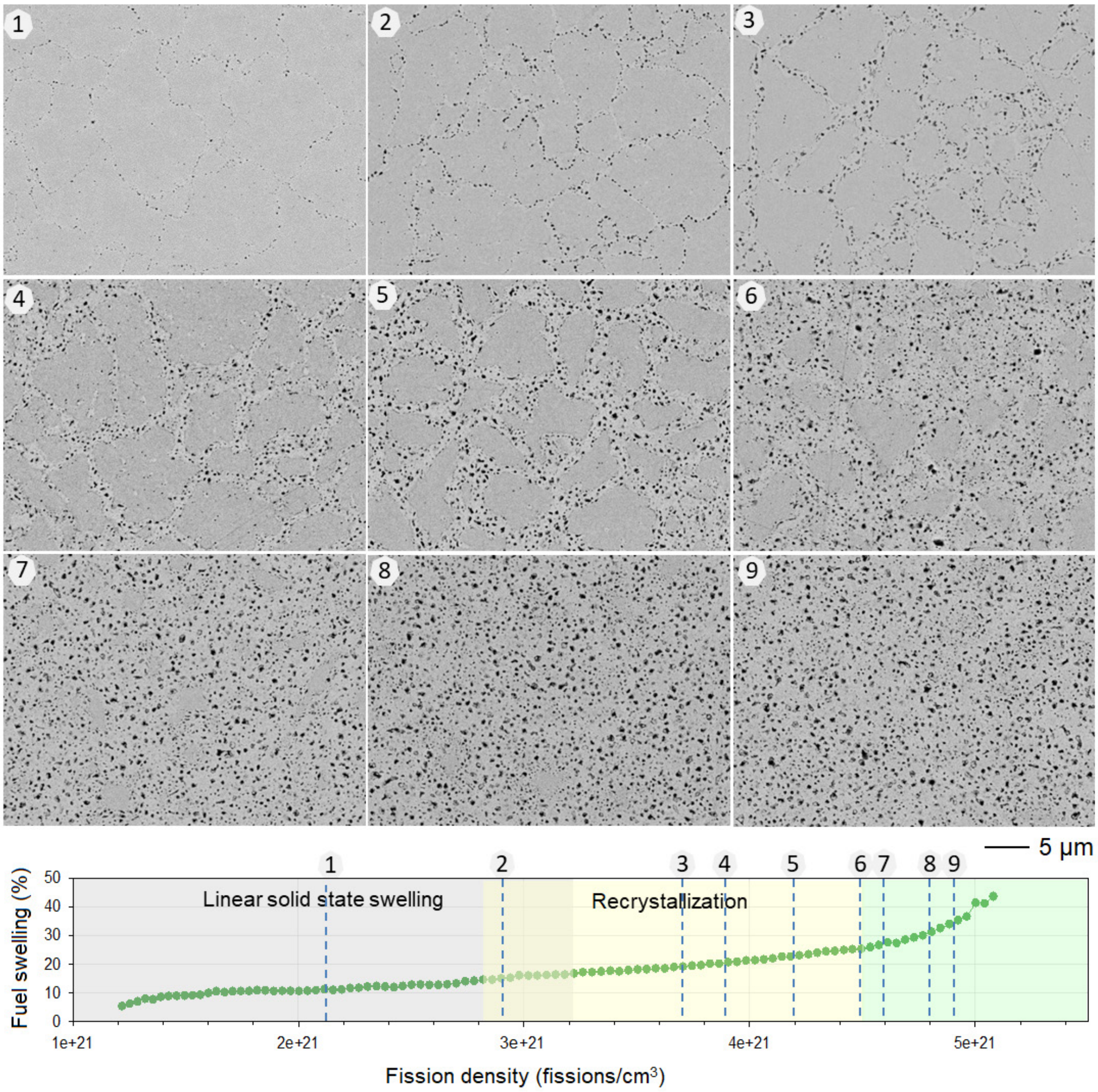

FIG. 54. Evolution of the microstructure observed in samples of a zirconium nitride coated U–Mo fuel plate having a fission density as indicated in the graph. (Adapted from Ref. [36] with permission from SCK•CEN.)

8.3.3. Phase distribution

Contrast variations in BSE images are caused by variations in density. These contrast variations can be used to investigate the distribution of phases in a microstructure. An example of the contrast variations in a dispersion fuel microstructure is presented in Fig. 56, where the U–Mo phase, the interaction layer and the aluminium matrix can be identified. Comparing this figure with Figs 40 and 42 shows that SEM is more effective than optical metallography for determining phase distributions, particularly owing to the ease of performing image analysis. However, optical microscopy may be preferred in the light of easier handling, speed of image acquisition and ability to handle larger sample sizes, while providing sufficient image quality.

By analysing scanning electron microscope images, such as those presented in Fig. 57 [2, 37], quantitative data can be obtained. Such images show the evolution of the features seen in optical microscopy

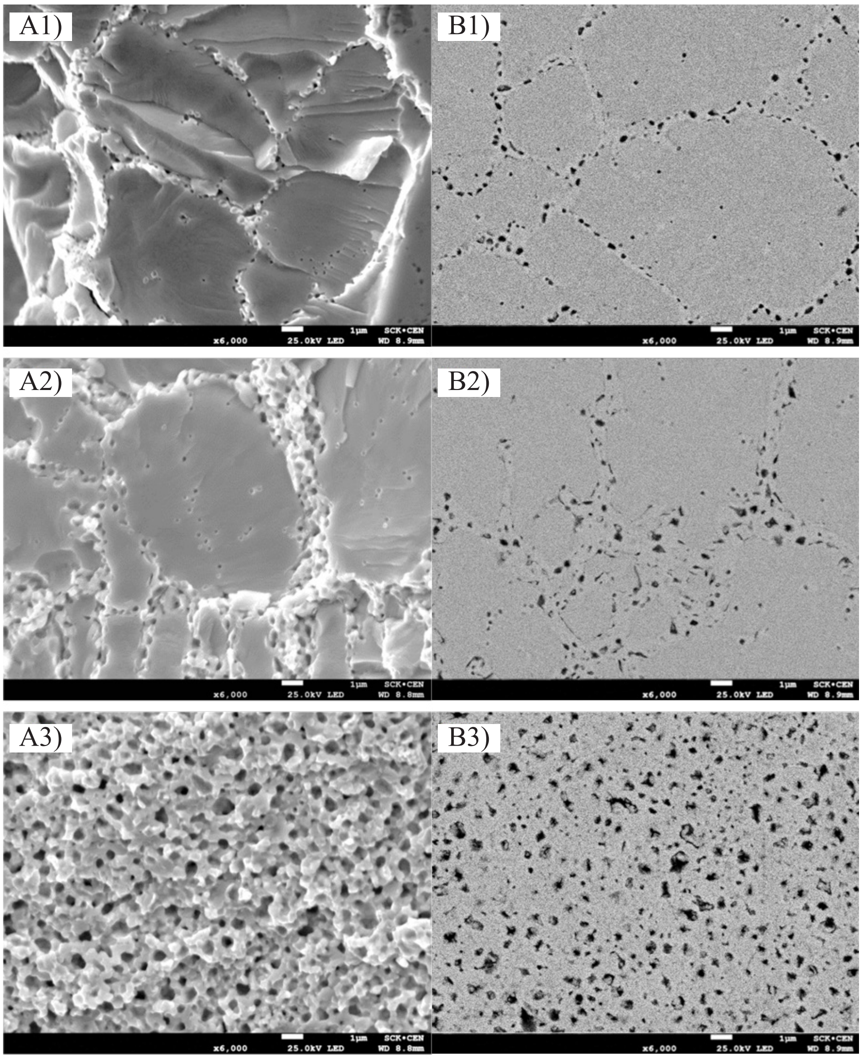

FIG. 55. Secondary electron images of the fractured (A) and polished (B) surface of a low burnup (1), intermediate burnup (2) and high burnup (3) sample showing the first steps in the recrystallization process. (Reproduced from Ref. [36] with permission from SCK•CEN.)

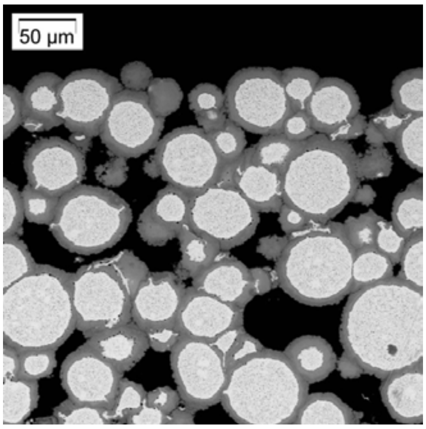

FIG. 56. BSE low magnification image from a scanning electron microscope of a U–Mo dispersion fuel. (Courtesy of CEA.)

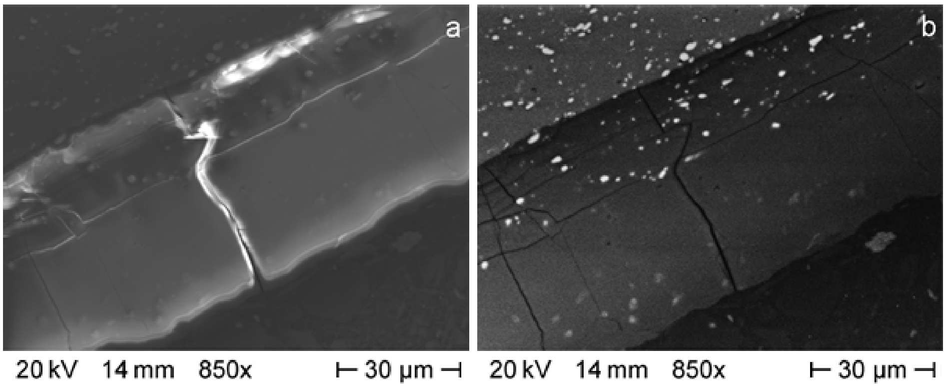

FIG. 57. (a) Secondary electron image showing cracks in the oxide layer. (b) The BSE image of the oxide layer reveals white particles, which are identified as AlFeNi precipitates. AlFeNi is an aluminium alloy composed of ~96 wt% Al, 1 wt% Fe, 1 wt% Ni, and 1 wt% Mg. (Reproduced from Refs [2, 37] with permission from SCK•CEN.)

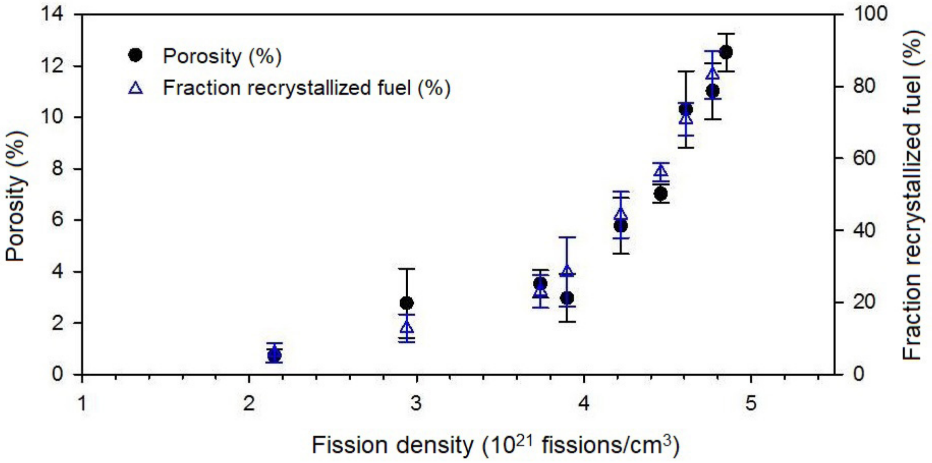

FIG. 58. Results of secondary electron image analysis; the recrystallized fraction and porosity progress with increasing burnup in U–Mo particles. (Adapted from Ref. [36] with permission from SCK•CEN.)

examinations (e.g. interaction layer, bubbles, recrystallization). As an example, Fig. 58 shows the increase of porosity and recrystallized fraction with increasing burnup, with data obtained through image analysis.

8.3.4. Electron backscatter diffraction

SEM systems dedicated to irradiated fuel examinations are increasingly equipped with electron backscatter diffraction (EBSD) systems [38, 39]. EBSD is a quantitative technique revealing local crystal orientation at the surface of polished samples. These orientations are generally presented as maps and deliver information on the crystallographic texture (i.e. the preferential orientations of crystallites in the polycrystalline sample). This technique consists of analysing the diffraction pattern of BSEs obtained on a phosphor screen. This diffraction pattern results from the interaction between the electrons emanating from the electron gun of the scanning electron microscope and the crystal lattice close to the surface of the polished sample. The pattern therefore depends on the crystal structure and on its local orientation (Fig. 59).

Applied on a multiphase sample, EBSD identifies the local phase and therefore gives it spatial distribution. This technique can also be used for local strain measurements. EBSD is used to analyse

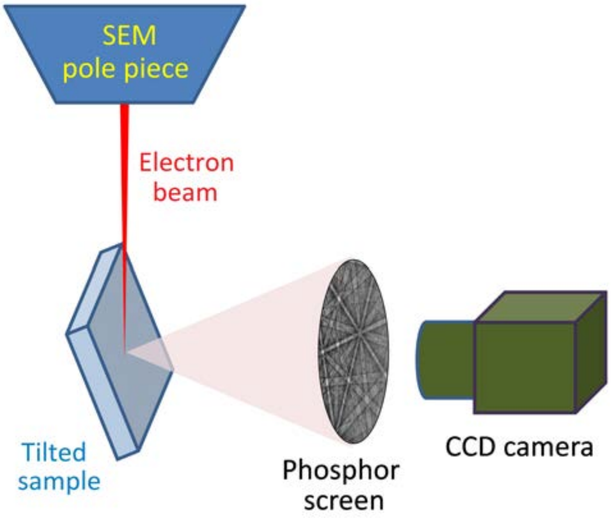

FIG. 59. Principle of the EBSD system.

centimetre sized specimens with millimetre sized grains, as well as thin films with nanograins. Spatial resolution is related to the resolution of the scanning electron microscope, but 10 nm grains can be distinguished in a modern field emission scanning electron microscope. The specimen depth implied in the measurement is less than 10 nm, and specimen size depends on the microscope's geometry and capability.

Typically, the sample is tilted at approximately 70° relative to the horizontal. The electron beam is vertical, and the phosphor screen, with its associated charge coupled device camera, is set roughly parallel to the beam, in front of the sample. The system requires an accurate insertion mechanism to control the position of the phosphor screen and the camera when in use, and to retract them to a safe position when not in use, to prevent interference with other scanning electron microscope operations. Because of the tilt, the lateral resolution is better than the longitudinal one.

Sample polishing is a key aspect of this technique. Each polishing step removes surface defects induced close to the sample surface by the previous polishing step. Surface oxidation, contamination and residual lattice damage are likely to reduce the quality of the diffraction pattern images. The final polishing step generally uses a colloidal silica suspension. For some samples, final ion milling can improve the results. When the scanning electron microscope used for the EBSD measurements is also equipped with a FIB, it can be used to remove possible contamination or oxide layers. Examples of produced images are shown in Figs 60 and 61. Colouring is used to depict local crystal orientation changes.

A pioneering work on EBSD with nuclear fuels can be found in Ref. [40] and more recent works include Refs [41, 42]. This technique has also been applied to non-irradiated fuel studies on sintering in Ref. [43] and on creep in Ref. [44], and to non-irradiated U–Mo fuels in Refs [45, 46] and to irradiated dispersion fuel in Ref. [47].

EBSD and EDS measurements can be performed simultaneously on small samples, thereby facilitating an understanding of the microstructure.

8.3.5. Scanning electron microscope–focused ion beam (dual beam)

FIB instruments can be used to prepare electron microscopy specimens from a wide range of materials, including semiconductors, ceramics, metals, polymers, biological materials and tissues [48]. A basic FIB instrument consists of a vacuum system and chamber, a liquid metal ion source, an ion column, a sample stage, detectors and a gas delivery system. Modern FIB instruments supplement a FIB column with an additional scanning electron microscope column so that the instrument has a dual beam arrangement, whereby a sample can be imaged and material removed and deposited at a length scale of a

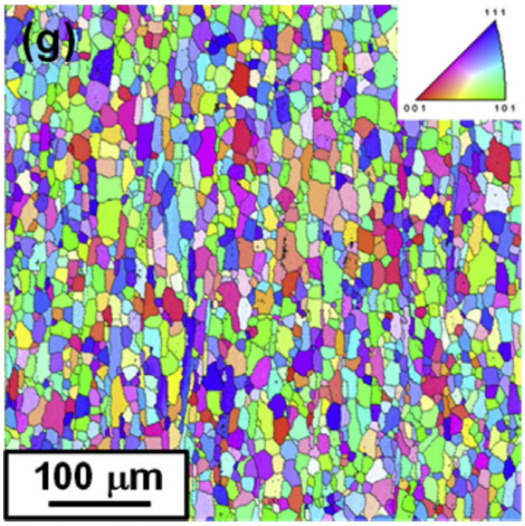

FIG. 60. EBSD inverse pole figure map of U–10 wt% Mo recrystallized grains after hot rolling at approximately 650°C and annealing at 700°C. (Reproduced from Ref. [45] with permission.)

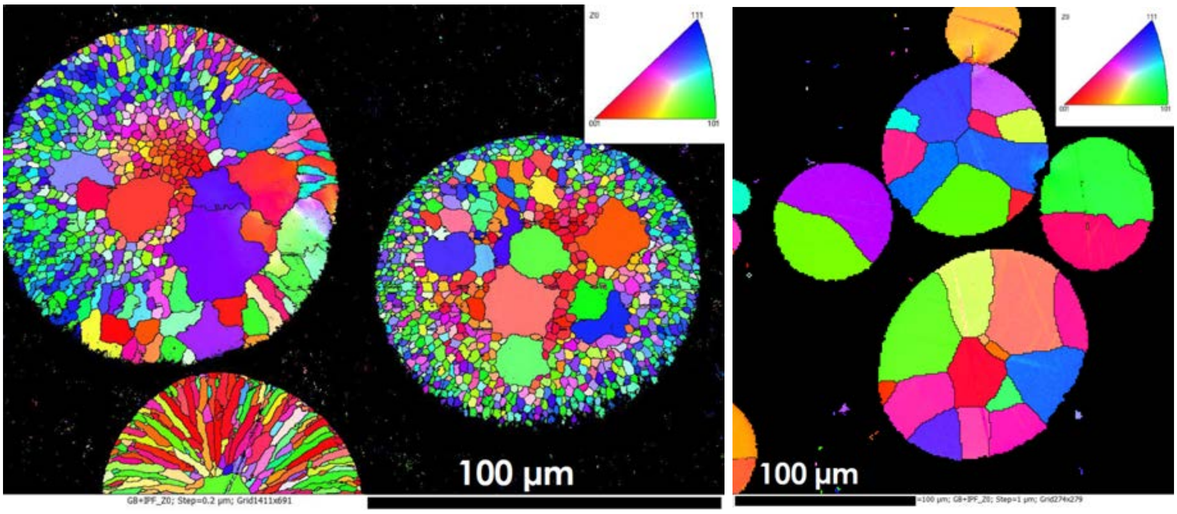

(a)

(b)

FIG. 61. EBSD grain orientation maps (a) as atomized powder and (b) after heat treatment at 1000°C for 1 h, showing a significant grain growth during the annealing. (Adapted from Ref. [46] with permission from CEA.)

few nanometres. To satisfy the basic functions of a FIB, imaging and sputtering with an ion beam requires a highly focused beam. A liquid metal ion source provides the brightest and most highly focused beam. The most widely used source is a gallium based blunt needle. Gallium is superior to other liquid metal ion sources, such as indium, bismuth, tin and gold, because it combines a low melting temperature (~30°C), low volatility and low vapour pressure [49]. Gallium does not react with the tungsten that typically defines the needle, and evaporation is negligible.

During FIB operation, gallium flows from a reservoir to the needle tip and is extracted by field emission. A collision cascade is generated by the gallium as it interacts with the sample, causing sputtering and generating secondary electrons that are gathered by secondary electron detectors. Material can be sputtered in a site specific manner. In a dual beam platform instrument, an electron column is mounted vertically, the ion column is mounted at an oblique angle, and the specimen is positioned at a height where the electron beam and the ion beam coincide, resulting in co-localized FIB processing and scanning electron microscope characterization. Electron induced characteristic X rays, electron backscattered diffraction, and other electron generated signals that are not directly generated by the ion beam enable site specific specimen characterization. The most widespread application of the dual beam scanning electron microscope–FIB is for the generation of site specific SEM and TEM specimens.

The challenges associated with using FIB to characterize irradiated nuclear fuels and materials are discussed in Ref. [49]. The advantages and disadvantages of using FIB to prepare TEM samples from irradiated U–10Mo monolithic fuel are discussed in Ref. [50].

When characterizing irradiated nuclear fuel, it is important to characterize the porosity in the microstructure. Much of this porosity is due to the development of fission gas bubbles. However, when samples are mechanically polished, some of the porosity can be lost. By employing a dual beam scanning electron microscope–FIB to generate samples with little smearing, SEM analysis can be used effectively to characterize the microstructure (Fig. 62), and samples can be produced for TEM. Traditional techniques have been employed for producing TEM samples (see Section 8.5) from irradiated nuclear fuels, but they are difficult to employ. FIB, however, is an effective technique that is relatively easy to employ and can be used in a site specific way to generate samples from specific locations of an irradiated fuel plate.

Once a small specimen is produced from a fuel plate in the hot cell, it is mounted and polished in a glovebox. The specimen is then transferred into a dual beam FIB to obtain cross-sections. The procedure is material- and process-dependent (i.e. beam current conditions change with changes in the process or the material). A detailed sample preparation method has been employed to produce cross-sections with viewable dimensions of ~15 µm × 10 µm [51]. The resulting sample microstructural features can be imaged using SEM (Fig. 62) and secondary electrons. Further sample thinning is performed using FIB to produce a sample that is thin enough to be characterized using TEM.

In addition to oxide layer thickness measurements, images from SEM can be used for the following:

(a) Measurement of local plate, cladding and fuel thickness. Of these three measurements, only the plate thickness measurements can be compared to NDT local measurements at the sampling position.
(b) Identification of cracks and other mesoscopic defects.
(c) Characterization of fission gas bubbles (size distribution (2-D), morphology, spatial distribution). These measurements are limited to micrometric bubbles (>~20 nm).

8.4. ELECTRON PROBE MICROANALYSIS

EPMA is used to measure the local chemical composition of the material on a micrometre level, allowing a local quantitative analysis of the material. Similar to a scanning electron microscope, an electron probe microanalyser employs an electron beam focused on a sample surface. The primary

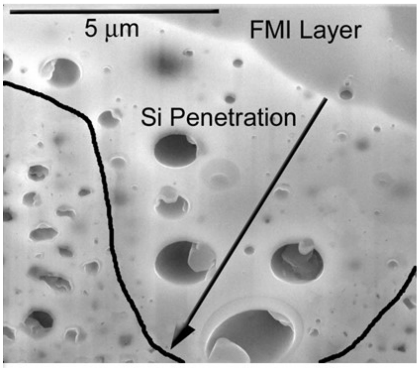

FIG. 62. Scanning electron microscope image of the FIB machined surface of a U–Mo particle periphery and of the interdiffusion layer. (FMI — fuel–matrix interaction). (Adapted from Ref. [51] with permission.)

electrons, interacting with the sample, induce the emission of secondary electrons, BSEs and characteristic X rays [52]. EPMA is based on the measurements of the peak intensities of these characteristic X rays. It allows the analysis of most existing elements that are present in a sample, from atomic number 5 (boron) to 92 (uranium). This analysis is an elemental analysis and does not identify isotopes of an element. It is sensitive enough to detect and measure elements down to a mass fraction of ~0.02 wt%.

The main measuring device for EPMA is a wavelength dispersive spectrometer. Its principle is illustrated in Fig. 63. Its main elements are a crystal, which is used as a monochromator, and a proportional counter, which is used as a detector. The X ray wavelength is selected through Bragg's diffraction law. For that, the monochromator and the proportional counter are set on mechanisms allowing displacements and rotations, keeping the sample surface, the crystal and the detector on a focusing circle (so-called Rowland circle). In Fig. 63, the WDS measurement system is represented for two possible measurement positions. The black dashed lines symbolize the trajectories of the crystal and of the counter covering the whole spectrum. The linear trajectory of the crystal aligned with the electron beam focusing point is an advantage of such a setting, with the emerging angle of the measured X rays always being the same. Various crystals or layered synthetic solids can be used, each with its own capacities, and in most WDS systems two to six crystals are set on a turret, allowing the selection of one crystal.

An example of a spectrum obtained from an irradiated U–Mo particle using a pentaerythritol (PET, molecular formula $C_5H_{12}O_4$) crystal is shown in Fig. 64.

An electron probe microanalyser usually has more than one WDS spectrometer (often four or five), usually set at equivalent positions but different azimuths around the electron beam and the samples. This allows measurement of more than one element at the same time, often with different crystals but using the same X ray emerging angle, which shortens the overall duration of the analysis that would otherwise be performed sequentially.

Obtaining a quantitative evaluation of the sample composition is not a straightforward process. First, the measurement needs to be calibrated using standards containing the considered elements at known concentrations. Since interferences between the lines of two elements occur, and since for some elements in a given sample each existing line is affected by interferences, these interferences have to be taken into account. An interference of a uranium line with a plutonium line can be seen in Fig. 64.

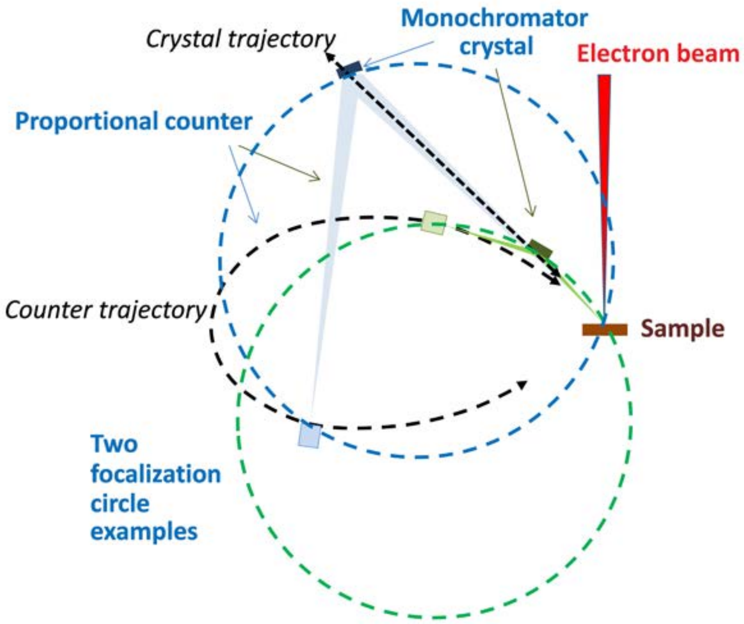

FIG. 63. Measurement principle in a WDS. Respective positions of the crystal and of the proportional counter for two counting positions used as examples.

Moreover, the electronic interaction with the sample is a complicated process, and several effects need to be considered before deducing a composition from a set of measurements. Indeed, an analysis is not a complete analysis of a known volume. The electron trajectories and interactions with the sample do not have a homogeneous density. Figure 65 shows a set of trajectories of electrons in a U–Mo particle and in aluminium simulated by the Monte Carlo code PENELOPE [53].

The deeper the X ray production position, the lower its emergence from the surface of the sample. The emission rate depends both on the X ray wavelength and on matrix effects linked with the content of the material, the atomic number of its constituents and its density. Figure 66 shows the depth distribution of the origin of the X ray emerging at the sample surface for uranium.

To take all these effects into account in a given quantitative EPMA, an iterative model based on all measurements is utilized to determine the real concentration of each component. More details on EPMA principles, theory and practice can be found in Refs [34, 54, 55].

Adaptations for the hot cell use of EPMA systems have been described in Refs [56–58]. In addition to protecting the operators from the irradiated fuel samples, the electron probe microanalyser has to be modified to enable the measurements. The detector used for the measurement is sensitive to the radiation

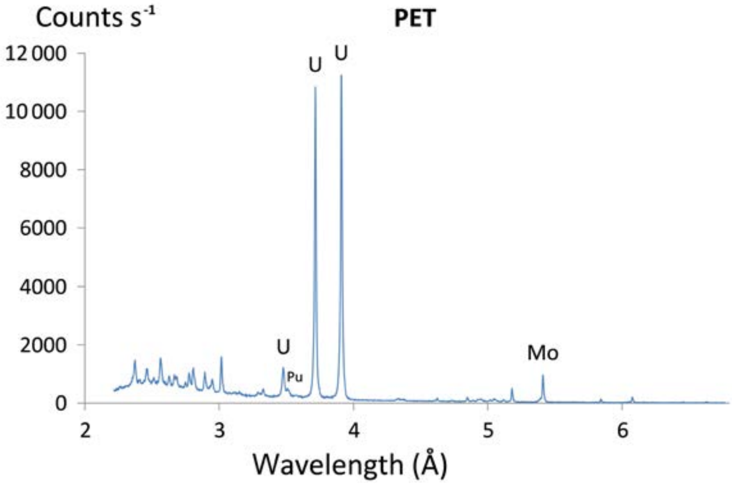

FIG. 64. Example of a spectrum obtained on an irradiated U–Mo particle using a PET crystal. (Courtesy of CEA.)

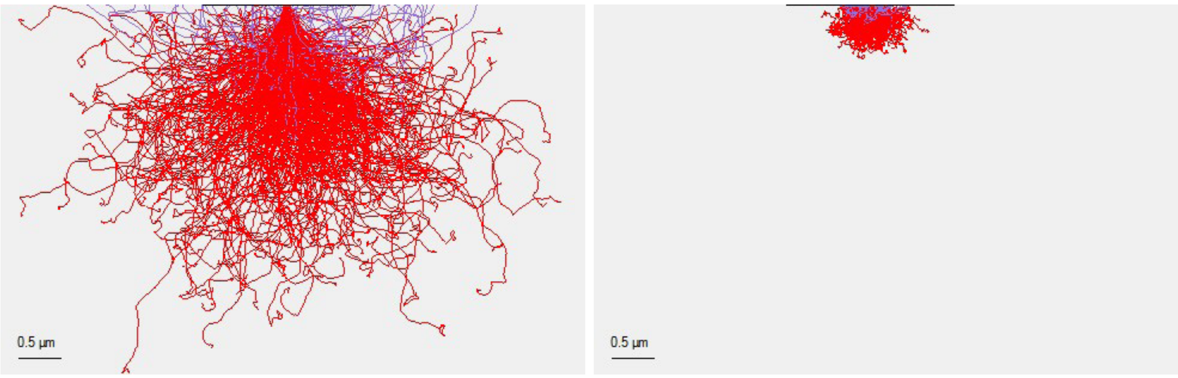

(a)
Al matrix

(b)
U–Mo matrix

FIG. 65. Simulation of 400 20 keV primary electron trajectories in an aluminium matrix and in a U–Mo matrix using the Monte Carlo code PENELOPE [53]. (Courtesy of CEA.)

emitted by the sample. It is possible to interpose dense shielding (usually tungsten alloys) between the sample and all positions where the detector may be without cutting the useful X ray path. This shielding can be seen in Fig. 67, with two high density tungsten alloy parts in the WDS itself but also with the sample stage weighing more than 80 kg.

In addition to local quantitative analyses, qualitative maps of the sample surface are obtained by scanning it, while the spectrometers are set on the peak positions of the lines of interest. This can be done using a scanning electron beam, or, for larger areas, by moving the sample. The time spent on each pixel of the image produced is usually shorter than the time used with quantitative analyses. A result is that the counting uncertainties for each point of an image are higher than for a local quantitative analysis. These maps are generally called qualitative, with the general understanding that the brighter the local grey level of the image (the local counting), the higher the local element concentration. By combining these images and detailed quantitative analyses performed along lines within the image field, it is sometimes possible to derive semiquantitative maps of the considered elements by establishing a link between the grey level

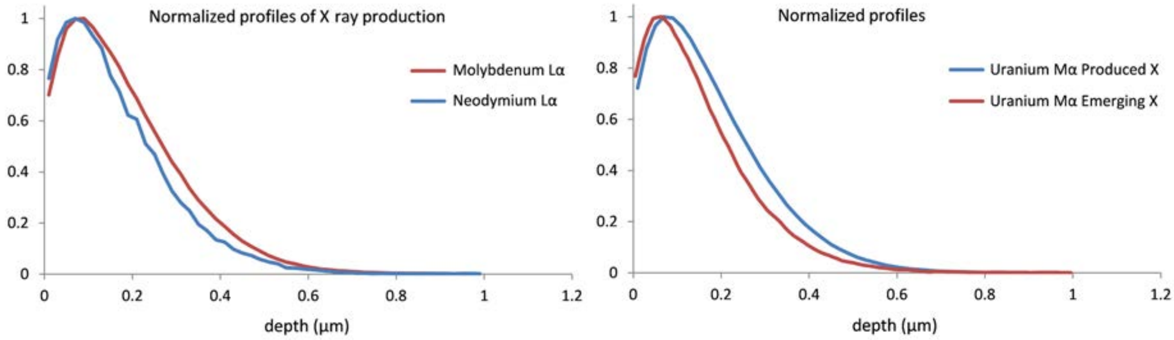

FIG. 66. Simulation of depth distributions for X ray production and the X ray emerging in the detector direction for a 20 keV measurement in a U–Mo particle using the Monte Carlo code PENELOPE [53]. (Courtesy of CEA.)

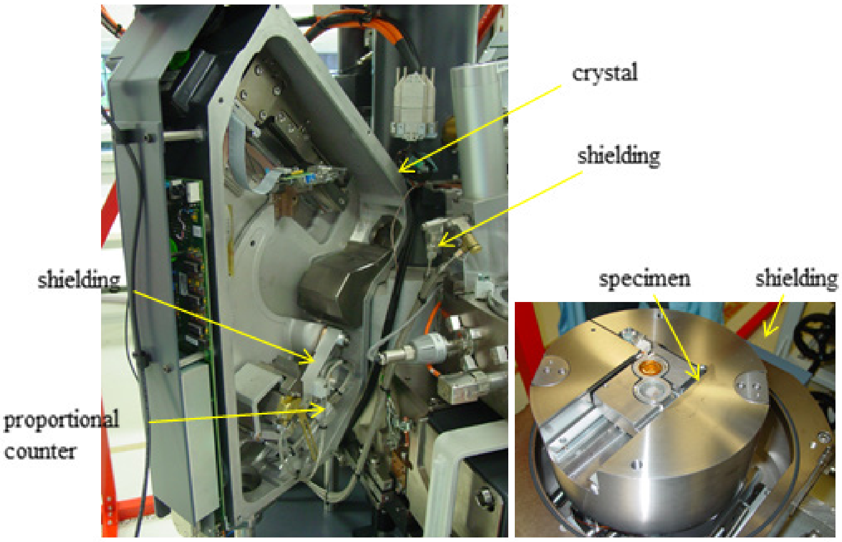

FIG. 67. Opened WDS and sample stage in a shielded CAMECA SX100 electron probe microanalyser. This snapshot of the spectrometer reveals the mechanisms used for the displacement of the crystals and of the counter. These images also show the high density tungsten alloy used in the stage and in the spectrometer. (Adapted from Ref. [58] with permission.)

of each image and the quantitative local concentration of the selected element. In the case of composite fuels, due to the high changes in the matrix, the maps of the fission products can be deceptive in the various zone comparisons, and quantitative analysis lines across the various areas of the fuel are preferred.

EPMA has the following advantages:

(a) It is possible to measure high gamma emitting samples using shielded devices.
(b) For the measurable elements, measurements are possible for concentrations down to ~0.02 wt%.
(c) Automation is possible, allowing long acquisition periods with no action from the operator.
(d) Large field maps (using sample movements) and detailed maps (using beam scanning) are used.

The limitations of EPMA include the following:

(a) No measurements are possible for the lightest elements.
(b) No measurements are possible for concentrations clearly lower than 0.02 wt%.
(c) No isotopic measurements are possible.
(d) There are interferences between various elements. These interferences need to be taken into account.
(e) Acquisition times are long.
(f) Uncertainty calculations are complex.
(g) Calibration using standards is necessary for each element analysed. Nevertheless, approaches without standards have been designed for some of the minor actinides, for which standards are not easily available [59].

Maps and quantitative analyses have both proved useful in research reactor fuel examinations. The maps are used to draw information on the evolution of the major constituents of the fuels and on the migration of the major fission products. Quantitative analyses are used to determine compositions in the various areas visible on the maps and to further understanding of the qualitative maps.

Figure 68 shows large area EPMA mappings across the fuel meat in a silicon coated U–Mo fuel plate with a fission density of 5.2×10^{21} fissions/cm^3 [60]. Using only the elements with a sufficiently high concentration (main fuel constituents and high yield fission products), the mappings provide an overview over a large field, showing the correlations between fission product concentrations and other microstructural features, such as the interaction layer. In this particular case, the image illustrates the formation of the interaction layer and its effect on the barium, neodymium and xenon fission product atoms that were ejected from the fuel particle into the aluminium matrix. As the interaction layer forms, the fission products are ‘swept up’ and end up on the interface between the interaction layer and the matrix. Where the formation of the interaction layer is suppressed by some means (silicon in this case), the fission products are distributed more diffusely in the matrix surrounding the particles.

Figure 69 shows a set of EPMA X ray maps obtained on a polished sample of an irradiated U–Mo dispersion fuel with silicon addition in the aluminium matrix [61]. In these maps, for a given element, the brighter the grey level, the higher the local concentration. In this fuel, optical micrographs and scanning electron microscope images, such as the BSE image in Fig. 69, show the formation of an interdiffusion layer between the U–Mo particles and the aluminium matrix. They also show small fission gas bubble formation in the U–Mo particles and larger bubbles in the interdiffusion layer, especially at interfaces. The EPMA maps confirm these observations, with maps of uranium, molybdenum and aluminium for the interdiffusion layer formation, and xenon maps for the gas bubble formation. Within the U–Mo particles, the molybdenum map shows lower molybdenum content along lines forming what appear to be the grain boundary network (darker lines within the U–Mo particles).

The molybdenum map also shows that this molybdenum inhomogeneity is not the same for all U–Mo particles. The bright spots within the U–Mo particles in the xenon map correspond to small fission gas bubbles very close to the polished surface, but unopened by this polishing. The neodymium and caesium maps also show a non-uniform concentration within the U–Mo particles, signalling migration of these elements during irradiation.

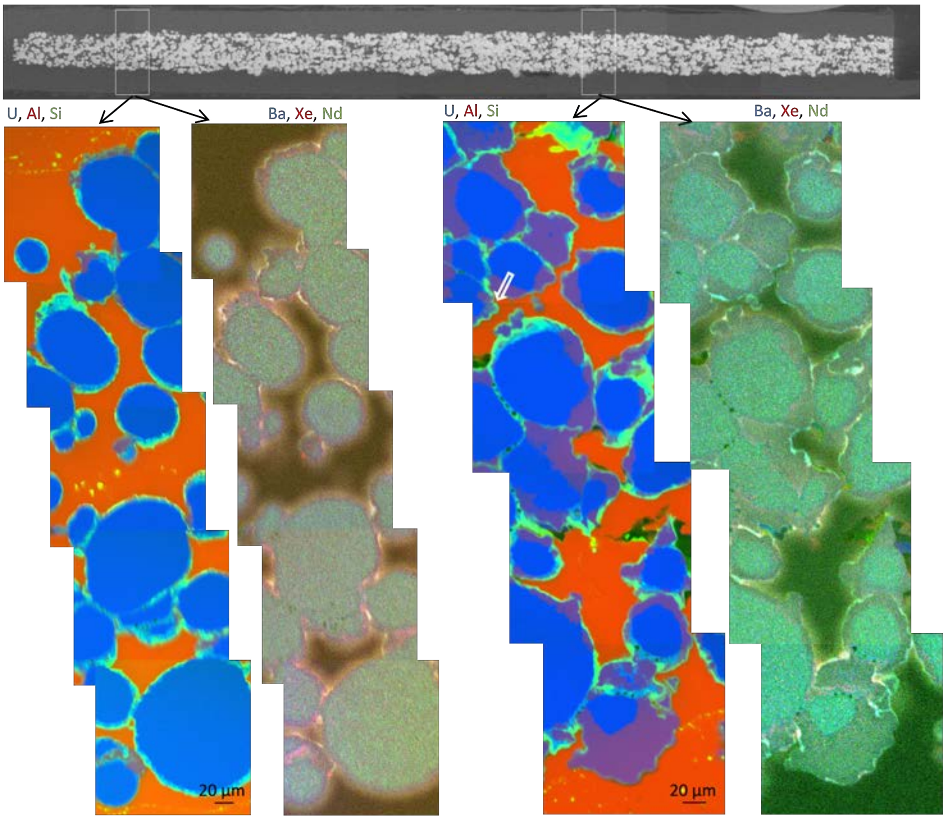

FIG. 68. EPMA overview maps of the main constituents (uranium, molybdenum, aluminium) and a selected number of fission products (barium, xenon, neodymium) across the width of the fuel meat in an irradiated U–Mo fuel plate at two locations. The maps illustrate how EPMA can clarify the correlation between fission product concentrations and other microstructural features, such as interaction layer formation. (Adapted from Ref. [60] with permission from SCK•CEN.)

In oxide nuclear fuels, neodymium is one of the least mobile fission products after its recoil subsequent to fission. Consequently, in oxide fuel EPMA examinations, measurements of neodymium production are generally used to deduce the distribution of more mobile fission products. The movements observed in neodymium maps in U–Mo dispersion fuels show that this element cannot be used this way in these cases. No good reference has been found, since all fission products exhibit signs of mobility. In addition to mobility inside the U–Mo particles, the fission product maps exhibit very bright areas corresponding to the accumulation of these fission products, especially along interdiffusion layer–aluminium interfaces, or what used to be these interfaces in cases where the local aluminium matrix has been totally consumed. The silicon map shows silicon precipitates within what remains of the aluminium matrix, but no precipitates are present in the interdiffusion layers.

Figure 70 illustrates fission product concentrations as a function of burnup. When there is no diffusion of the fission products, leading to changes in the local compositions and precipitation, the quantified fission product concentrations rise in proportion to the yield of the fission products. Therefore, as soon as the fission products become mobile (either thermal or athermal), deviations from the linear evolution are visible. In the case of U–Mo fuel, from which the measurements in Fig. 70 are taken, the recrystallization effect (see also Section 8.3) causes precipitation of fission products. At around a fission density of 4.5×10^{21} fissions/cm^3, the recrystallization of this fuel is complete and the analyses can no longer be performed in an undisturbed region of the grain. This affects the reliability of the measurements, which is visible in the deviation from the linear evolution.

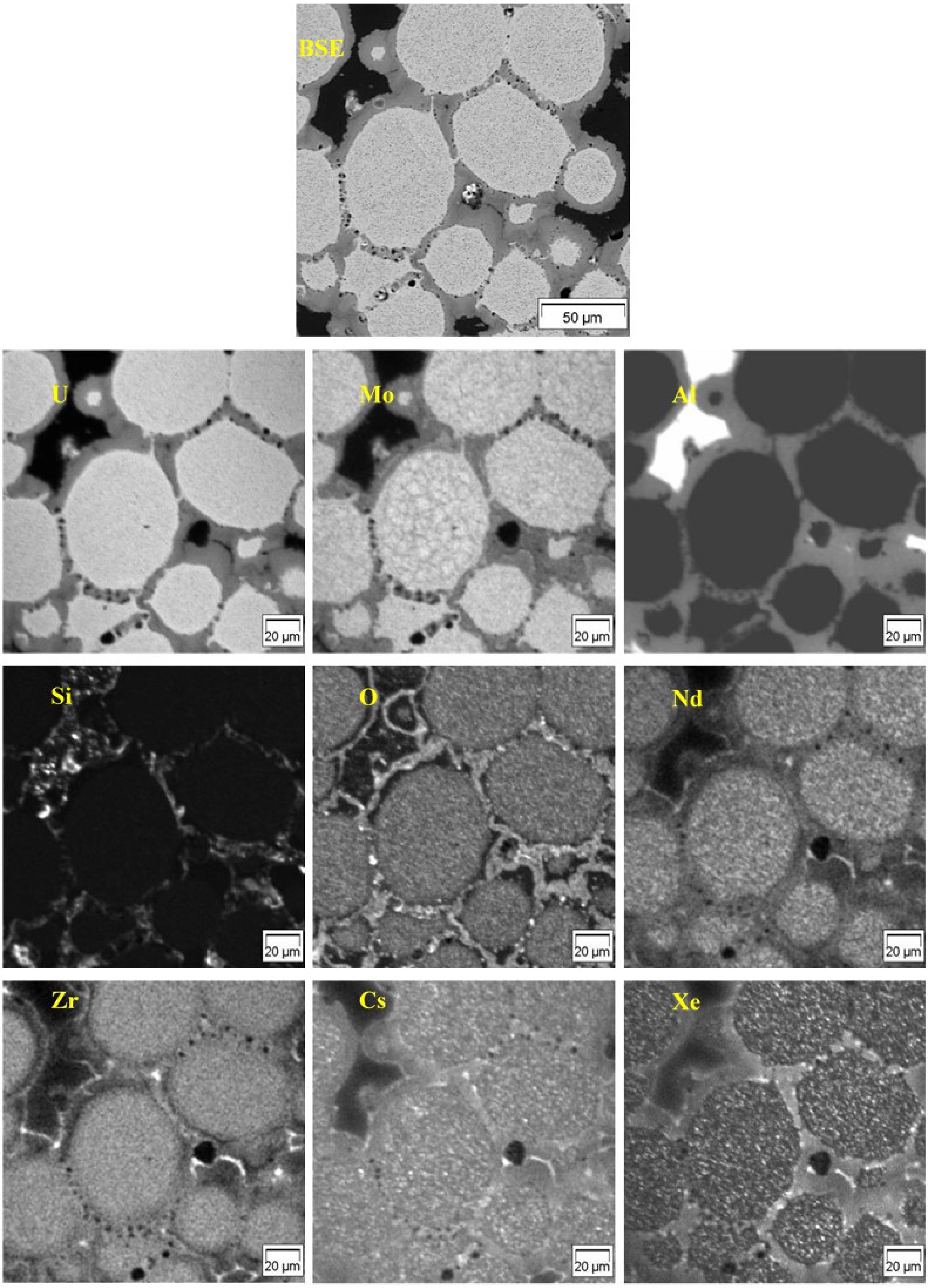

FIG. 69. Detailed EPMA maps for some of the main constituents and some of the main fission products in an irradiated U–Mo dispersion fuel with silicon addition in the aluminium matrix. (Courtesy of CEA.)

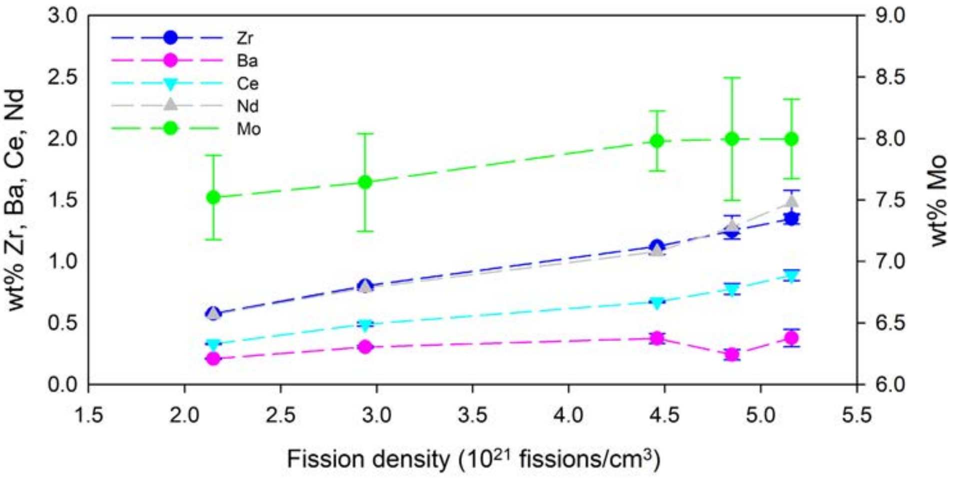

FIG. 70. *Example of quantitative EPMA performed in the centre of fuel particles and showing the accumulation of fission products with burnup. (Courtesy of SCK•CEN.)*

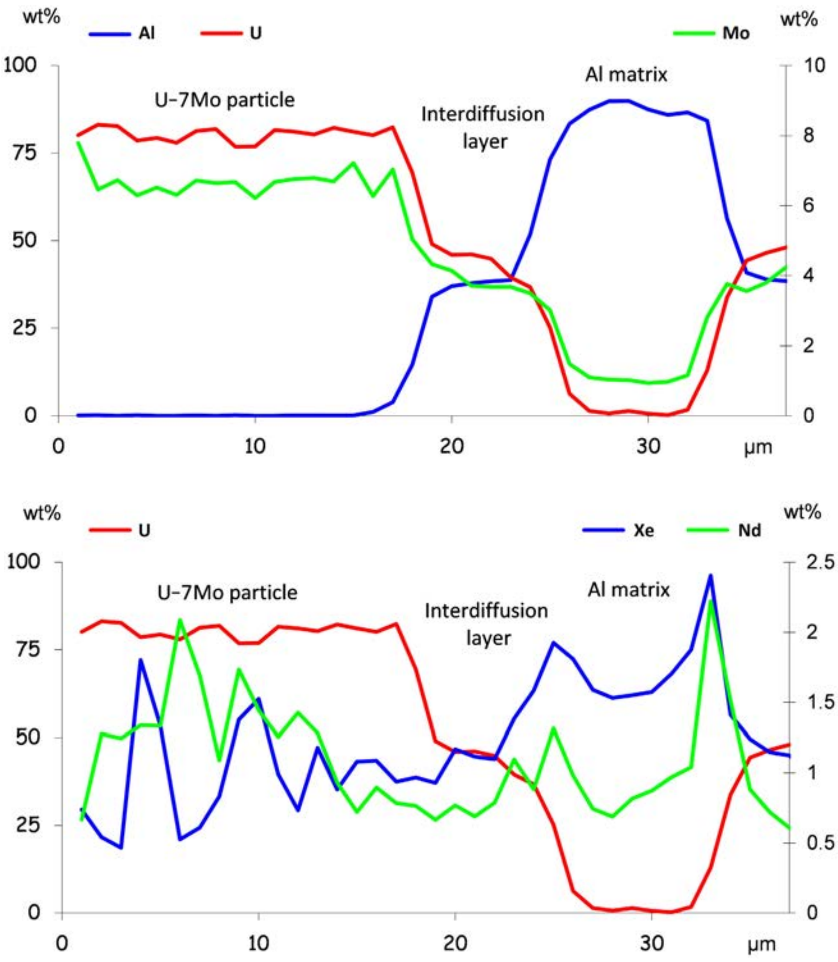

FIG. 71. *Example of quantitative EPMA along a line. This line goes across an interdiffusion layer formed in an irradiated U–Mo dispersion fuel. (Adapted from Ref. [31] with permission from CEA.)*

Figure 71 gives an example of quantitative analyses along a line on another irradiated U–Mo dispersion fuel. This line was designed to cover all phases in this fuel. On the left of the graphs, the analyses are in a U–Mo particle. They then cross the interdiffusion layer and an aluminium matrix remnant, ending again in an interdiffusion layer. The analyses of the initial components allow determination of their relative content in the interdiffusion layer, showing that, for this fuel, in this field, its composition is close to $(U,Pu,Mo)Al_6$. These analyses also show the high concentration of fission products such as neodymium or xenon at the interdiffusion layer–aluminium matrix interfaces. In addition, they show the absence of uranium in the aluminium matrix, and the high level of fission product implantation. The molybdenum level in the aluminium matrix remnants is not due to a diffusion of the initial molybdenum of the U–Mo particles in the aluminium, but corresponds to the recoil of the molybdenum produced by nuclear fission. Examinations of the cladding material have also been performed. In the case of non-conductive materials, the charges brought by the electron beam tend to accumulate and then modify the primary beam electron trajectory, so that no analysis is possible. To prevent this, it is necessary to coat the surface of the sample with a conductive layer. This layer is usually carbon, to avoid too much influence on the measurement results. In this case, the results have to be computed, taking the carbon layer into account.

8.5. TRANSMISSION ELECTRON MICROSCOPY

TEM supplies morphological, compositional and crystallographic data for samples. Many features of interest in an irradiated nuclear fuel plate are too small to resolve using optical microscopy and SEM. TEM has a resolution limit of around 0.1 nm, which is necessary to observe features such as fission product precipitates, fission gas bubbles, grain boundaries, dislocations, voids and vacancies. A single column of atoms can be examined, which is three orders of magnitude smaller than the smallest resolvable object in a light microscope. Information about these features is needed for the development of computer models that describe fuel performance, and to understand the underlying mechanisms that dictate the performance of a specific type of nuclear fuel.

In general, samples for TEM characterization are more difficult to prepare than those for optical microscopy and SEM analysis. As a result, it is only practical to perform TEM analysis on a few samples from a given fuel plate. Candidate plates for additional analysis using TEM can be identified using data from optical microscopy and SEM analysis. Results from optical microscopy and SEM can be used to identify unique microstructural features in the fuel plate that may affect irradiation behaviour. For example, TEM analysis would be beneficial if there was some indication of the presence of impurity phases in the microstructure. Overall, TEM analysis is only performed if absolutely necessary.

Transmission electron microscopes use a beam of electrons transmitted through an ultrathin specimen that interacts with the specimen as it passes through it. This interaction creates an image that is magnified and focused onto an imaging device, such as a fluorescent screen (or a charge coupled device camera). TEM image contrast originates from the absorption of electrons in the material. This is a result of the thickness and composition of the material. A transmission electron microscope contains an emission source that emits electrons when it is connected to a high voltage source (~100–300 kV). Other components of a transmission electron microscope include electromagnetic lenses, a vacuum chamber, two condensers, a sample stage, a phosphor or fluorescent screen, and a computer. A transmission electron microscope functions under the same basic principles as an optical microscope.

TEM offers the following advantages:

(a) Powerful magnification of the sample microstructure, providing information on element and compound structure;
(b) High quality detailed images;
(c) Information on surface features, shape, size and structure;
(d) Easy to operate;

(e) Because of the small sample size, radiation levels are low enough so that additional shielding is typically not required.

The disadvantages of TEM include the following:

(a) Instruments are large and expensive.
(b) Laborious sample preparation may be required.
(c) Specialized training is required for operation.
(d) Instruments can only characterize samples that are electron transparent, can tolerate exposure to a vacuum chamber and are small enough to fit into the chamber.
(e) Instruments require special housing and maintenance.
(f) The images produced are black and white.
(g) Instruments are sensitive to vibration and electromagnetic fields and have to be located in special isolation areas.

As discussed above, sample preparation can be a major challenge for performing TEM. Irradiated plate type fuels have been characterized using TEM and samples produced using a traditional approach [62, 63]. In these studies, a small sample from the fuel plate, approximately 1 mm thick, is prepared. The sample is glued inside a 3.0 mm diameter molybdenum ring using epoxy, and it is mechanically wet polished from both sides down to ~100 µm thickness inside a glovebox. The sample is then jet electropolished and finally ion polished until perforation occurs. The finished sample is characterized using a JEOL2010 transmission electron microscope operated at 200 kV. These samples can be used to investigate the behaviour of fission products in the fuel plate microstructure and to determine the crystal structures of different phases. In Ref. [64], the results of microstructural characterization of an irradiated plate type fuel are discussed, where samples produced using a FIB have been analysed. In Ref. [65], the appropriateness of different sample preparation techniques for TEM analysis of nuclear materials is discussed.

Examples of major features that have been identified using TEM are shown in Figs 72–74, with examinations showing the existence of a fission gas bubble superlattice in the U–Mo phase, high

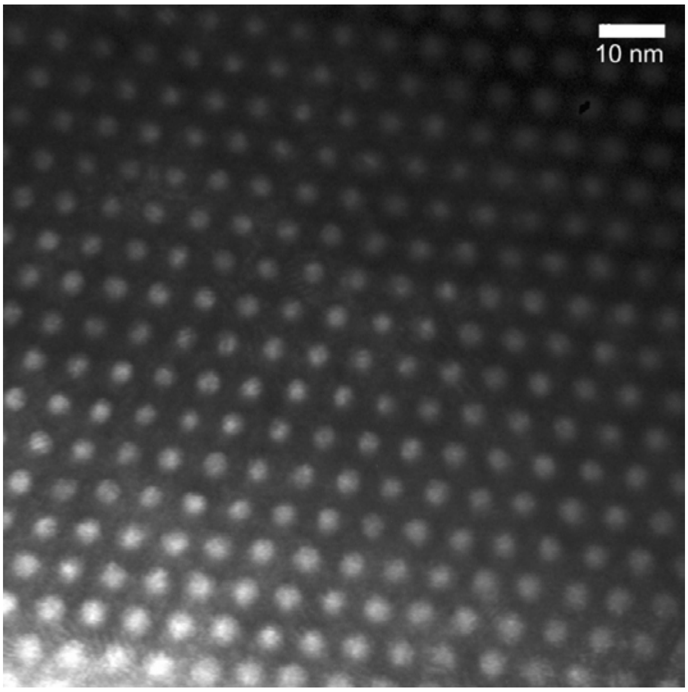

FIG. 72. TEM micrograph of fission gas bubble superlattice in an irradiated U–Mo phase. (Courtesy of INL.)

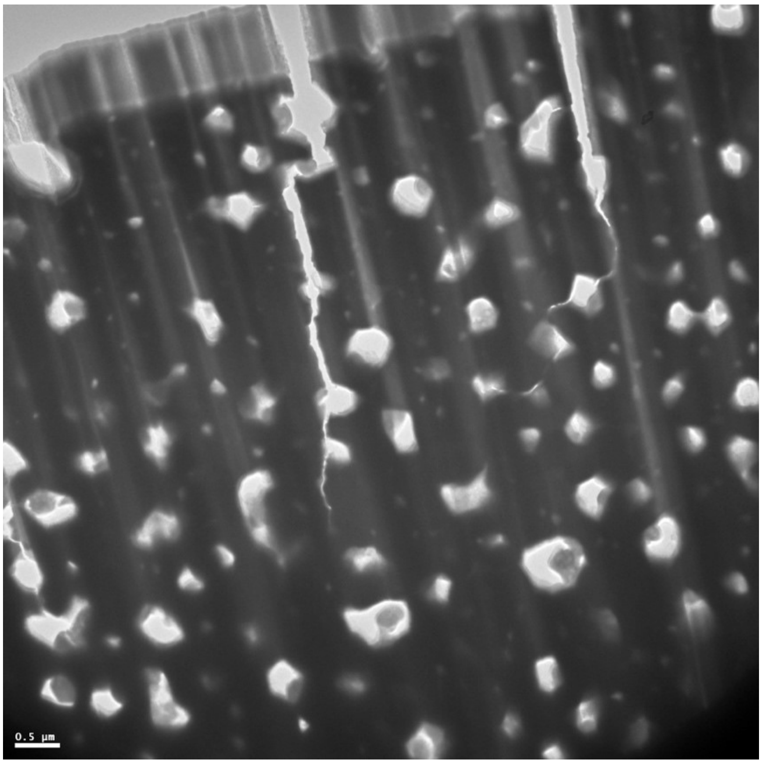

FIG. 73. TEM micrograph of highly irradiated U–Mo dispersion fuel. (Courtesy of INL.)

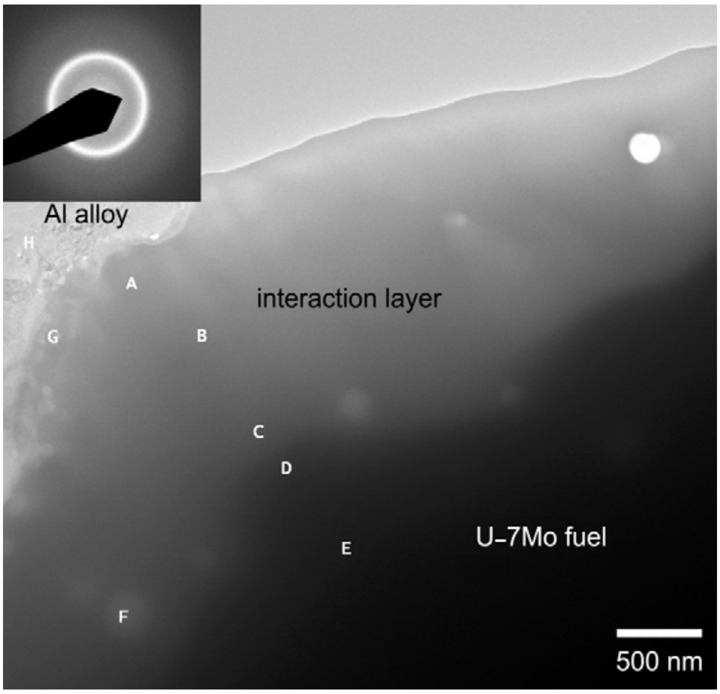

FIG. 74. TEM examination with microdiffraction image showing the amorphous nature of the interaction layer and locations where EDS composition measurements were taken (results not shown here). (Courtesy of INL.)

burnup structure formation at higher burnup and the amorphous nature of the interdiffusion layer. This amorphous nature was shown indirectly by X ray diffraction examinations, with the absence of any new phase appearing in the diffractograms (see Section 8.6). TEM examinations provided direct proof of the amorphous nature of the interdiffusion layer. In Fig. 74, the letters A–H refer to the locations at which the EDS measurements were taken.

8.6. X RAY DIFFRACTION

X ray diffraction tools are used in all material science fields. Generally applied to crystallized materials, they can also be used to study amorphous compounds.

These tools utilize the existence of an elastic interaction between X rays and the electronic orbital of each atom of a material. This elastic interaction leads each electron to become the source of X rays of the same wavelength as the incident X rays, emitted in all directions. It can be considered as an elastic diffusion of the X rays. The regularity of the positions of the atoms in a crystal leads these diffused X rays to form constructive interferences in specific directions, depending on the atoms in the crystal and the positions of these atoms.

In an X ray diffraction measurement, the studied material is subjected to X rays of a selected wavelength, and the resulting X ray intensity is measured around the sample. The positions of the constructive interferences and the properties of the measured peaks are used to derive information on the studied material.

Since its beginning, this technique has been one of the main methods used to determine the geometric arrangement of the atoms in crystallized materials. Databases have been compiled and serve as a reference source, so that X ray diffraction can now be used to identify the compounds in a material as well as its crystalline phase. Some knowledge of the elements anticipated in the sample, obtained using other microanalysis techniques, is usually necessary before the compounds can be identified and preselected. This technique determines the quantitative distribution of the compounds and their lattice parameters. Careful analysis of the peaks provides microstructural information on the average size of the diffracting crystallites, on internal stresses and on defect densities. Samples can be powders or solid samples.

Various configurations are possible. Figure 75 shows a schematic diagram for one of the most common geometries used. Alternatively, the counter can be set directly along the measurement circle, without the monochromator. This monochromator is useful to reduce the background, fluorescence and secondary peaks due to the source, such as the Kβ. In the examination of active materials such as irradiated nuclear fuels, shielding is necessary to protect the proportional counter from gamma radiation. In a geometry without a monochromator, this shielding cannot be effective; no shielding is possible along the direct line between the sample and the proportional counter. However, with a monochromator and a geometry similar to that shown in Fig. 75, shielding material can be set along the direct line between the sample and the proportional counter, without cutting the X ray path. This is the most common geometry in hot cell facilities.

Even with very small samples, most X ray diffraction devices have to operate in a hot cell. In most cases, the device gradually becomes contaminated and maintenance becomes difficult. Using the experience from a past device, in which the whole apparatus was placed in a glovebox inside a lead cell, the actual X ray diffraction device used on irradiated fuels in the LECA-STAR facility (CEA Cadarache, France) was designed to avoid this problem [66]. The goniometer with the X ray tube and the X ray detector are set up inside the hot cell, below the glovebox. The glovebox has a beryllium window at the bottom of the pit. With this configuration, the studied sample is always in the glovebox, either in the main compartment or on the sample holder in front of the beryllium window. When no sample is in the cell, the doors of the cell can be opened, providing easy access to the uncontaminated X ray tube and X ray detector (Fig. 76).

The use of X ray diffraction on fresh fuel in pre-irradiation characterizations combined with post-irradiation X ray diffraction can determine lattice parameters and their evolution as a function of composition. In the case of the U–Mo system, an important aspect of interpreting lattice parameters after

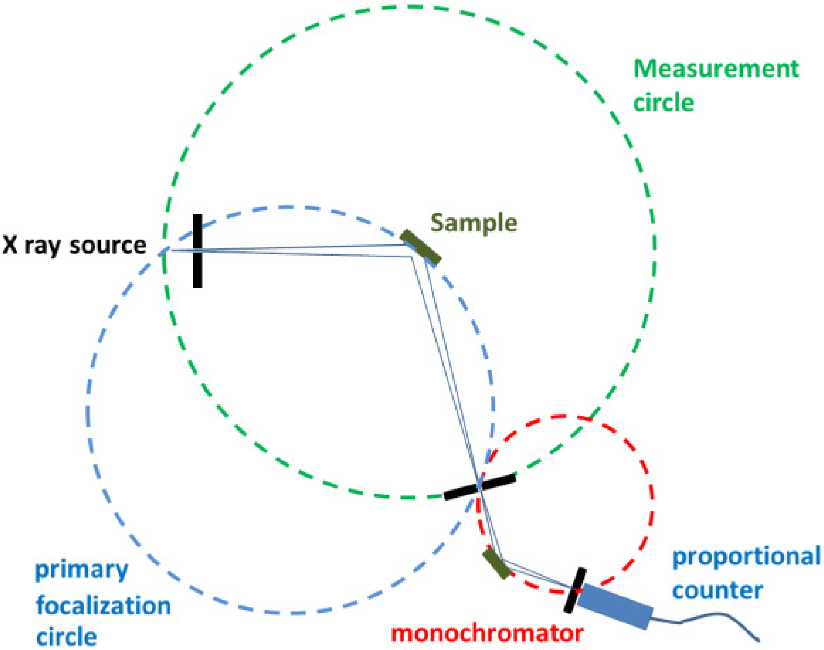

FIG. 75. Schematic diagram of an X ray diffractometer with a Bragg–Brentano parafocusing geometry.

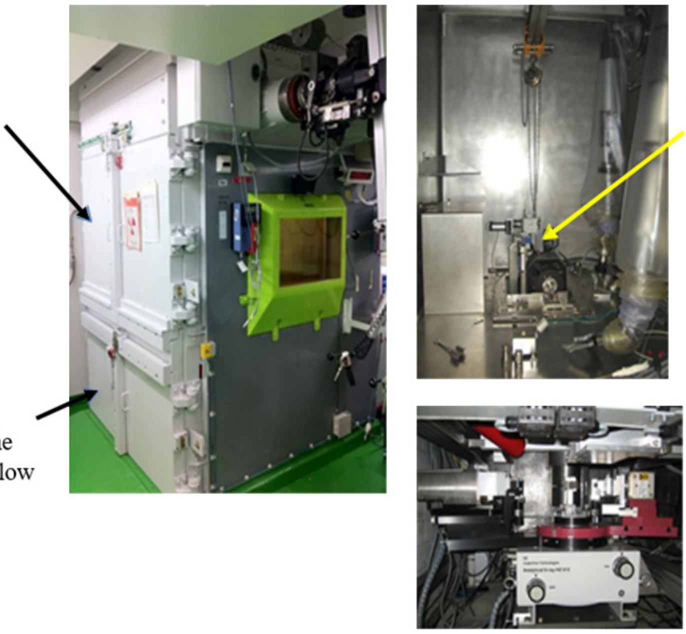

Top doors for access to the glovebox

Bottom doors for access to the goniometer, below the glovebox

Sample holder inside the glovebox inside the cell. Samples are manipulated by remote handling telemanipulators through the cell wall and the glovebox panel

Goniometer, below the glovebox, but inside the cell

FIG. 76. Example of an X ray diffractometer in a hot cell. (Courtesy of CEA.)

irradiation is their evolution as a function of molybdenum content. As molybdenum is a relatively high yield fission product, the molybdenum fraction of the fuel increases with irradiation, even more so because the uranium concentration decreases as uranium is consumed by nuclear fission. This is shown in Fig. 77.

Figure 78 shows an example of a diffractogram obtained on an irradiated U–Mo dispersion fuel with a local fission density of ~2.7 × 10^{21} fissions/cm^3. X ray diffraction results obtained on the same unirradiated fuel had shown the presence of the α-U–Mo phase. This α-U–Mo phase had completely disappeared from the diffractogram after irradiation, as expected.

Only aluminium and the γ-U–Mo phase were clearly visible after irradiation. Moreover, the counts of aluminium were clearly lower than the initial counts, consistent with the formation of the interdiffusion layer and the decrease of the aluminium phase evidenced by optical metallography. No sign was found of the formation of any other phase. This was an indirect proof of the amorphous nature of the interdiffusion layer formed in-pile. The amorphous nature was later confirmed by TEM [67]. The very wide and dissymmetric shape of the γ-U–Mo peaks in Fig. 78 was due to the decrease of uranium by nuclear fission and the presence of fission products. The new average lattice parameter was found to be 0.7% higher after irradiation.

A similar example is shown in Fig. 79 with a pair of diffractograms obtained at the Joint Stock Company State Scientific Centre — Research Institute of Atomic Reactors (Dimitrovgrad, Russian Federation) [68]. In this dispersion fuel, α-phase was present in the fuel before irradiation, but was no longer detectable in the diffractogram obtained after irradiation at ~67% burnup. In this case, the new average lattice parameter was found to be 0.39% higher after irradiation. Moreover, despite significant interdiffusion layer formation, no extra phase was detected, a sign of the probable amorphous structure of the newly formed material.

Another illustration of the use of X ray diffraction on irradiated research reactor materials is given in Fig. 80, where a diffraction analysis of the oxide material growing on the outer surface of fuel plates during irradiation is presented. When the plates are removed from the cooling water, the drying out of the oxide can alter the properties of the material, for example by removal of the crystal water. The drying out of the oxide is evident by the crack pattern it displays, illustrated in the same figure.

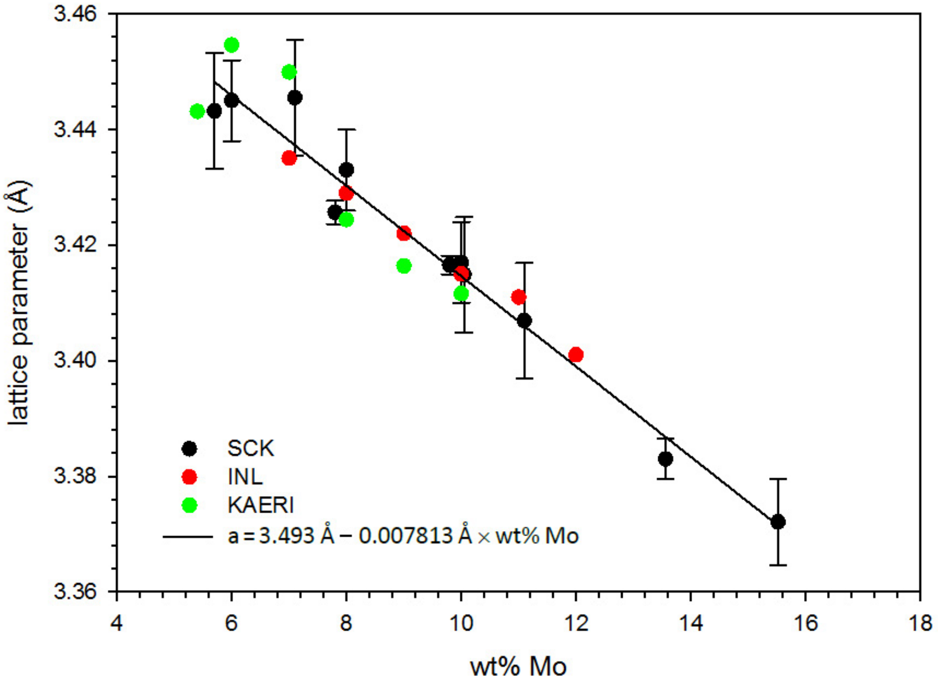

FIG. 77. X ray diffraction based lattice parameter analysis of U–Mo as a function of molybdenum content. The deviations found for the KAERI data are related to the use of atomized fuel particles instead of well annealed arc melt buttons. (Adapted from Ref. [2] with permission from SCK•CEN.)

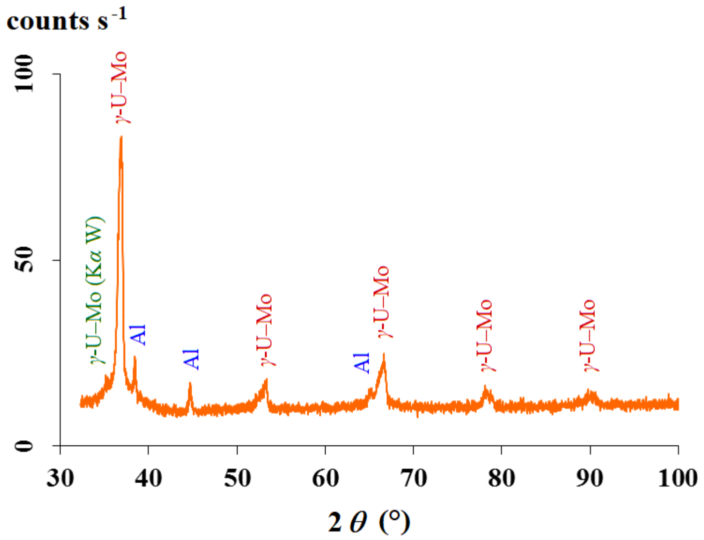

FIG. 78. X ray diffractogram of an irradiated U–Mo dispersion fuel meat. (Courtesy of CEA.)

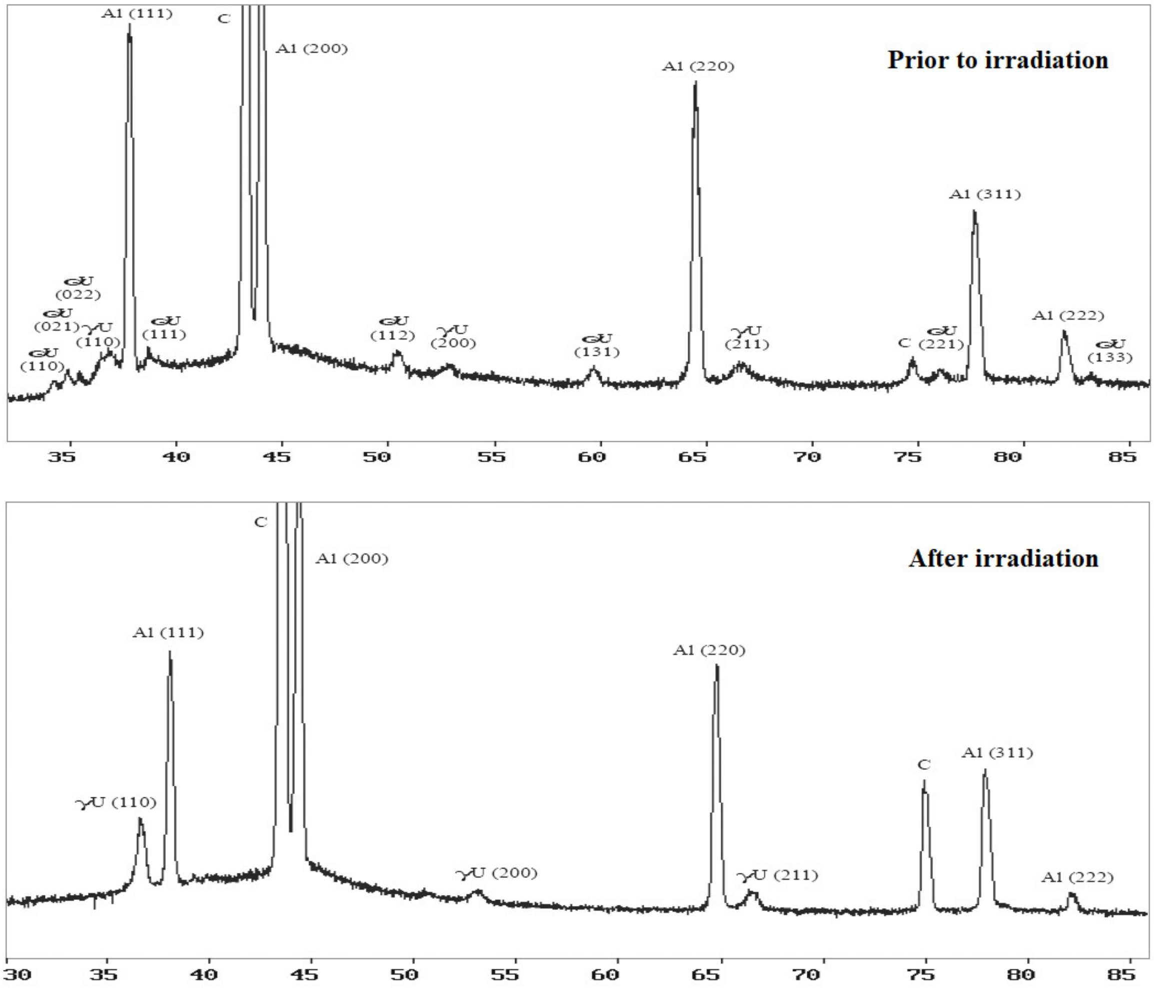

FIG. 79. X ray diffractograms of an unirradiated U–7.5%Mo with γ and α phases and the same fuel at ~67% burnup. (Reproduced from Ref. [68] with permission from Research Institute of Atomic Reactors.)

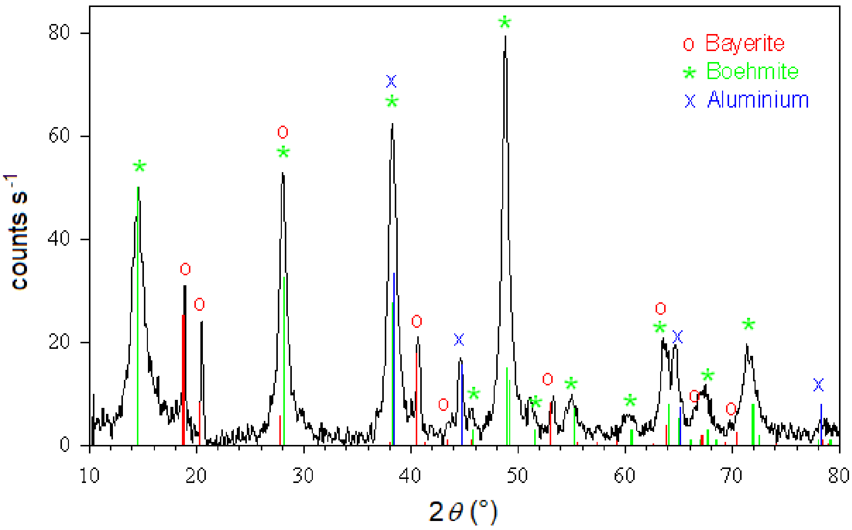

(a)

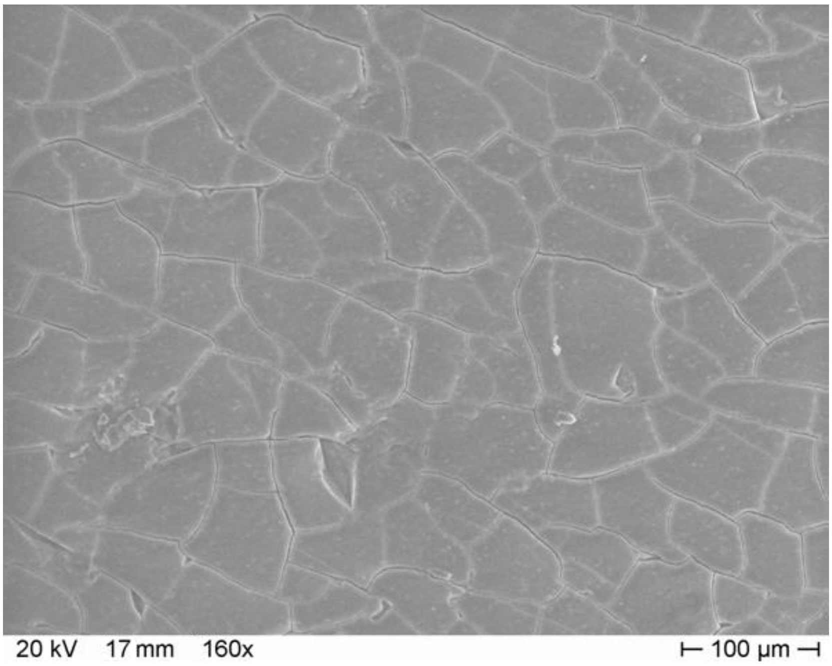

(b)

FIG. 80. (a) X ray diffractogram of oxide material scraped from the surface of an irradiated fuel plate showing that the phase composition of the oxide is mainly boehmite, AlO(OH), with some contribution from bayerite, $Al(OH)_3$. (b) The scanning electron microscope image shows the morphology of the oxide layer as it is present on a typical fuel plate surface after drying out in the hot cell. (Adapted from Refs [2, 37] with permission from SCK•CEN.)

8.7. RADIOCHEMICAL BURNUP DETERMINATION

In radiochemistry, fuel burnup is expressed as the number of fissions relative to the number of heavy metal atoms initially present in the fuel and is calculated according to Eq. (2):

$$F = \frac{\sum \Delta N}{\sum N_0} \times 100 = \frac{\sum \Delta N}{\sum N_{\mathrm{E}} + \sum \Delta N} \times 100 \tag{2}$$

where

F is the percentage of burnup fissions per initial metal atom;
$\sum \Delta N$ is the number of heavy atoms split into smaller nuclei;
$\sum N_0$ is the number of heavy atoms initially present;

and $\sum N_{\mathrm{E}}$ is the number of heavy atoms at the end of irradiation.

In irradiated fuel, $\sum N_{\mathrm{E}}$ can be determined using a combination of mass spectrometry and radiochemical measurement techniques. $\sum \Delta N$ can be derived from an appropriate fission product monitor for which the concentration in the fuel is proportional to the number of heavy atoms split. Commonly used burnup monitors are neodymium isotopes, ^{137}Cs and ^{144}Ce [69–71]. In the literature, ^{148}Nd is recommended as an ideal burnup monitor [72].

8.7.1. Sample dissolution, separation and analyses

8.7.1.1. Hot cell dissolution

A first requirement for an accurate destructive burnup determination and fuel characterization is a quantitative dissolution of the fuel material and the complete recovery of uranium, plutonium, minor actinides and the majority of the fission products in solution. Special attention needs to be paid to the dissolution efficiency of the fission product monitors of interest, such as ^{148}Nd, ^{137}Cs and ^{144}Ce. Figure 81 shows the system used in the hot cell for the dissolution of an irradiated fuel sample for aluminium cladding.

Depending on the amount and the type of fuel and fuel cladding, the fuel sample is dissolved in two or more steps using a mixture of concentrated (8–10M) nitric acid (HNO_3) and hydrofluoric acid (HF). The weight of the remaining fuel residue ought to be <0.5% of the initial fuel weight. In general, the cladding is not dissolved with the fuel. However, when the fuel is confined as a wafer between thin aluminium plates, the fuel as well as the cladding material need to be dissolved. Nitric acid itself is not a good reagent to dissolve pure aluminium, as it forms an inert layer on the surface of the metal, preventing further attack on the underlying layers. Adding a small amount of mercury ions as a catalyst to the nitric acid gives rise to the formation of an amalgam and facilitates dissolution of the aluminium.

The obtained mother solution is diluted to a dose rate of a few millilitres, which is low enough for the solution to be brought out of the hot cell for subsequent separation and analyses in the laboratory.

8.7.1.2. Description of chemical separation

In order to calculate a radiochemical burnup, the concentration of the heavy atoms at the end of irradiation and the concentration of one or more burnup monitors need to be determined. The concentration of these burnup monitors is analysed using different techniques. Caesium-137 and ^{144}Ce are measured via HPGe spectrometry, while the neodymium isotope and heavy atom concentrations are determined using thermal ionization mass spectrometry (TIMS). Prior to the TIMS analysis, it is necessary that uranium, plutonium and neodymium are separated from interfering radionuclides. The chemical separations used

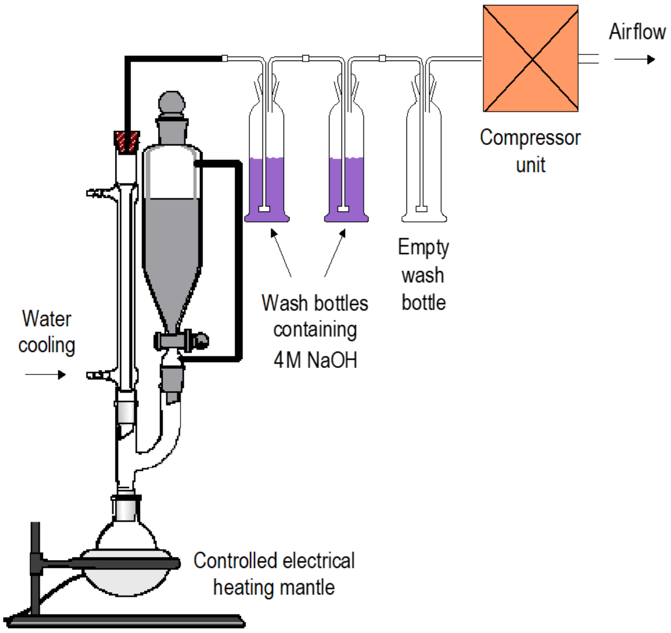

FIG. 81. *Schematic representation of the dissolution set-up for an aluminium clad nuclear fuel sample.*

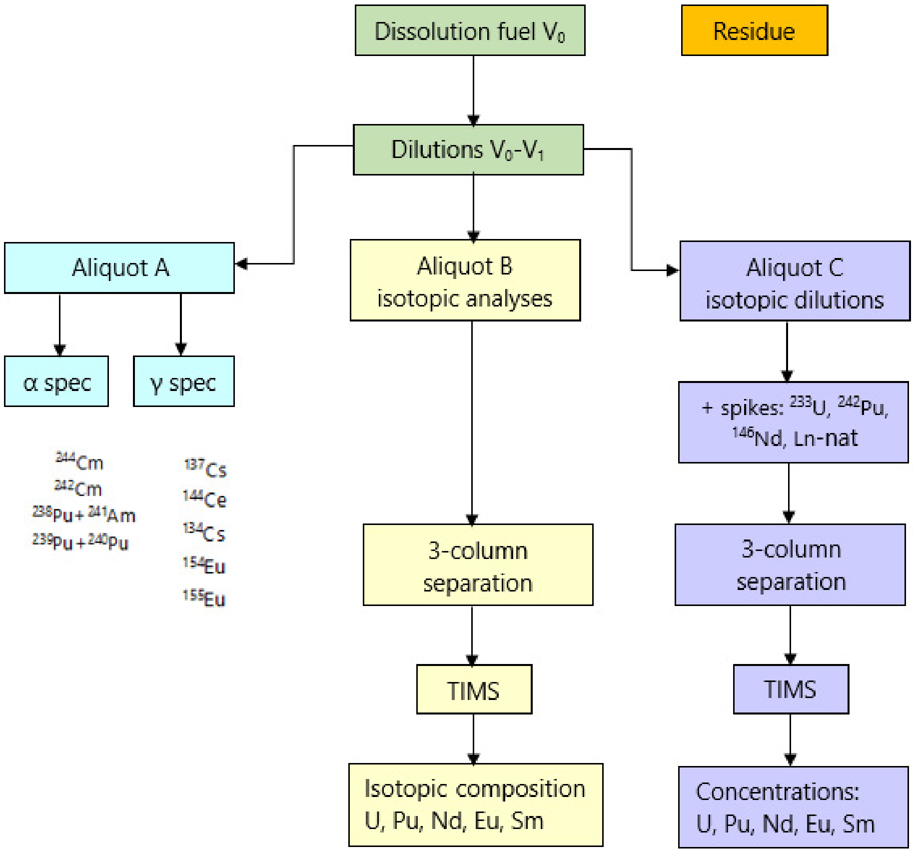

FIG. 82. *Overview of the chemical separations performed on the fuel solution.*

are modifications of the original methodology developed at SCK•CEN, as described in Ref. [69]. The flowchart in Fig. 82 gives a schematic overview of the separations involved.

8.7.1.3. Analytical techniques: Alpha and gamma spectrometry

Alpha spectrometry can be used to analyse ^{242}Cm and ^{244}Cm. Standard and sample sources are prepared by weighing and evaporating a small aliquot on a tantalum disc. From a suitable diluted spent fuel solution, three separate discs are prepared for measurement.

Total alpha measurements are performed using solid scintillation zinc sulphide detectors that are efficiency calibrated against a standard source prepared from a ^{241}Am standard solution with an uncertainty of 1.5% at a 99% confidence level and traceable to a standard of the Physikalisch-Technische Bundesanstalt (PTB).

Alpha spectrometric measurements of the different alpha energy groups (i.e. ^{239}Pu + ^{240}Pu, ^{238}Pu + ^{241}Am, ^{243}Cm + ^{244}Cm and ^{242}Cm) are performed using passivated ion-implanted planar silicon detectors that are energy calibrated and allow the alpha emitters to be identified and their relative contribution to the total alpha activity to be determined.

Gamma spectrometry can be used to analyse ^{137}Cs, ^{144}Ce, ^{154}Eu, ^{155}Eu and ^{241}Am. For gamma spectrometric measurements of the spent fuel solution, three separate 5 mL ampoules are prepared, each containing a decreasing amount of spent fuel. Each ampoule is measured using two different HPGe detectors, resulting in a total of six measurements. The HPGe detectors are energy and efficiency calibrated over an energy range of 60–2000 keV using a gamma ray reference solution with a mixture of ten different radionuclides. The detectors are calibrated using an ELMA 60 standard solution traceable to the National Institute of Standards and Technology (NIST).

8.7.1.4. Thermal ionization mass spectrometry

TIMS can be used to analyse ^{234}U, ^{235}U, ^{236}U, ^{238}U, ^{238}Pu, ^{239}Pu, ^{240}Pu, ^{241}Pu, ^{242}Pu, ^{142}Nd, ^{143}Nd, ^{144}Nd, ^{145}Nd, ^{146}Nd, ^{148}Nd and ^{150}Nd. The isotopic compositions and concentrations of uranium and plutonium are determined using TIMS. For the elements uranium, plutonium and neodymium, a separation is performed prior to the actual measurement to eliminate isobaric interferences. For concentration experiments, the samples are spiked with the appropriate isotopic or elemental standard solutions. An overview of the spikes and their concentrations and uncertainties is given in Table 2 [73].

TABLE 2. OVERVIEW OF THE SPIKES USED FOR TIMS ANALYSIS [73]

Element	Spike
Uranium	Mixed U/Pu spike (U-233) IRM-046c[a], uncertainty regarding the concentration of 0.024% (2s)
Plutonium	Mixed U/Pu spike (Pu-242) IRM-046c[a], uncertainty regarding the concentration of 0.041% (2s)
Neodymium	Nd spike, custom-made from 97.49% enriched Nd-146–neodymium oxide[b], standardized by TIMS by isotopic composition/concentration with natural Nd_2O_3[c], uncertainty regarding the concentration of 1.5% (2s)

[a] From Institute for Reference Materials and Measurements.

[b] From Oak Ridge National Laboratory.

[c] From Specpure, Johnson Matthey Chemicals Ltd.

Purified isotopic composition or concentration fractions of the elements are selected. Typically, 1 μL of the resulting concentrate is evaporated on a rhenium filament, which serves as the ionization source in TIMS.

During the TIMS measurement, attention is paid to possible isobaric interferences resulting from specific isotopes or their oxides. For neodymium, for example, the efficiency of its separation from other lanthanides having isotopes with the same nominal atomic masses as the neodymium isotopes is monitored. Interferences from the ^{142}Ce isotope on ^{142}Nd and from ^{148}Sm or ^{150}Sm on ^{148}Nd or ^{150}Nd, respectively, are monitored by measurement of the signals at $m/z = 140$ for cerium and at $m/z = 149$ or 151 for samarium. Contamination of the separated neodymium fraction with natural neodymium is monitored using the ^{142}Nd peak. Neodymium-142 is not formed by nuclear fission in a spent fuel, although small amounts can be present as a result of (n,γ) reactions of ^{141}Pr. When the isotopic abundance of ^{142}Nd in the spent fuel sample is very low (i.e. <1%), no corrections have to be made for possible contamination by natural neodymium.

8.7.1.5. Inductively coupled plasma mass spectrometry

In the case of plated fuels, the cladding is dissolved together with the fuel material. However, to calculate the radiochemical burnup, it is necessary to know the weight of the fuel material. Therefore, inductively coupled plasma mass spectrometry is used to analyse the concentration of the elements of the cladding. By combining the measurement results with knowledge of the cladding and fuel composition, the total fuel weight can be determined.

8.7.2. Burnup calculations

8.7.2.1. Calculation of $\sum N_E$

The concentrations of the different uranium, plutonium, americium and curium isotopes obtained from analysis are converted from the time of measurement (T_M) to the end of irradiation (T_{EOL}). For the uranium isotopes with half-lives >10^5 years, no corrections have to be made for decay. Plutonium, americium and curium isotopes are corrected for decay and/or for in-pile buildup owing to the decay of higher actinides. The radionuclides for which the concentration is influenced owing to the decay of a parent radionuclide are ^{241}Am, ^{238}Pu and, to a lesser extent, ^{240}Pu.

Combining the number of atoms of uranium, plutonium and minor actinides at the end of irradiation (so-called 'end of life', EOL) gives $\sum N_E$, the total number of heavy atoms present in the sample at EOL.

8.7.2.2. Calculation of $\sum \Delta N$

The total number of heavy atoms that split into smaller nuclei, $\sum \Delta N$, is directly proportional to the number of atoms of a fission product monitor according to Eq. (3):

$$\sum \Delta N = \frac{N_n}{\mathrm{MWFY}_n} \tag{3}$$

where

N_n is the total atom production of isotope n;

and MWFY_n is the mean weighted fission yield for fission product n.

The total atom production N_n for stable fission products, such as the neodymium isotopes, can be derived easily from the chemical analyses without further corrections. The only exception is the isotope ^{144}Nd, which is the daughter product of ^{144}Ce ($t_{1/2}$ = 284.9 days).

When using radioactive fission products such as ^{137}Cs and ^{144}Ce as burnup monitors, an additional correction factor for in-pile and out-pile decay has to be determined, taking into account the irradiation history of the fuel. These correction factors are calculated using Eqs (4) and (5):

$$F_{\text{in-pile}} = \frac{\lambda_n \times \Delta T_1}{1 - e^{-\lambda_n \times \Delta T_1}} \tag{4}$$

$$F_{\text{out-pile}} = \frac{1}{e^{-\lambda_n \times \Delta T_2}} \tag{5}$$

where

T_1 is the duration of the irradiation cycle;

and T_2 is the time elapsed between end of cycle and EOL.

Multiplying the number of atoms at EOL by these correction factors gives the actual number of fissions resulting in the formation of ^{137}Cs and ^{144}Ce.

Two of the neodymium isotopes that are formed as a result of fission show a relatively high cross-section for (n,γ) capture, namely ^{143}Nd (325 b) and ^{145}Nd (42 b), resulting in the formation of ^{144}Nd and ^{146}Nd, respectively. To eliminate the impact on the burnup calculations from the buildup and burnout due to thermal irradiation, these isotopes are summed for the actual burnup calculations (i.e. ^{143}Nd + ^{144}Nd and ^{145}Nd + ^{146}Nd).

Contributions to ^{148}Nd from (n,γ) capture of the short lived ^{147}Nd isotope are negligible for most nuclear power reactor fuels, but may become more prominent for test fuels in reactors with high neutron fluxes.

To calculate an accurate mean weighted fission yield, MWFY$_n$, for each burnup monitor, the mean fissile composition at any given moment of the irradiation has to be known. As this is virtually impossible, a more practical approach is taken and the average fissile composition is derived from the composition of the initial fuel (so-called ‘beginning of life’, BOL) and the composition at the end of irradiations (EOL). For the calculation of MWFY$_n$, only ^{235}U, ^{239}Pu and ^{241}Pu are assumed to undergo fission.

For each burnup monitor, MWFY$_n$ is calculated using Eq. (6):

$$\text{MWFY}_n = \frac{1}{2}\left[\left(\frac{\sum_i N_i \sigma_i Y_i}{\sum_i N_i \sigma_i}\right)_{\text{BOL}} + \left(\frac{\sum_i N_i \sigma_i Y_i}{\sum_i N_i \sigma_i}\right)_{\text{EOL}}\right] \tag{6}$$

where

σ_i is the thermal fission cross-section for ^{235}U, ^{239}Pu and ^{241}Pu;
Y_i is the fission yield for each burnup monitor;

and N_i is the number of fissile atoms at BOL and EOL.

The number of fissile atoms at BOL is calculated from the initial fuel composition data. The concentrations of ^{235}U, ^{239}Pu and ^{241}Pu are obtained from mass spectrometry analysis results and are converted from the time of measurement (T_{M}) to the end of irradiation (T_{EOL}).

8.7.2.3. *Mass balance calculations*

As a measure of the overall quality of the burnup determination, the mass balance, MB, is calculated. MB is calculated by dividing the determined sum of heavy atoms and average number of fissions, as derived from the destructive radiochemical analyses, by the number of heavy atoms initially present in the fuel, as derived from the weight of the analysed fuel sample and the composition of the fuel at BOL (Eq. 7):

$$\mathrm{MB}_1 = \frac{\left(\Sigma N_{\mathrm{E}} + \Sigma \Delta N\right)_{\mathrm{EOL}}}{\left(\Sigma N_0\right)_{\mathrm{BOL}}} \tag{7}$$

9. SPECIALIZED CHARACTERIZATION TECHNIQUES

The techniques discussed in this section are not routinely part of a research reactor fuel PIE campaign, but they are used occasionally when the specific data that they can produce are needed.

9.1. NANOINDENTATION

Because of its finer resolution compared with microindentation, nanoindentation can be applied more effectively to evaluate the mechanical properties of relatively small phases. Traditional tensile testing is often impractical because of the nature, cost or availability of the phases in question. In lieu of tensile testing, quasi-static nanoindentation can be performed. The resulting unloading curves (see Fig. 83) are

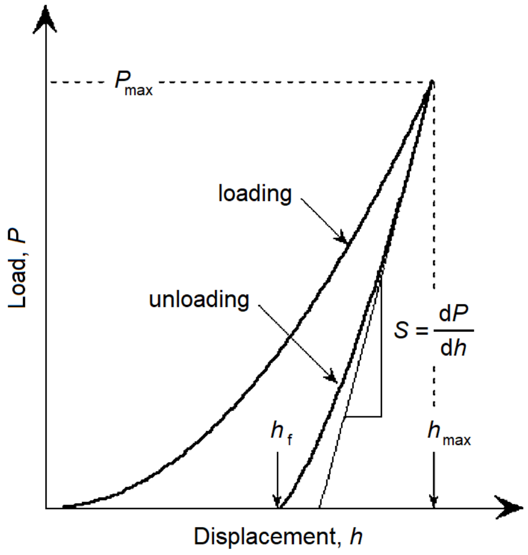

FIG. 83. Typical loading/unloading curve with critical measured parameters.

analysed for elastic modulus and hardness using the method described in Ref. [74]. According to this method, the hardness is dependent on the area function and peak load, in accordance with Eq. (8):

$$H = \frac{P}{A_\mathrm{c}} \tag{8}$$

where

H represents the hardness;
P represents the peak load;

and A_c represents the area function, which is a function of the contact depth.

The reduced modulus is dependent upon the initial slope of the unloading curve and the contact area, according to Eq. (9):

$$E_\mathrm{r} = \frac{\sqrt{\pi}}{2} \frac{S}{A_\mathrm{c}} \tag{9}$$

where

E_r represents the reduced modulus

and S represents the initial slope of the unloading curve.

Young's modulus of the specimen can be calculated from the reduced modulus if both Young's modulus and Poisson's ratio of the indenter tip and Poisson's ratio of the specimen are known, according to Eq. (10):

$$\frac{1}{E_\mathrm{r}} = \frac{1 - v_\mathrm{s}^2}{E_\mathrm{s}} + \frac{1 - v_\mathrm{i}^2}{E_\mathrm{i}} \tag{10}$$

where

E_s represents Young's modulus of the specimen;
v_s represents Poisson's ratio of the specimen;
E_i represents Young's modulus of the indenter tip;

and v_i represents Poisson's ratio of the indenter tip.

For a diamond indenter tip, E_i and v_i are 1140 GPa and 0.07, respectively. The tip area function is calibrated using 100 indentations of varying loads on a fused quartz standard, and the subsequent testing indentations are performed within or above the depth range at which the area function is calibrated.

An example of using nanoindentation to better understand the mechanical properties of phases in a nuclear fuel can be found in Ref. [75]. In order to analyse the phases in question, hot isostatic pressing plates were used in conjunction with solid state diffusion couples for indentation testing. Bulk phases available in the hot isostatic pressing plate samples were used for indentation testing in this experiment. However, several phases of interest were not observed in continuous and sufficiently large quantities and as a result were insufficient for indentation. These phases were fabricated intentionally through diffusion couple experiments on a larger scale so that the interaction layers could be indentation tested. Arrays of indentations on diffusion couples yield a high number of data points and often simultaneous testing of several different materials or phases (Figs 84 and 85). This type of high throughput testing eliminates the necessity for the fabrication of several samples to yield statistically significant data.

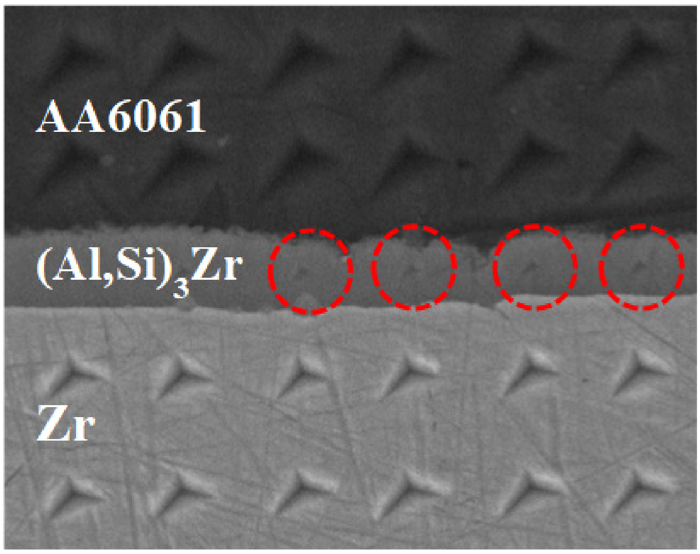

FIG. 84. Scanning electron microscope image of nanoindentations within a 2–3 µm thick interaction layer present at the interface between the cladding and the zirconium diffusion barrier. (Courtesy of INL.)

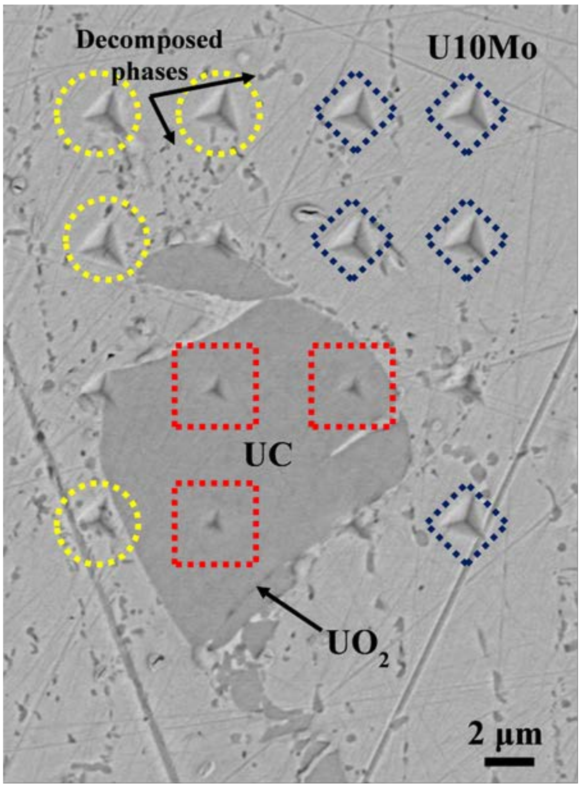

FIG. 85. Nanoindentations in phases found in U–10Mo. (Courtesy of INL.)

9.2. BEND TEST AND LASER SHOCK FOR BONDING

Mechanical testing of unirradiated fuel is used to provide data on the linkages between material chemistry, process parameters, microstructure and mechanical properties. Mechanical property measurements on irradiated fuel provide information on the evolution of properties under irradiation and, along with the results of pre-irradiation material properties testing, allow the impact of fabrication and irradiation variables on material properties to be related to overall fuel performance. Mechanical testing of irradiated fuel also provides critical data needed to understand and analyse the mechanisms of failures in fuel plates, including the fuel failure threshold. Bend testing and hardness testing are typical methods used.

Bond strength measurements focus on answering important questions related to fuel performance. For example, fuel–cladding bond strength measurements provide information about the resistance of fuel to delamination during irradiation, as well as an understanding of the mechanism for delamination, both of which are required to ensure that the cladding and fuel meat maintain intimate contact throughout irradiation. It is also necessary to understand whether the strength of the fuel–cladding bond prior to irradiation (which may be dependent on key fabrication process variables, such as cold rolling, or key microstructural features, such as interaction layer thickness) is correlated with post-irradiation bond strength and resistance to delamination.

Bend testing is used to generate data that support the assessment of geometric stability, mechanical integrity and stable and predictable behaviour of nuclear fuel plates, and it provides inputs for fuel performance modelling and reactor safety analyses. To test the bonding characteristics of the cladding–cladding interface for fuel plates, the bend test is typically performed on material sheared from the perimeter of a fuel plate (i.e. shear drop material). The test involves placing a cladding piece (approximately 6.35 cm by 19 mm wide) in a clamping fixture and bending the sample (at its approximate mid-length) 90° and then 180° (back through the starting position), and then 90° back to the starting position. Bend test samples are then inspected by a qualified visual inspector. Samples that show any visual cladding delamination along the sample edge that was previously adjacent to the candidate plate are rejected.

To test the bonding characteristics of the fuel–diffusion barrier interface in a monolithic fuel plate, the cladding is first removed through dissolution in natrium hydroxide (NaOH) and the test is then performed on the zirconium coated fuel meat alone. Tests are conducted using the four point bending capability provided by a remote load frame in a hot cell. This allows for the bend strength, strain at failure and elastic modulus of the irradiated fuel to be estimated.

Bond strength can also be tested in a hot cell using a combination of two complementary experimental methods — laser shock testing and laser ultrasonic imaging, referred to collectively as the laser shockwave technique. A high energy pulsed laser generates a large amplitude compression wave at the top surface of a specimen. The compressive shock wave travels through the material and is reflected off the free surface as a tensile stress wave that travels back through the specimen. This tensile stress generated at the film or coating interface may debond the film or coating from the substrate if it is sufficiently large. From the specimen response, combined with shockwave propagation models, it is possible to determine the stress required to debond the film or coating from the substrate. These techniques have been adapted for characterizing the adhesion between layers in thicker structures, such as epoxy bonded carbon/carbon composites [76], which is the basis for bond strength measurements in monolithic U–Mo fuel plates.

The critical stresses necessary to create a debond (i.e. the bond strength) as measured by laser shock may be substantially higher than the values measured by low strain rate methods, such as pull testing [77]. The laser shock method relies upon a variety of hardware, software and analysis techniques that are combined into an integrated testing system. The optical energy of the source laser is not an accurate predictor of internal stresses, because the shockwave energy imparted to the specimen by the generation of a confined plasma is difficult to reproduce consistently or calculate. Therefore, the system measures the real time specimen bottom surface velocity during the shock experiments using an optical interferometer, which is more accurate than optical energy measurements. Before and after each laser shot, a pulse echo laser–ultrasonic testing inspection capability integrated into the system is used to determine when a debond has occurred and to measure the through-thickness location of the debond, allowing a more accurate estimate of the internal stress at that location [78].

9.3. THERMOPHYSICAL MEASUREMENTS

Thermophysical property measurements are used to ensure that the internal plate operating temperatures are quantifiable and that temperature dependent behaviour — such as fission gas driven swelling, blistering, thermal stresses and interdiffusion rates — can be predicted. The development of techniques and equipment to evaluate the thermophysical properties of fresh and irradiated fuels and the conduct of measurements on historical samples are important. Measurements include laser flash thermal diffusivity and specific heat capacity as a function of temperature and burnup, and room temperature density measurements as a function of burnup. Metallography, microscopy and chemical analysis are conducted as needed for correlation development [79].

9.3.1. Specific heat capacity

The specific heat capacity of an alloy can be determined using a differential scanning calorimeter [79]. Platinum–rhodium crucibles hold the specimen and reference material for analysis. Ultra-high purity argon cover gas passes through an oxygen gettering furnace. Multiple differential scanning calorimeter runs are recommended, from ambient temperature to approximately 1073 K, each followed by controlled cooling to ambient temperature, with the heating rate being the same for both the heating and cooling cycles. Data are collected during both the heating and cooling cycles, and specific heat capacity is determined using analytical software based on American Society for Testing and Materials (ASTM) Standard E1269 – 05 [80].

9.3.2. Laser flash thermal diffusivity

The laser flash method was first introduced in 1960 to obtain non-contact measurements of thermal diffusivity, specific heat capacity and thermal conductivity for different materials [81]. The laser flash method involves the rapid heating of one surface of a small disc of the material with a single pulse from a laser or other flash energy source, followed by the monitoring of the arrival of the resulting temperature. Details on how to perform this test are provided in Ref. [82] and a schematic diagram illustrating the process is presented in Fig. 86.

Thermal property measurements have been made on U–Mo fuel, using samples extracted from alloys produced with 3, 5, 7, and 10 wt% molybdenum [83], as well as on samples from the AFIP-1 reactor experiment in the ATR [84]. In the latter case, two irradiated U–7Mo/aluminium–silicon matrix dispersion fuel plates (one with an Al–2Si matrix and the other with an AA4043 alloy matrix) were measured. The results from these measurements were used to calculate the thermal conductivity. It was observed that, during irradiation, the thermal conductivity of the dispersion fuel decreased from around 60 $W \cdot m^{-1} \cdot K^{-1}$ to about 10–20 $W \cdot m^{-1} \cdot K^{-1}$.

9.3.3. Dilatometry

A dilatometer can be used to determine the coefficient of linear thermal expansion [79]. Data are collected from room temperature to 1073 K for both the heating and cooling cycles, using ASTM Standard E228 – 06 [85] as a reference. Helium cover gas flowing through the chamber minimizes sample oxidation at elevated temperatures. The values of the instantaneous coefficient and of the average coefficient of linear thermal expansion are determined from the dilatometer curves as a function of temperature.

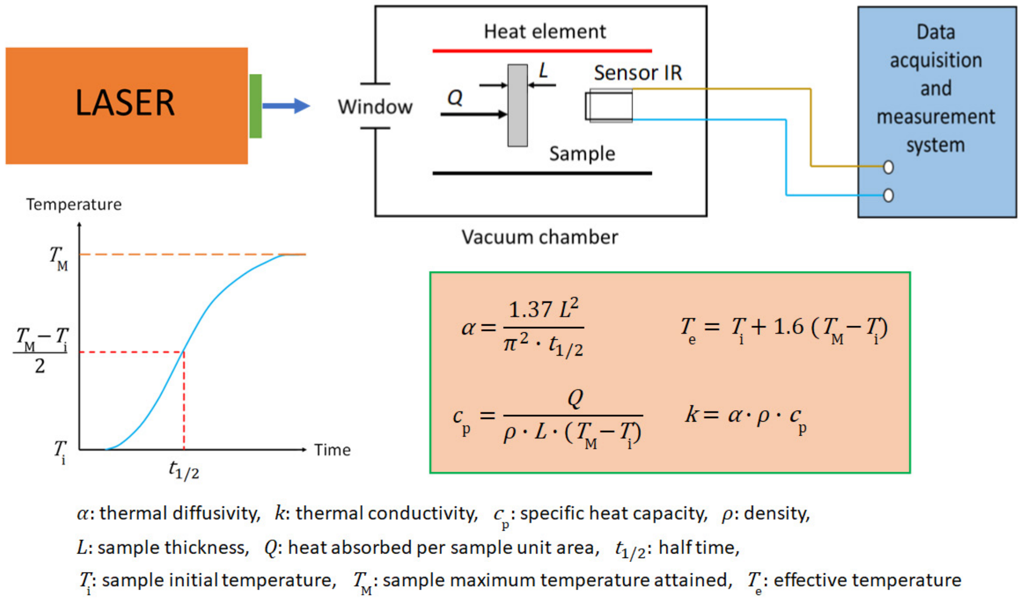

FIG. 86. Principle of the laser flash method.

9.4. SECONDARY ION MASS SPECTROMETRY

In a secondary ion mass spectrometer, an ion beam is focalized on the surface of a solid sample. The resulting interaction leads to a sputtering of the top layers with an emission of atoms and molecules. A small number of these atoms and molecules escape as positively or negatively charged species, called secondary ions, which are then measured in a mass spectrometer.

SIMS techniques have the capacity to determine the isotopic composition of any element with uncertainty levels lower than a few per cent in many applications. With measurement along the sputtering process, SIMS can be used to measure depth profiles starting from the uppermost atomic layers down to several micrometres below the sample surface. The ability of SIMS to record ionic images is widely used to map the distribution of isotopes and then to make correlations with the sample microstructure. On newest instruments, the lateral resolution can be as low as 50 nm with a depth resolution of ~1 nm. Another advantage of SIMS is its sensitivity, which can extend to the parts per billion range for many elements. However, quantitative measurements are not easy and are not always possible, in part because of the significant matrix effects discussed below.

The main components of a SIMS instrument include the following:

(a) A set of primary ion sources, which can be oxygen (O^{2+}, O^-) or caesium (Cs^+).
(b) A primary column used to drive and focalize the primary ion beam on the surface of the sample.
(c) A chamber where the sample is under high vacuum and set to a high voltage.
(d) A secondary column to extract, accelerate and transport secondary ions towards the mass spectrometer.
(e) A mass spectrometer, which can be based on a quadrupole, a magnetic sector or a time of flight mass filter. To date, secondary ion mass spectrometers installed in hot cell facilities are equipped with either quadrupole (Atomika) or magnetic field (CAMECA) systems.
(f) Ion detection systems, with a Faraday cup and electron multiplier for ion counting and a microchannel plate for ion mapping.

A comprehensive view of the SIMS principles and applications can be found in Ref. [86].

To have the capacity to examine irradiated nuclear fuels, radiological shielding and other changes are necessary [87]. Due to the size of the secondary ion mass spectrometer, the operators' radiation protection is ensured by surrounding the sample chamber with lead walls, but not the whole apparatus. Extra shielding has been added at the back of the instrument to allow easy access to the primary and secondary columns (Fig. 87). Additionally, motorized slits and diaphragms have been developed to replace the genuine manual adjustable devices that are no longer accessible because of irradiation and shielding.

The secondary ion mass spectrometer chamber was connected to a glovebox to limit contamination from fuel samples to specific areas. The sample introduction system was adapted with a motorized transfer rod backed up by a manual remote system in case of a defect in the automated part.

Containment, monitoring and cleaning are important because the measurement process begins with sample sputtering. The measurement uses only a small part of the sputtered material, while most of the contamination is deposited on the immersion lens, very close to the fuel sample. Nevertheless, other parts, such as the primary column diaphragm and the entrance slit, have been modified to facilitate their maintenance in the case of contamination.

SIMS techniques have been found to be valuable for the characterization of irradiated nuclear fuels in the past [88–97] and more recently [98–101]. They have been applied to isotopic measurements, isotope mapping and fission gas measurements in light water reactor fuels.

SIMS measurements are strongly affected by matrix effects. Depending on the matrix, the sputtering rate for a given primary beam as well as the ionization rate of the various elements can change significantly. For the analysis of samples where three main phases are present — particles, matrix and interdiffusion layers — data processing is complicated or even impossible. Moreover, because SIMS is sensitive to the oxidation state of the matrix, variable surface oxidation of these phases after sample polishing can lead to a more complicated analysis of results.

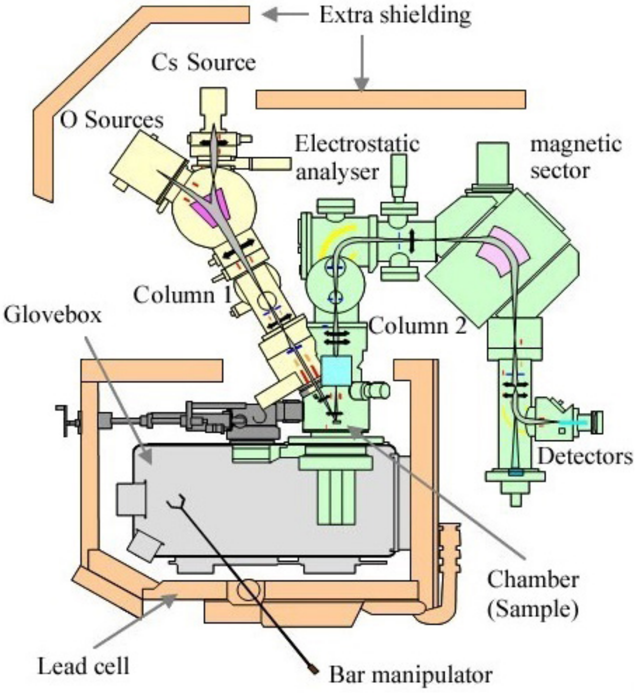

FIG. 87. Scheme of a sector field secondary ion mass spectrometer (CAMECA IMS 6f R). Hot cell adaptation in the CEA LECA-STAR facility. (Adapted from Ref. [87] with permission.)

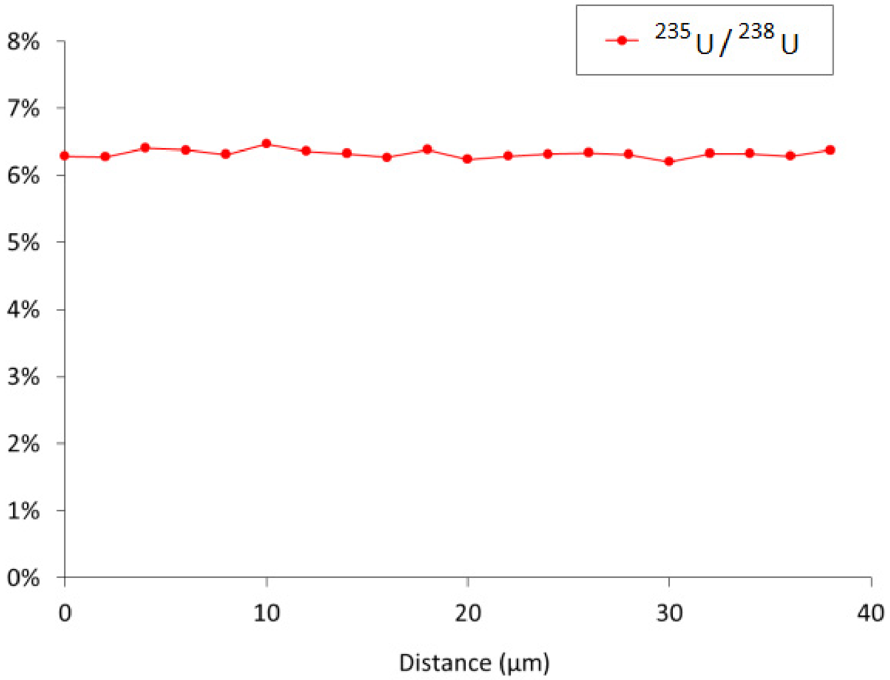

FIG. 88. $^{235}U/^{238}U$ *ratios across a particle and an interdiffusion layer. (Courtesy of CEA.)*

Finally, as mentioned previously, isotopic compositions can be measured by SIMS. Figure 88 shows ^{235}U/^{238}U measurements across a particle and an interdiffusion layer, indicating a stable measurement with a mean ratio slightly higher than 6%.

9.5. NEUTRON DIFFRACTION

Because of their high penetration depth, neutrons can be employed to perform diffraction analysis on bulk samples [102]. The neutron scattering that occurs when a beam of neutrons is applied to a sample can be used to determine the atomic structure of the material. The technique is similar to X ray diffraction, but, owing to different scattering properties, neutron diffraction is complementary to X ray diffraction.

The beam of neutrons that is required for this technique can be produced using a nuclear reactor, and the neutron beam can then be combined with a crystal monochromator and filters to generate the desired neutron wavelength. Neutron diffraction not only has a high penetration depth, but it is also sensitive to light atoms, distinguishes isotopes and does not generate radiation damage.

Neutron diffraction measurements of irradiated fuel element samples have been performed at the Canadian Nuclear Laboratory (CNL) [103, 104]. To perform the measurements on samples with radiation fields that measured, at a distance of 1 m, approximately 600 µSv/h (60 mrem/h) per centimetre length of fuel meat, a special lead filled 'castle' was developed with a thickness of lead sufficient to permit the execution of neutron powder diffraction experiments at the National Research Universal (NRU) reactor without exposing personnel to the high external radiation fields emitted from the specimen. Thermal neutrons enter the castle through a removable port and diffract from the phases within the fuel meat. A segment of the neutron diffraction pattern travels through an 80° scattering aperture and leaves the cell. The aperture can be raised during a measurement and closed and locked to facilitate safe transportation and handling of the fuel element.

To obtain a specimen that would yield an unambiguous diffraction pattern from the crystalline phases in the fuel meat, the aluminium cladding was machined away from the fuel element prior to the diffraction experiment. This allowed for the use of quantitative Rietveld refinement analysis techniques so that the phase volume fractions with the fuel meat could be determined with accuracy. The specimens were subsequently loaded into a specially designed canister fabricated from vanadium, which has a coherent thermal neutron scattering cross-section close to zero, and thus the canister did not contribute any Bragg peaks to the spectrum. The diffraction experiments were conducted in a spectrometer that was equipped with a banana shaped 800 element boron trifluoride position-sensitive detector. An incident monochromatic beam of thermal neutrons was obtained from a silicon single crystal oriented to scatter from the 531 reflection (λ = 1.33 Å) at a take off angle of 92.7°. The position-sensitive detector of the spectrometer was positioned to achieve nominal coverage of the Bragg peaks from 20–100° 2θ.

Prior to conducting any diffraction experiments on an irradiated fuel element, experiments were performed on a calibration specimen of known composition to assess the accuracy of the analysis. This specimen was an unirradiated U–10 wt% molybdenum fuel element that contained γ-phase particles, with a nominal composition of 62 wt% γ-phase (balance aluminium). Data were collected after 12 h exposure, and quantitative analysis of the data using Rietveld refinement showed that the phases present in the specimen were aluminium and γ-U, with trace amounts of UO_2 and α-U. These results compared well with the actual composition of the fuel meat. The results of the analysis of the irradiated sample were compared with the unirradiated sample results (see Fig. 89) to show a reduction in the quantity of the original aluminium and γ-U–Mo phases in the sample during irradiation, and the phases UAl_3, UAl_2 and UAl_4 had formed owing to reactions of the fuel and matrix. The mass fraction of the γ-U–Mo phase had reduced from 60 to 24 wt%, and the unreacted aluminium from 36.5 to 8 wt%.

Neutron diffraction experiments have also been performed on irradiated (U–Mo)/aluminium fuel samples (40% and 80% mean equivalent burnup) at the IVV-2M research reactor in the Russian Federation [105]. One of the goals of the work was to measure lattice parameter changes for the U–Mo fuel and the aluminium matrix as a function of burnup. Some irradiated samples were subsequently annealed from 150°C to 580°C at 50°C increments, and the change in lattice parameter was determined as a function of annealing temperature. The experimental data were obtained over the angle interval from (5–105)° 2θ with a spacing of 0.1°. The results of this work were used to plot the lattice parameter of U–Mo as a function of fuel burnup. Three regions of parameter change were identified: the first region with 0–50% burnup exhibited an increase of the parameter with growing burnup; the second region with up to 75% burnup exhibited little change in parameter; and the third region with burnups higher than 75%, where

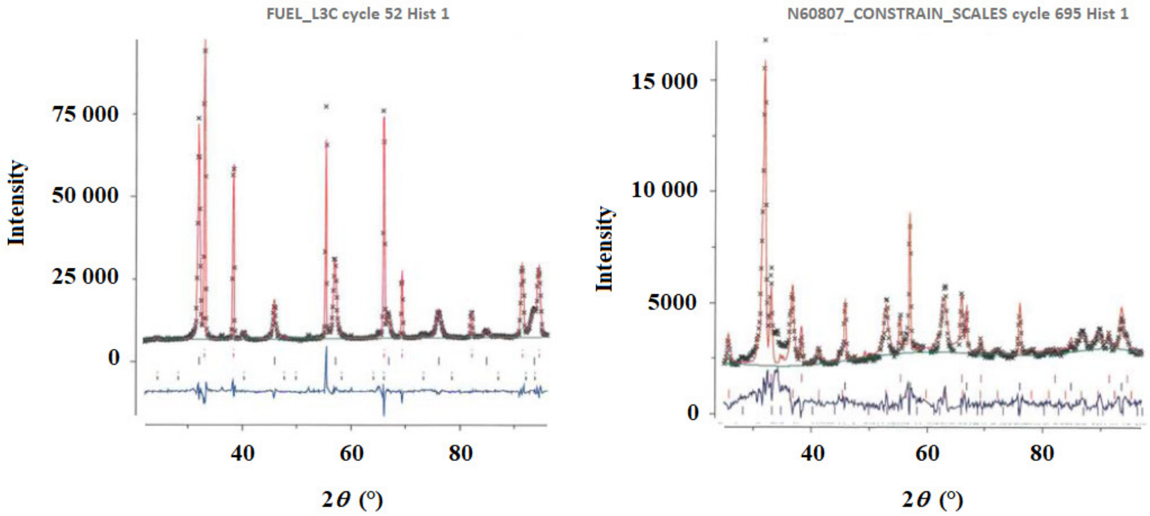

FIG. 89. Neutron powder diffraction patterns of (a) an unirradiated U–10 wt% Mo dispersion fuel element (with nominal overall composition of ~62 wt% γ-U–Mo) and (b) an irradiated U–10 wt% Mo dispersion fuel element (with nominal overall composition of ~24 wt% γ-U–Mo). (Adapted from Ref. [104] with permission from CNL.)

the parameter decreased and reached values relevant to what was observed for unirradiated samples. For the annealed samples, the lattice parameters for both the U–Mo and aluminium decreased monotonically within the range of annealing temperatures employed. The exact changes in the lattice parameters as a function of annealing temperature differed depending on the burnup values for the samples.

9.6. SMALL ANGLE NEUTRON SCATTERING

Small angle neutron scattering utilizes elastic neutron scattering at a small scattering angle to assess the nuclear structure of various materials or isotopes. Examination of materials is performed within a spatial scale of 1–100 nm. A neutron beam radiates a material sample during the measurement. The sample may consist of an aqueous solution or a solid composite material. The neutron beam is scattered elastically by interacting with the sample atomic nucleus and with the magnetic moments of unpaired electrons. The small angle neutron scattering technique is related to the 'scattering length density' and is a measure of the strength of the interaction (i.e. small angle neutron scattering cross-section) of the neutron wave with the nucleus of the sample. Further details of the technique are given in Ref. [106].

The small angle neutron scattering technique can be applied to dispersion fuel irradiated to high burnup levels [107]. The material structure changes and new phases (i.e. a (U–Mo)Al$_x$ interaction layer between an aluminium matrix and the fuel material), as well as gas pores, form in U–Mo/aluminium dispersion fuel under irradiation. All these changes affect the behaviour of U–Mo dispersion fuel, especially for high burnup conditions.

9.7. TEMPERATURE TRANSIENT TESTS

The two methods discussed below require heating of irradiated samples after the irradiation period.

9.7.1. Fission gas release studies

Out of pile tests can be performed to evaluate fuel behaviour and in particular fission product release in cases of unusual fuel temperature, whatever its origin, such as coolant blockage or loss. Temperature transient test results have been reported for U–Mo dispersion fuel samples at CEA Cadarache [61] and for monolithic fuel samples at Pacific Northwest National Laboratory (PNNL) [108]. In these tests, the fission gas release was monitored online. Figures 90 and 91 show schematic views of the devices used for these studies. The figures illustrate that several methods can be used to perform this type of measurement or study. In one case, the furnace was a high frequency induction furnace (Fig. 90), whereas in the other the furnace was the platinum wire wound furnace of a thermogravimetric/differential thermal analysis device (Fig. 91). In the former, the analysis of the released fission gases uses gamma spectrometry and gas μ chromatography situated outside the hot cell [109], while in the latter, the analysis is performed with a mass spectrometer in the hot cell. At CEA, the crucible was made of tungsten, while at PNNL an alumina crucible was used. Nevertheless, both devices used argon as a carrier gas.

These techniques are also applied to other fuels, mainly to simulate accidental conditions, such as loss of coolant [93, 110, 111], for high temperature diffusion experiments [99, 112] and also for some specific measurements, such as the amount of intergranular gas in an irradiated oxide fuel [113, 114].

With this type of device, it is necessary to know the fuel sample temperature for the duration of the test [115]. Irrespective of the system, the release measurement does not take place immediately when this release occurs. Therefore, it is important to design a data processing system that enables the correlation of the fuel temperature and the release time.

Figure 92 shows the release history of ^{85}Kr during a temperature transient test at CEA LECA-STAR on a U–Mo dispersion fuel, obtained with a gamma spectrometry device. The temperature was brought up to 1800°C. Equivalent measurements by μ chromatography showed that xenon, krypton and helium have

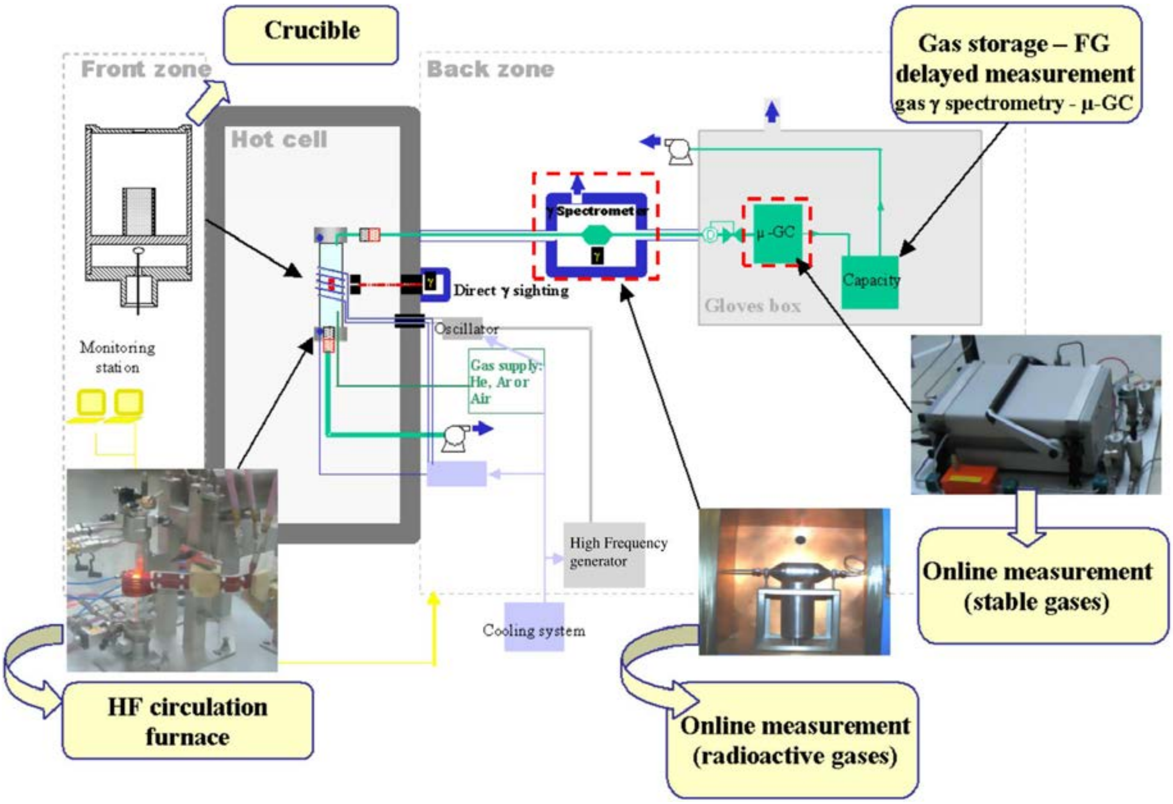

FIG. 90. Schematic diagram of the MERARG-2 loop in the CEA LECA-STAR facility. The furnace is a high frequency (50 kHz) induction furnace surrounding a quartz tube. Online measurement of the fission gas release is performed using a γ spectrometer and a gas μ chromatograph, both situated outside the hot cell. (Reproduced from Ref. [61] with permission.)

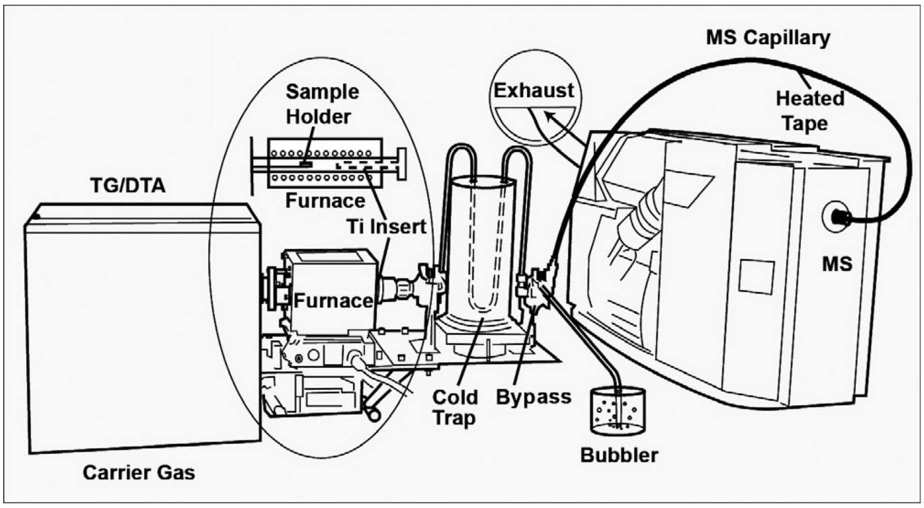

FIG. 91. Scheme of the device used in the PNNL hot cell facility. The furnace is a thermogravimetric/differential thermal analysis (TG/DTA) device with a platinum wire wound furnace surrounding a fused quartz tube. On-line measurement of the fission gas release uses a mass spectrometer (MS) inside the hot cell (Ti — titanium). (Reproduced from Ref. [108] with permission.)

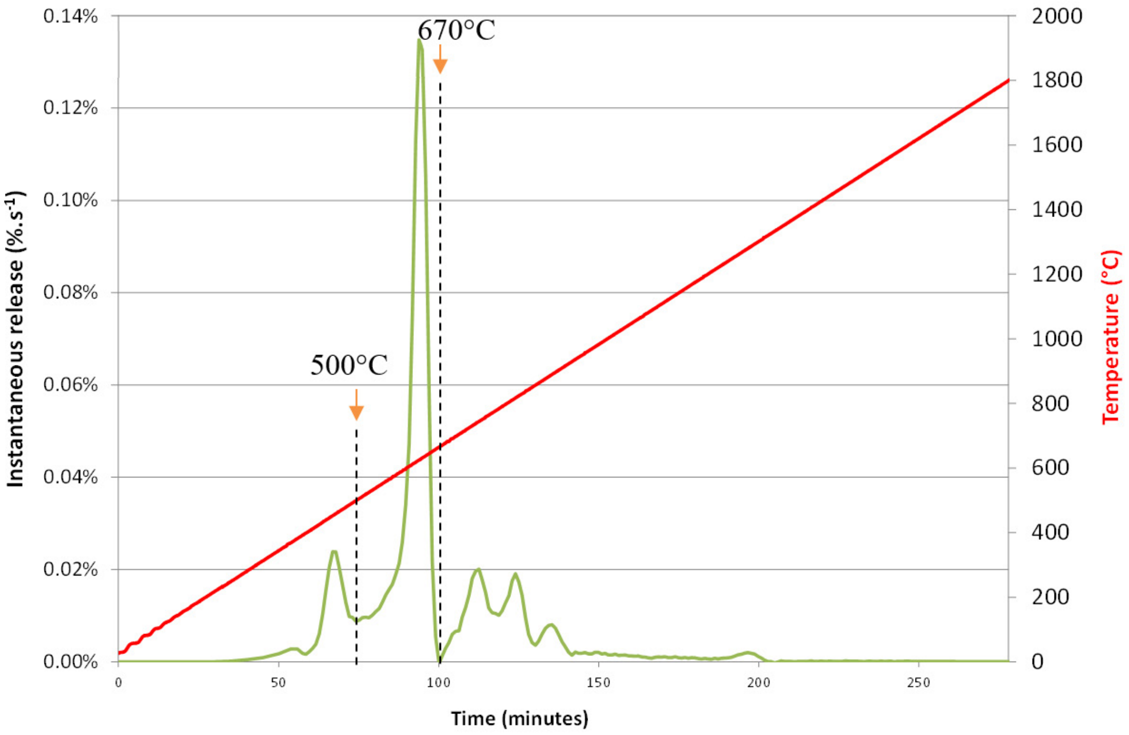

FIG. 92. Temperature ramp in a test at CEA LECA-STAR and ^{85}Kr release history. The dashed lines after the two first release peaks correspond to the maximum temperatures assigned to other tests followed by post-test examinations of the specimens. (Adapted from Ref. [61] with permission.)

the same release history, with the main release event occurring at ~620°C. These gases were completely released when the temperature reached 1350°C. Nevertheless, H_2 release was still detected at the end of the test. This is understood as being an effect of the decomposition, at high temperature, of the aluminium hydroxides formed by corrosion of the external surface of the cladding during the fuel irradiation.

Figure 93 shows the fission gas release as a function of the temperature during a temperature transient test on an irradiated monolithic fuel sample at PNNL. The fission gas release appears to be similar to that in Fig. 92, with the difference being that the main peak is at slightly higher temperatures (651°C instead of 620°C). The differential thermal analysis and thermogravimetric results in Fig. 94 illustrate the onset of cladding melting at (612 ± 5)°C and the onset of an exothermic reaction at (654 ± 5)°C in the main release peak vicinity, giving some indication of the release mechanisms.

After the temperature transient tests in this type of experiment, it is valuable to examine the specimen using the other techniques described in this publication, such as optical microscopy, SEM and EPMA. Figure 95 shows a selection of the EPMA maps obtained from the polished surface of a sample that had been submitted to a temperature transient test stopped at 670°C after the main fission gas release peak [61]. Together with the associated quantitative analyses using image analyses to derive semiquantitative profiles from these maps, it was possible to deduce that during the test there had been a massive diffusion of the cladding elements inside the plate and the remaining aluminium matrix had disappeared.

9.7.2. Blister testing

Blister anneal testing is a destructive characterization method used to detect defects, non-uniform and excessive porosity, and the coalescence of gas bubbles. The test has been applied as a tool for measuring adhesion strength in thin coatings [116, 117]. Blisters themselves can be indicative of an excess of defect

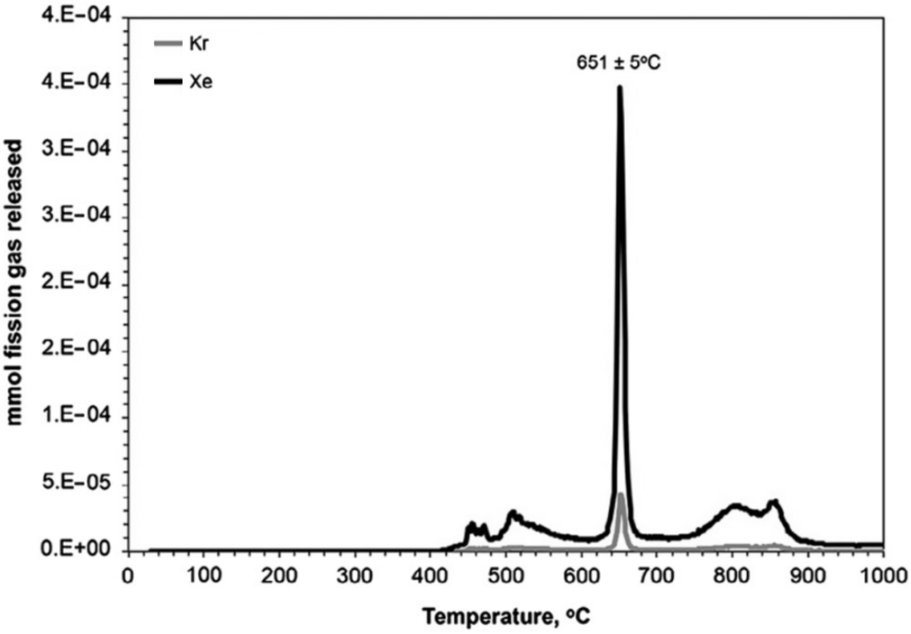

FIG. 93. Fission gas release as a function of temperature during a heating test on an irradiated monolithic fuel at PNNL. (Adapted from Ref. [108] with permission.)

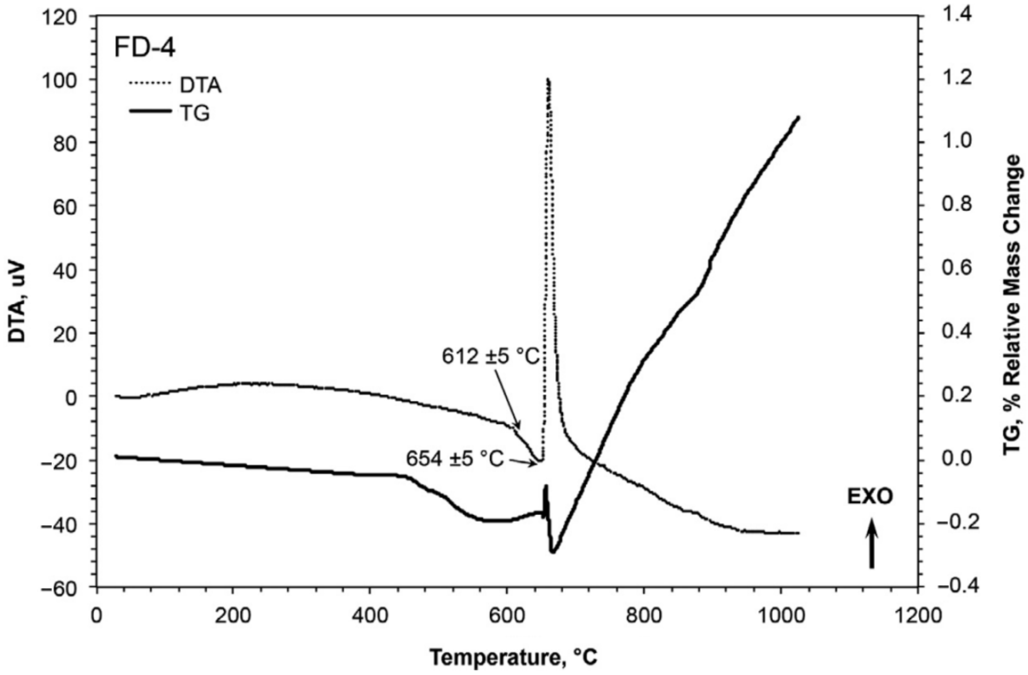

FIG. 94. Differential thermal analysis and thermogravimetric results for the same PNNL test as in Fig. 93. (Adapted from Ref. [108] with permission.)

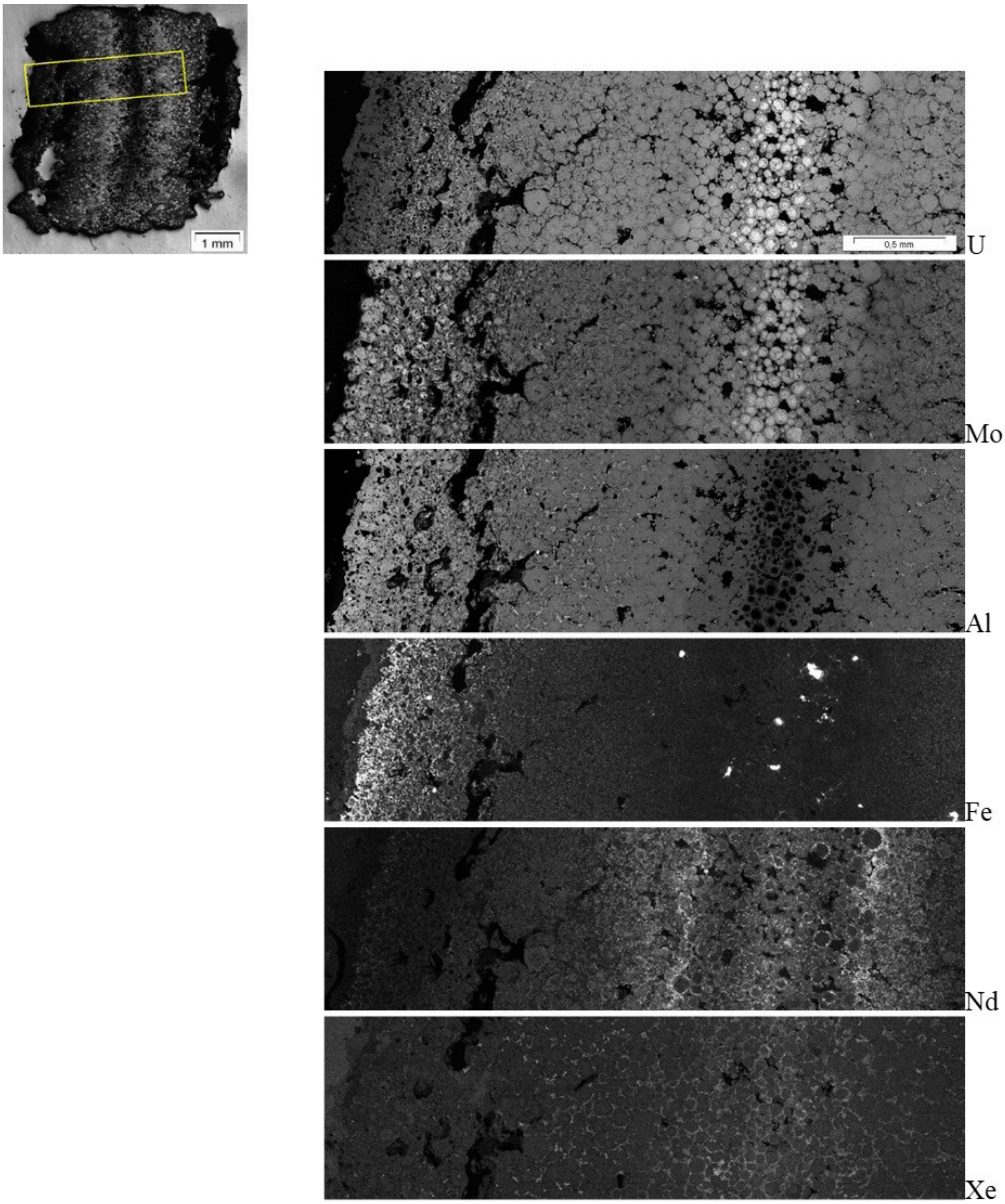

FIG. 95. EPMA maps obtained at CEA LECA-STAR from the polished surface of an irradiated U–Mo dispersed fuel sample after a test was stopped when the temperature reached 670°C (i.e. just after the main fission gas release peak). (Adapted from Ref. [61] with permission.)

and impurity sites for hydrogen gas coalescence in cast materials. Blister size, shape and location can be characterized to determine initiation sites and failure mechanisms in plate type nuclear fuels.

The Nuclear Regulatory Commission's report, NUREG-1313 [118], pertaining to research reactor fuel qualification, states: “The resistance of a fuel plate to blistering (caused by gas bubble agglomeration) when it is heated to elevated temperatures has been used as a measure of fuel plate stability for many years in the development of dispersion fuels”. Although blistering in U–10Mo monolithic fuel may involve different mechanisms than for dispersion fuels, blister threshold temperatures and morphologies have been evaluated for a range of fission densities using miniature and full size test plates.

Blister threshold temperature data are obtained by heating irradiated fuel plates at successively higher temperatures of between 350°C and 550°C. A plate is held at temperature for a period of time (20 min), the furnace is turned off, and then the plate is moved from the furnace to the hot cell (an argon atmosphere at ~30°C) and examined visually for blisters. If no blister is observed, the plate is returned to the still warm (~70–130°C) furnace to be heated further in 25°C increments. This process is repeated until a blister is observed. The test is then concluded, and the temperature at which the blister was first observed is recorded as the blister threshold temperature.

The visual examination for the detection of blisters is accomplished using a telescopic camera lens, binoculars and additional local in-cell lighting (Fig. 96). Verification of the presence or absence of blisters is provided by at least two observers. Photographs of both surfaces of the plate are taken between each blister anneal cycle to provide a record of blisters and other changes in the appearance of the plate.

The inherent temperature uncertainty of the system and test protocol is ±13°C (comprising the accuracy of the thermocouple and controller/readout, furnace temperature uniformity and test environment noise) and ±24°C (introduced by the temperature increment increase), respectively.

Blister test results are reported, for example, in Refs [2, 119]. Blister threshold measurements were completed in conjunction with the Extended Life Aluminide Fuel (ELAF) testing campaign in the 1980s [119]. The ELAF programme irradiated UAl_2 fuel with 40, 45 and 50 vol.% fuel meat loading to fuel meat fission densities of up to 3×10^{21} fissions/cm^3, along with 50 vol.% UAl_x reference plates (UAl_x in this reference denotes the mass composition of UAl_2 and UAl_3). These fuel plates contained 1.4–1.5 wt% B_4C as a burnable absorber. During irradiation, ^{10}B generates helium. Because of the additional helium gas inventory and high fission density, blister testing of the ELAF plates is likely to represent the most

(a)

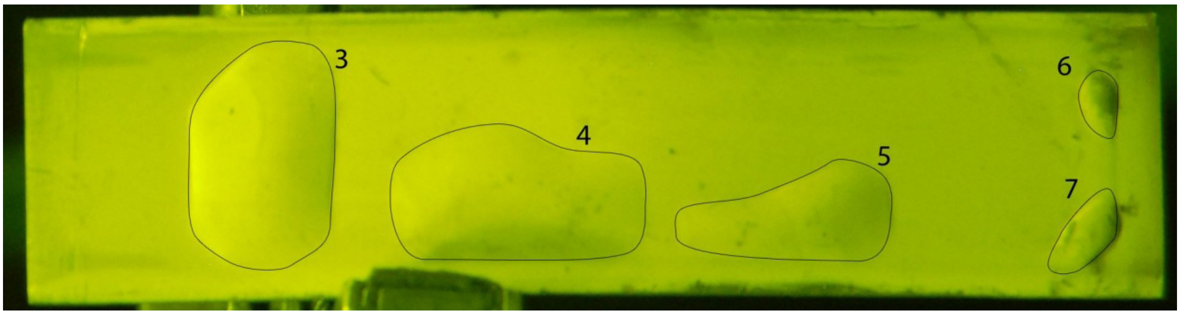

(b)

FIG. 96. Visual examination of two miniplates after blister tests. The blisters are outlined to highlight the blister location and extent. (Courtesy of INL.)

severe testing conditions for aluminide fuel blister threshold temperature. Many of the blister threshold data on UAl_x fuels that preceded the ELAF programme are summarized in Ref. [120]. These fuel plates also contain B_4C as a burnable poison.

References [121, 122] report the testing of aluminide fuel plates in a sodium bonded experimental capsule to compare the blister threshold temperature occurring in the reactor to that measured in post-irradiation testing. Although sample temperatures sufficient to test in-pile blistering were not achieved, post-irradiation out of pile blister threshold temperature data were collected. The fission densities reported in Ref. [120] differ from those reported in Refs [121, 122]. Whitacre published similar data in 1990 [123].

The data reported in Ref. [124] for aluminide fuel mini-plates that did not contain boron, irradiated in the Oak Ridge Research Reactor, provide additional information, summarized as ranges of blister threshold temperature for ranges of fission density.

U_3Si_2 was developed as a high density fuel for the conversion of research reactors that require a uranium density in the fuel meat of up to 4.8 g U/cm^3. Many of the low power research reactors were successfully converted to LEU using this fuel type. The blister threshold behaviour of U_3Si_2 is similar to that of UAl_x, with both being intermetallic compounds. The blister threshold temperature of U_3Si_2 is relatively insensitive to fuel meat fission density at the qualified fuel density limit of 4.8 g U/cm^3. Most of the available U_3Si_2 blister threshold data were acquired from testing of fuel plates from the qualification irradiation of six fuel test assemblies in the Oak Ridge Research Reactor [125]; the results are also reported in Refs [126–130].

9.8. ATOM PROBE TOMOGRAPHY

The very small scale (e.g. nanometre or atomistic) chemical structure of a material can affect fuel behaviour. For example, nuclear fuel swelling can be affected by very low length scale phenomena. It is

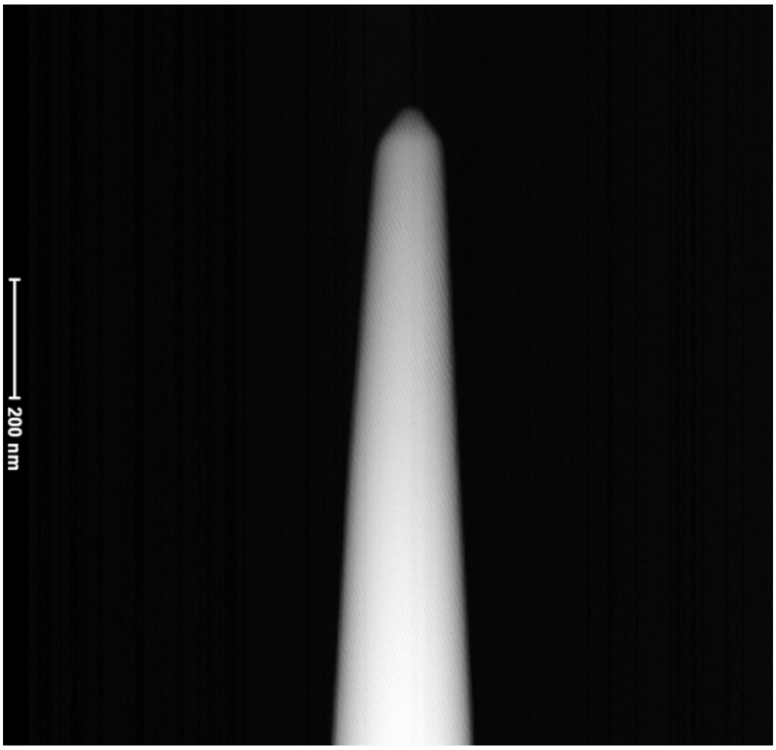

FIG. 97. Scanning electron microscope image of the APT tip of irradiated U–10Mo fuel. (Courtesy of INL.)

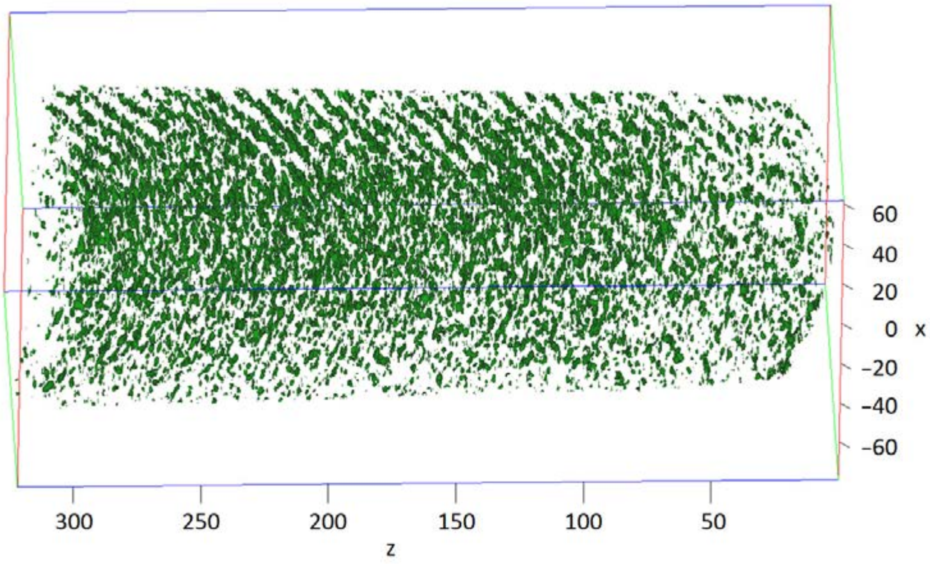

FIG. 98. APT 3-D reconstruction showing the distribution of xenon atoms in an irradiated U–10Mo sample containing a fission gas bubble superlattice. (Courtesy of INL.)

important to trace the earliest stages of microstructural evolution in an irradiated nuclear fuel or material (e.g. clustering, nucleation, precipitate growth). Atom probe tomography (APT) is a versatile tool that allows the characterization of 3-D information at the subnanometre length scale.

APT extracts individual atoms from the surface of needle-like specimens via controlled field ionization and evaporation (Fig. 97) [131]. The evaporated ions are accelerated towards a position sensitive detector that records the position and time of flight, atom by atom. A reconstruction is generated that has an accuracy of a few ångströms. The time of flight determines the chemical identity of the ions (Fig. 98). An example of the utilization of APT would be a case where small precipitates in a material need to be analysed. This tool can be employed to analyse the atom size distribution, density, solute concentrations in the matrix and morphology of a nuclear fuel or material. Some preliminary data from analysis of irradiated U–Mo fuel showed where solid and gaseous fission products were located in the microstructure, with xenon being a fission gas of particular interest (Fig. 98).

10. CONCLUSIONS

The set of post-irradiation techniques to be used in the examination of irradiated fuels depends on the questions that need to be answered. The researcher needs to apply a subset of the techniques described above to gather the relevant data. Which techniques are selected depends on criteria such as availability (not all techniques are available at all laboratories), the specific problem to be addressed and available materials. An alternative is to transport the samples to other laboratories to apply techniques that are only available there. Given the cost and time required for transportation, obtaining as much information as possible to pass on to the external laboratory is the best way to proceed.

The researcher generally has to apply multiple techniques to arrive at a correct and reliable interpretation. Unexpected results need to be verified carefully before new theories are formulated. In particular, the novel techniques that have become available or accessible with irradiated fuels over the last decade have created possibilities for complementing the work already carried out over the last 50 years.

This creates opportunities for improved understanding, but also carries the risk of diverting away from the purpose of the irradiations and post-irradiation examinations, which is the qualification or improvement of research reactor fuel.

It is advisable to perform non-destructive and basic destructive characterizations (optical microscopy, SEM, EPMA) prior to the application of more advanced techniques. When a mechanistic understanding is targeted, the level of comprehension ought to be increased gradually, starting with NDT, moving onto classical destructive testing, and then employing more advanced destructive testing and specialized techniques. A typical example is the way in which the pillowing of U–Mo–Al fuel is addressed. Non-destructive thickness measurements reveal that at high power/burnup locations in U–Mo–Al fuel plates, a significant increase in the thickness of the plate is present. By performing optical and electron microscopy on samples taken at high power/burnup locations, the pillowing is shown to originate in the formation of large cavities between the interaction layer and the matrix. An accumulation of fission products, including fission gas, at the interface between the interaction layer and the matrix is demonstrated by EPMA. Puncturing of a pillow shows that the cavities are gas filled. X ray and neutron diffraction suggests that the interaction layer is amorphous, as confirmed by TEM. This amorphous nature is seen as part of the cause of the formation of defects. A deeper understanding is still being acquired using more advanced techniques.

All microscopy techniques require careful sample preparation and the identification of artefacts introduced by the preparation process. A good example of this is the damage to the surface layers of polished samples that is revealed when a transverse section is taken using FIB technology. The use of ions for sample preparation can also induce defects, particularly when transmission electron microscopy is involved. Polishing artefacts (and in general sample preparation artefacts) can be avoided, but this sometimes requires a trial and error approach. When observations are made that are difficult to correlate with other results, it is often a good policy to first investigate whether defects induced during sample preparation are involved.

The handling of highly radioactive materials in post-irradiation work requires either hot cells for the protection of the operators or sample miniaturization to limit the radiation level and contamination risks. The use of FIB allows samples to be taken that are small enough to be handled without radiation protection and sometimes even outside the controlled area. This opens up possibilities for using techniques that were previously only available with non-active materials. One example is the use of synchrotron X ray sources in PIE, such as the work performed at the Advanced Photon Source at ANL on FIB cubes of irradiated U–Mo fuel produced at INL [132].

PIE results are often fed into computer models to improve understanding of the phenomenology of in-pile fuel behaviour. Data are used to calibrate and validate models and eventually expand their domain of validity. Likewise, the preparation and interpretation of experimental work, such as irradiations or PIE, can be influenced by modelling irradiation phenomena and fuel behaviour. Data gaps in the establishment and validation of the predictive power of models can be filled using suitable experimental techniques.

Validation of experimental techniques is sometimes the subject of a so called ‘round robin exercise’. These exercises revolve around the examination of a single sample, or highly similar samples, by different laboratories, each using its own experimental approach. The results are compared, and flaws in procedures can be identified and corrected. This highlights the value of collaborative research. Such collaboration across different laboratories also enables complementary studies on the same material. Such complementary work can be performed with or without overlap. However, it is recommended to provide overlapping results to link the results together.

As many of the properties of fuels undergo significant evolutions during irradiation, it is vital to apply a systematic approach to sampling and examinations. A series of samples with a systematic variation in burnup–fission density, power–fission rate, composition, microstructure, etc. is needed to establish how certain fuel properties change. The simultaneous modification of too many parameters will make it difficult to identify differences across a series, and in turn make it difficult to separate phenomena and parameterize models.

REFERENCES

[1] INTERNATIONAL ATOMIC ENERGY AGENCY, Applications of Research Reactors, IAEA Nuclear Energy Series No. NP-T-5.3, IAEA, Vienna (2014).

[2] LEENAERS, A., Surface-engineered Low-enriched Uranium–Molybdenum Fuel for Research Reactors, PhD Thesis, University of Ghent/SCK•CEN, Ghent (2014).

[3] MEYER, M.K., et al., Irradiation performance of U–Mo monolithic fuel, Nucl. Eng. Technol. **46** (2014) 169–182.

[4] REST, J., "A microstructurally-based model for the evolution of irradiation-induced re-crystallization in U–Mo monolithic and Al-dispersion fuels", Proc. 26th Int. Mtg on Reduced Enrichment for Research and Test Reactors, Vienna, 7–12 November 2004, Argonne Natl Lab., IL (2004).

[5] OLANDER, D.R., Fundamental Aspects of Nuclear Reactor Fuel Elements, TID-26711-P1, ERDA Technical Information Center, Oak Ridge, TN (1976).

[6] IDAHO NATIONAL LABORATORY, Specification for Experimental Plates for the RERTR-11A and RERTR-ALT Campaigns, Idaho Natl Lab., ID (2012).

[7] WIGHT, J.M., et al., "Testing and Acceptance of Fuel Plates for RERTR Fuel Development Experiments", Proc. 30th Int. Mtg on Reduced Enrichment for Research and Test Reactors, Washington, 5–9 October 2008, Idaho Natl Lab., ID (2008).

[8] WIGHT, J.M., Fuel Plate Specification for the AFIP-1 Fuel Irradiation in the ATR Fabricated at BWXT, Idaho Natl Lab., ID (2008).

[9] WOOLSTENHULME, N.E., et al., Fabrication of Contoured Monolithic Foils, Idaho Natl Lab., ID (2008).

[10] TAYLOR, S.C., RERTR 12 Fuel Plate Ultrasonic Debond and Mini-Clad Thickness Test Results, Idaho Natl Lab., ID (2012).

[11] TAYLOR, S.C., COTTLE, D.L., JUE, J.F., RERTR Program Review of Ultrasonic Fuel Characterization, Idaho Natl Lab., ID (2007).

[12] WINTERGERST, M., DACHEUX, N., DATCHARRY, F., HERMS, E., KAPUSTA, B., Corrosion of the AlFeNi alloy used for the fuel cladding in the Jules Horowitz research reactor, J. Nucl. Mater. **393** (2009) 369–380.

[13] SACRISTAN, P., et al., "MTR fuel plate qualification in OSIRIS reactor", Proc. 26th Int. Mtg on Reduced Enrichment for Research and Test Reactors, Vienna, 7–12 November 2004, Argonne Natl Lab., IL (2004).

[14] SACRISTAN, P., et al., "A full programme for a world wide qualified UMo fuel", Trans. 4th Int. Topical Mtg on Research Reactor Fuel Management, Colmar, 19–21 March 2000, European Nuclear Society, Berne (2000) 93–98.

[15] RIPERT, M., et al., "Results of the IRIS4 irradiation in OSIRIS reactor", Proc. 31st Int. Mtg on Reduced Enrichment for Research and Test Reactors, Beijing, 1–5 November 2009, Argonne Natl Lab., IL (2009).

[16] WACHS, D.M., et al., Swelling of U–7Mo/Al–Si dispersion fuel plates under irradiation — non-destructive analysis of the AFIP-1 fuel plates, J. Nucl. Mater. **476** (2016) 270–292.

[17] TAYLOR, S.C., KRAFT, N.C., Ultrasonic Transducer, US Patent 2007/0000329 A1, 2007.

[18] INTERNATIONAL ATOMIC ENERGY AGENCY, Review of Fuel Failures in Water Cooled Reactors, IAEA Nuclear Energy Series No. NF-T-2.1, IAEA, Vienna (2010).

[19] SMITH, M.L., BIGNELL, L.J., ALEXIEV, D., MO, L., Sipping test: checking for failure of fuel elements at the OPAL reactor, Nucl. Eng. Technol. **42** (2010) 125–130.

[20] VAN DEN BERGHE, S., et al., Swelling of U(Mo) dispersion fuel under irradiation — non-destructive analysis of the SELENIUM plates, J. Nucl. Mater. **442** (2013) 60–68.

[21] VAN DEN BERGHE, S., et al., Swelling of U(Mo)–Al(Si) dispersion fuel under irradiation — non-destructive analyses of the LEONIDAS E-FUTURE plates, J. Nucl. Mater. **430** (2012) 246–258.

[22] LEHMANN, E.H., VONTOBEL, P., HERMANN, A., Non-destructive analysis of nuclear fuel by means of thermal and cold neutrons, Nucl. Instrum. Methods Phys. Res. A **515** (2003) 745–759.

[23] INTERNATIONAL ATOMIC ENERGY AGENCY, Advanced Post-irradiation Examination Techniques for Water Reactor Fuel: Proceedings of a Technical Committee Meeting held in Dimitrovgrad, Russian Federation, 14–18 May 2001, IAEA-TECDOC-CD-1277, IAEA, Vienna (2002) CD-ROM.

[24] CRAFT, A.E., et al., Neutron radiography of irradiated nuclear fuel at Idaho National Laboratory, Phys. Procedia **69** (2015) 483–490.

[25] CRAFT, A.E., WILLIAMS, W.J., ABIR, M.I.K., WACHS, D.M., AFIP-7 Tomography — 2013 Status Report, Idaho Natl Lab., ID (2013).

[26] UNIVERSITY OF CAMBRIDGE, Optical Microscopy and Specimen Preparation, Metallographic Specimen

Preparation (2019),
http://www.icbl.hw.ac.uk/learnem/doitpoms/OpticalMicroscopy/metallography.htm

[27] VANDER VOORT, G.F. (Ed.), Metallography and Microstructures, ASM Handbook, Vol. 9, ASM International, Materials Park, OH (2004).

[28] GEELS, K., FOWLER, D.B., KOPP, W.U., RUCKERT, M., Metallographic and Materialographic Specimen Preparation, Light Microscopy, Image Analysis and Hardness Testing, ASTM International, West Conshohocken, PA (2007).

[29] LEENAERS, A., et al., Post-irradiation examination of uranium–7 wt% molybdenum atomized dispersion fuel, J. Nucl. Mater. **335** (2004) 39–47.

[30] EVANS, J.H., "Remote metallography", Interpretive Techniques for Microstructural Analysis, Proceedings of a Symposium (McCALL, J.L., FRENCH, P.M., Eds), Plenum Press, Minneapolis, MN (1977).

[31] HUET, F., MARELLE, V., NOIROT, J., SACRISTAN, P., LEMOINE, P., "Full-sized plates irradiation with high UMo fuel loading — final results of IRIS 1 experiment", Proc. 25th Int. Mtg on Reduced Enrichment for Research and Test Reactors, Chicago, 5–10 October 2003, Argonne Natl Lab., IL (2003).

[32] DUBOIS, S., et al., "Comprehensive overview on IRIS program: Irradiation tests and PIE on high density UMo/Al dispersion fuel", Trans. 11th Int. Topical Mtg on Research Reactor Fuel Management and Meeting of the International Group on Research Reactors, Lyon, 11–15 March 2007, European Nuclear Society, Brussels (2007).

[33] LEENAERS, A., et al., "Post-irradiation examination of AlFeNi cladded U_3Si_2 fuel plates irradiated under severe conditions", Trans. 11th Int. Topical Mtg on Research Reactor Fuel Management and Meeting of the International Group on Research Reactors, Lyon, 11–15 March 2007, European Nuclear Society, Brussels (2007).

[34] GROUPEMENT NATIONAL DE MICROSCOPIE ÉLECTRONIQUE À BALAYAGE ET DE MICROANALYSES, Microscopie Électronique à Balayage et Microanalyses, (BRISSET, F., REPOUX, M., Eds), EDP Sciences, Les Ulis, France (2008).

[35] ZACHARIE-AUBRUN, I., BLAY, T., "New capabilities of analyses with a versatile nuclearized dual beam", Proc. 2016 Plenary Mtg of the European Working Group "Hot Laboratories and Remote Handling", Karlsruhe, 2–6 October 2016 (2016).

[36] LEENAERS, A., VAN RENTERGHEM, W., VAN DEN BERGHE, S., High burn-up structure of U(Mo) dispersion fuel, J. Nucl. Mater. **476** (2016) 218–230.

[37] LEENAERS, A., et al., Post-irradiation examination of AlFeNi cladded U_3Si_2 fuel plates irradiated under severe conditions, J. Nucl. Mater. **375** (2008) 243–251.

[38] SCHWARTZ, J., KUMAR, M., ADAM, B.L., FIELD, D.P., Electron Backscatter-Diffraction in Materials Science, Springer, Berlin (2009).

[39] GROUPEMENT NATIONAL DE MICROSCOPIE ÉLECTRONIQUE À BALAYAGE ET DE MICROANALYSES, EBSD: Analyse par Diffraction des Électrons Retrodiffusés, Applications et Techniques Couplées, (BRISSET, F., Ed.), EDP Sciences, Les Ulis, France (2015).

[40] INTERNATIONAL ATOMIC ENERGY AGENCY, Advances in Fuel Pellet Technology for Improved Performance at High Burnup, IAEA-TECDOC-1036, IAEA, Vienna (1998).

[41] TEAGUE, M., GORMAN, B., MILLER, B., KING, J., EBSD and TEM characterization of high burn-up mixed oxide fuel, J. Nucl. Mater. **444** (2014) 475–480.

[42] JADERNAS, D., TEJLAND, P., "Electron backscatter diffraction of nuclear materials", Proc. Microscopy & Microanalysis 2014, Hartford, 3–7 August 2014, Microsc. Microanal. **20** (2014) Suppl. 3, 1804–1805.

[43] RUDMAN, K., et al., Three-dimensional characterization of sintered UO_{2+x}: Effects of oxygen content on microstructure and its evolution, Nucl. Technol. **182** (2012) 145–154.

[44] ILTIS, X., GEY, N., CAGNA, C., HAZOTTE, A., SORNAY, P., Microstructural evolution of uranium dioxide following compression creep tests: an EBSD and image analysis study, J. Nucl. Mater. **456** (2015) 426–435.

[45] CLARKE, A.J., et al., Microstructural evolution of a uranium–10 wt.% molybdenum alloy for nuclear reactor fuels, J. Nucl. Mater. **465** (2015) 784–792.

[46] VANNI, F., et al., "Characterization of ALD and PVD coated U(Mo) powders for EMPIRE experiment", Proc. 37th Int. Mtg on Reduced Enrichment for Research and Test Reactors, Antwerp, 23–27 October 2016, Argonne Natl Lab., IL (2016).

[47] JADERNAS, D., et al., Microstructural characterization of as-fabricated and irradiated U–Mo fuel using SEM/EBSD, J. Nucl. Mater. **509** (2018) 1–8.

[48] GIANUZZI, L.A., STEVIE, F.A., A review of focused ion beam milling techniques for TEM specimen preparation, Micron **30** (1999) 197–204.

[49] VOLKERT, C.A., MINOR, A.M., Focused ion beam microscopy and micromachining, microscopy and micromachining, MRS Bull. **32** (2007) 389–395.

[50] MILLER, B.D., et al., Advantages and disadvantages of using a focused ion beam to prepare TEM samples from irradiated U–10Mo monolithic nuclear fuel, J. Nucl. Mater. **424** (2012) 38–42.

[51] KEISER, D.D., Jr., MILLER, B., MADDEN, J., JUE, J.F., GAN, J., Nano-scale fission product phases in an irradiated U–7Mo alloy nuclear fuel, Microsc. Today (2014) 30–34.

[52] ZSCHORNACK, G., Handbook of X-Ray Data, Springer, Berlin (2007).

[53] SALVAT, F., The PENELOPE code system: Specific features and recent improvements, Ann. Nucl. Energy **82** (2015) 98–109.

[54] CASTAING, R., et al., Electron Probe Quantitation, Springer, New York (1991).

[55] GOLDSTEIN, J.I., Scanning Electron Microscopy and X-ray Microanalysis, Kluwer/Plenum, New York (2003).

[56] WALKER, C.T., Electron probe microanalysis of irradiated nuclear fuel: an overview, J. Anal. At. Spectrom. **14** (1999) 447–454.

[57] PERROT, M., Microanalyse d'Échantillons Irradiés par la Microsonde de Castaing. Application au Combustible Nucléaire MOX, PhD Thesis, Paris Sud University, Paris (1995).

[58] LAMONTAGNE, J., BLAY, T., NAVARRA, P., "Renewal of the shielded electron probe microanalyser (EPMA) in the CEA LECA-STAR hot laboratory: Safety and technical improvements", Proc. 2010 Plenary Mtg of the European Working Group "Hot Laboratories and Remote Handling", Dimitrovgrad, 6–10 September 2010 (2010).

[59] MOY, A., MERLET, C., DUGNE, O., Standardless quantification of heavy elements by electron probe, Anal. Chem. **87** (2014) 7779–7786.

[60] LEENAERS, A., et al., Fuel swelling and interaction layer formation in the SELENIUM Si and ZrN coated U(Mo) dispersion fuel plates irradiated at high power in BR2, J. Nucl. Mater. **458** (2015) 380–393.

[61] ZWEIFEL, T., et al., Annealing tests of in-pile irradiated oxide coated U–Mo/Al–Si dispersed nuclear fuel, J. Nucl. Mater. **452** (2014) 533–547.

[62] GAN, J., et al., Microstructure of the irradiated U_3Si_2/Al silicide dispersion fuel, J. Nucl. Mater. **419** (2011) 97–104.

[63] GAN, J., et al., Transmission electron microscopy characterization of irradiated U–7Mo/Al–2Si dispersion fuel, J. Nucl. Mater. **396** (2010) 234–239.

[64] GAN, J., et al., Microstructural characterization of irradiated U–7Mo/Al–5Si dispersion fuel to high fission density, J. Nucl. Mater. **454** (2014) 434–445.

[65] AITKALIYEVA, A., MADDEN, J.W., MILLER, B.D., COLE, J.I., GAN, J., Comparison of preparation techniques for nuclear materials for transmission electron microscopy (TEM), J. Nucl. Mater. **459** (2015) 241–245.

[66] VALOT, C., VLAY, T., CAILLOT, L., FERROUD-PLATTET, M.P., "A new device for X ray diffraction analyses of irradiated materials", Proc. 2007 Plenary Mtg of the European Working Group "Hot Laboratories and Remote Handling", Bucharest, 20–21 September 2007 (2007).

[67] VAN DEN BERGHE, S., et al., Transmission electron microscopy investigation of irradiated U–7wt%Mo dispersion fuel, J. Nucl. Mater. **375** (2008) 340–346.

[68] IZHUTOV, A.L., et al., Comparative analysis of structural changes in U–Mo dispersed fuel of full-size fuel elements and mini-rods irradiated in the MIR reactor, Nucl. Eng. Technol. **45** (2013) 859–870.

[69] DE REGGE, P., BODEN, R., Determination of neodymium isotopes as burnup indicator of highly irradiated (U, Pu)O_2 LMFBR fuel, J. Radioanal. Nucl. Chem. **35** (1977) 173–184.

[70] DE REGGE, P., HUYS, D., BODEN, R., "Radiochemical analysis methods for burnup determination in irradiated fuel", Vortragstagung: Kern-, Radio-, und Strahlenchemie — Grundlagen und Anwendungen, Jülich, 22–26 September 1980.

[71] BODEN, R., Methodology, Calculation and Interpretation in the Destructive Burnup Determination of Nuclear Fuel, Rep. NCS/72/D4301/RB/Ir/1398, SCK•CEN, Mol, Belgium (1992).

[72] AMERICAN SOCIETY FOR TESTING AND MATERIALS, ASTM Standard E321 – 96(2012), Standard Test Method for Atom Percent in Uranium and Plutonium Fuel (Neodymium-148 Method), ASTM International, West Conshohocken, PA (2012).

[73] SCK•CEN, BELGONUCLEAIRE, REBUS International Programme PWR – Reactivity Tests for a Direct Evaluation of the Burnup Credit on Selected Irradiated LWR Fuel Bundles, Destructive Radiochemical Spent Fuel Characterization of a PWR UO_2 Fuel Sample, RE 2005/35, Rev. A, BN Ref.: 0502640/221, SCK•CEN, Mol, Belgium (2006).

[74] OLIVER, W., PHARR, G., An improved technique for determining hardness and elastic modulus using load and displacement sensing indentation experiments, J. Mater. Res. **7** (1992) 1564–1583.

[75] NEWELL, R., Mechanical properties examined by nanoindentation for selected phases relevant to the development of monolithic uranium–molybdenum metallic fuels, J. Nucl. Mater. **487** (2017) 443–452.

[76] PERTON, M., BLOUIN, A., MONCHALIN, J.-P., Adhesive bond testing of carbon–epoxy composites by laser shockwave, J. Phys. D: Appl. Phys. **44** (2011) 34012.

[77] ARRIGONI, M., et al., Comparative study of three adhesion tests (EN 582 similar to ASTM C633 — LASAT (LASer Adhesion Test) — bulge and blister test) performed on plasma sprayed copper deposited on aluminium 2017 substrates, J. Adhes. Sci. Technol. **20** (2006) 471–487.

[78] SMITH, J.A., COTTLE, D.L., RABIN, B.H., Characterization of Bond Strength of U–Mo Fuel Plates Using the Laser Shockwave Technique: Capabilities and Preliminary Results, Rep. INL/EXT-13-30312, Idaho Natl Lab., ID (2013).

[79] BURKES, D.E., PAPESCH, C.A., MADDISON, A.P., HARTMANN, T., RICE, F.J., Thermo-physical properties of DU–10 wt.% Mo alloys, J. Nucl. Mater. **403** (2010) 160–166.

[80] AMERICAN SOCIETY FOR TESTING AND MATERIALS, ASTM Standard E1269 – 05, Standard test method for determining specific heat capacity by differential scanning calorimetry, ASTM International, West Conshohocken, PA (2005).

[81] PARKER, W.J., JENKINS, R.J., BUTLER, C.P., ABBOTT, G.L., Flash method of determining thermal diffusivity, heat capacity, and thermal conductivity, J. Appl. Phys. **32** (1961) 1679–1684.

[82] AMERICAN SOCIETY FOR TESTING AND MATERIALS, ASTM Standard E1461 – 13, Standard test method for thermal diffusivity by the flash method, ASTM International, West Conshohocken, PA (2013).

[83] FERREIRA, R.A.N., et al., "Thermophysical properties determination of uranium-molybdenum fuel by the flash laser method", Proc. Int. Nuclear Atlantic Conf. (INAC), Belo Horizonte, 24–28 October 2011, Brazilian Nuclear Energy Association, Sao Paulo (2011).

[84] BURKES, D.E., HUBER, T.K., CASELLA, A.M., A model to predict thermal conductivity of irradiated U–Mo dispersion fuel, J. Nucl. Mater. **473** (2016) 309–319.

[85] AMERICAN SOCIETY FOR TESTING AND MATERIALS, ASTM Standard E228 – 06, Standard test method for linear thermal expansion of solid materials with a push-rod dilatometer, ASTM International, West Conshohocken, PA (2006).

[86] VAN DER HEIDE, P., Secondary Ion Mass Spectrometry: An Introduction to Principles and Practices, Wiley, Hoboken, NJ (2014).

[87] RASSER, B., DESGRANGES, L., PASQUET, B., A new shielded SIMS instrument for analysis of highly radioactive materials, Appl. Surf. Sci. **203**–**204** (2003) 673–678.

[88] DESGRANGES, L., PASQUET, B., Measurement of xenon in uranium dioxide (UO_2) with SIMS, Nucl. Instrum. Meth. Phys. Res. B **215** (2004) 545–551.

[89] DESGRANGES, L., et al., "Characterisation of volatile fission products, including iodine, after a power ramp", Proc. Pellet-clad Interaction in Water Reactor Fuels, Aix-en-Provence, 2004, CEA, Paris (2004).

[90] DESGRANGES, L., VALOT, C., PASQUET, B., Characterisation of irradiated nuclear fuel with SIMS, Appl. Surf. Sci. **252** (2006) 7048–7050.

[91] DESGRANGES, L., et al., A method for the quantification of total xenon concentration in irradiated nuclear fuel with SIMS and EPMA, Nucl. Instrum. Meth. Phys. Res. B **266** (2008) 147–154.

[92] DESGRANGES, L., VALOT, C., PASQUET, B., ROURE, I., SIMS characterisation of actinide isotopes in irradiated nuclear fuel, J. Nucl. Mater. **385** (2009) 99–102.

[93] NOIROT, J., et al., "LWR fuel gas characterization at CEA Cadarache LECA-STAR hot laboratory", Post-irradiation Examination and In-pile Measurement Techniques for Water Reactor Fuels, IAEA-TECDOC-CD-1635, IAEA, Vienna (2009) CD-ROM.

[94] NOIROT, J., et al., High burnup changes in UO_2 fuels irradiated up to 83 GWd/t in M5 claddings, Nucl. Eng. Technol. **41** (2009) 155–162.

[95] WALKER, C.T., et al., SIMS analysis of an UO_2 fuel irradiated at low temperature to 65 MWd/kgHM, J. Nucl. Mater. **393** (2009) 212–223.

[96] RESTANI, R., MARTIN, M., KIVEL, N., GAVILLET, D., Analytical investigations of irradiated inert matrix fuel, J. Nucl. Mater. **385** (2009) 435–442.

[97] PORTIER, S., BREMIER, S., WALKER, C.T., Secondary ion mass spectrometry of irradiated nuclear fuel and cladding: an overview, Int. J. Mass Spectrom. **263** (2007) 113–126.

[98] NOIROT, J., et al., Heterogeneous UO_2 fuel irradiated up to a high burn-up: investigation of the HBS and of fission product releases, J. Nucl. Mater. **442** (2013) 309–319.

[99] NOIROT, J., et al., Post-irradiation examinations and high-temperature tests on undoped large-grain UO_2 discs, J. Nucl. Mater. **462** (2015) 77–84.

[100] HANIFI, K., et al., "A method for the quantification of total xenon concentration in each phase of MOX irradiated nuclear fuel with SIMS and EPMA", Proc. Microscopy and Microanalysis 2014, Hartford, 3–7 August 2014, Microsc. Microanal. **20** (2014) Suppl. 3, 1842–1843.

[101] PORTIER, S., DEGUELDRE, C., KIVEL, N., Solving isobaric interferences in secondary ion mass spectrometry: The case of Am and Pu in irradiated thorium-based fuel, Spectrochim. Acta B **73** (2012) 35–38.

[102] IBBERSON, R.M., DAVID, W.I.F., "Neutron powder diffraction", Structure Determination from Powder Diffraction Data, (DAVID, W.I.F., SHANKLAND, K., McCUSKER, L.B., BÄRLOCHER, C., Eds), IUCr Monographs on Crystallography 13, Oxford Science Publications, Oxford (2002) Ch. 5.

[103] CONLON, K.T., SEARS, D.F., "Neutron diffraction of UMo–Al dispersion fuels — latest results", Proc. 30th Int. Mtg on Reduced Enrichment for Research and Test Reactors, Washington, 5–9 October 2008, Argonne Natl Lab., IL (2008).

[104] CONLON, K.T., SEARS, D.F., "Neutron powder diffraction of irradiated low-enriched uranium–molybdenum dispersion fuel", Trans. 10th Int. Topical Mtg on Research Reactor Fuel Management, Sofia, 30 April – 3 May 2006, European Nuclear Society, Brussels (2006) 104–108.

[105] GOLOSOV, O.A., LYUTIKOVA, M.S., SEMERIKOV, V.B., TEPLYKH, A., "The effect of fuel burnup followed by annealing on changes in structure and structural parameters of U–9% Mo dispersion fuel", Trans. 12th Int. Topical Mtg on Research Reactor Fuel Management, Hamburg, 2–5 March 2008, European Nuclear Society, Brussels (2008).

[106] JACKSON, A.J., Introduction to Small Angle Neutron Scattering and Neutron Reflectometry, NIST Center for Neutron Research, Gaithersburg, MD (2008).

[107] GOLOSOV, O.A., SEMERIKOV, V.B., BOGDANOV, S.G., LYUTIKOVA, M.S., "Small angle neutron scattering by U–9% Mo/Al dispersion fuel irradiated to high burn-ups", Proc. 29th Int. Mtg on Reduced Enrichment for Research and Test Reactors, Prague, 23–27 September 2007, Argonne Natl Lab., IL (2007).

[108] BURKES, D.E., et al., Measurement of fission gas release from irradiated U–Mo monolithic fuel samples, J. Nucl. Mater. **461** (2015) 61–71.

[109] MEUNIER, B., et al., "He and fission product release from irradiated nuclear fuels: MERARG 2 capabilities", Proc. 2007 Plenary Mtg of the European Working Group "Hot Laboratories and Remote Handling", Bucharest, 20–21 September 2007 (2007).

[110] PONTILLON, Y., et al., "Experimental and theoretical investigation of fission gas release from UO_2 up to 70 GWd/t under simulated LOCA type conditions: the GASPARD program", Proc. Int. Mtg LWR Fuel Performance, Orlando, 2004, ANS, La Grange Park, IL (2004).

[111] NOIROT, J., PONTILLON, Y., YAGNIK, S., TURNBULL, J.A., TVERBERG, T., Fission gas release behaviour of a 103 GWd/tHM fuel disc during a 1200°C annealing test, J. Nucl. Mater. **446** (2014) 169–171.

[112] ZACHARIE, I., et al., Microstructural analysis and modelling of intergranular swelling of an irradiated UO_2 fuel treated at high temperature, J. Nucl. Mater. **255** (1998) 92–104.

[113] RAVEL, S., EMINET, G., MULLER, E., CAILLOT, L., "Partition of grain boundary and matrix gas inventories: Results obtained using the ADAGIO facility", Proc. Seminar Fission Gas Behaviour in Water Reactor Fuels, Cadarache, 26–29 September 2000, OECD Nuclear Energy Agency, Paris (2002) 347–356.

[114] PONTILLON, Y., DESGRANGES, L., POULESQUEN, A., ADAGIO technique: from UO_2 fuels to MOX fuels, J. Nucl. Mater. **385** (2009) 137–141.

[115] PONTILLON, Y., et al., "Fission gas release under normal and off-normal conditions: new analytical device implemented at the CEA-Cadarache", Proc. 2005 Plenary Mtg of the European Working Group "Hot Laboratories and Remote Handling", Petten, 23–25 May 2005 (2005).

[116] ESCOBAR GALINDO, R., et al., A modified blister test to study the adhesion of thin coatings based on local helium ion implantation, Thin Solid Films **471** (2005) 170–176.

[117] HEITZMANN, M.T., et al., Measurements of interface fracture strength between fiber-reinforced composite laminates and thin surface films using blister test, Key Eng. Mater. **471–472** (2011) 315–319.

[118] NUCLEAR REGULATORY COMMISSION, Safety Evaluation Report Related to the Evaluation of Low-Enriched Uranium Silicide–Aluminum Dispersion Fuel for Use in Non-Power Reactors, NUREG-1313, US Govt Printing Office, Washington, DC (1988).

[119] KIM, Y.S., Uranium intermetallic fuels (U–Al, U–Si, U–Mo), Compr. Nucl. Mater. **3** (2012) 391–422.

[120] BEESTON, J.M., HOBBINS, R.R., GIBSON, G.W., FRANCIS, W.C., Development and irradiation performance of uranium aluminide fuel in test reactors, Nucl. Technol. **49** (1980) 136–149.

[121] HOBBINS, R.R., et al., "Irradiation testing to verify failure predictions produced by post-irradiation testing",

Nuclear Technology Division Annual Progress Report for Period Ending June 30, 1971 ANCR-1016, Aerojet Nuclear Company Report, Rancho Cordova, CA (1971).

[122] HOBBINS, R.R., INC-16-2 Irradiation Experiment, Idaho National Engineering Laboratory, Idaho Falls, ID (1974).

[123] WHITACRE, R.F., The UAl_x Fuel Dispersion System, Rep. EGG-PRP-8783, Rev. 2, Idaho Natl Lab., ID (1990).

[124] SNELGROVE, J.L., DOMAGLA, R.F., WIENCEK, T.C., COPELAND, G.L., Fuel Development Activities for the US RERTR Program, Proc. 6th Int. Mtg on Reduced Enrichment for Research and Test Reactors, Tokai, 24–27 October 1983, Rep. JAERI-M 84-073, Japan Atomic Energy Research Institute, Tokai (1983).

[125] COPELAND, G.L., HOFMAN, G.L., SNELGROVE, J.L., “Examination of U_3Si_2–Al fuel elements from the Oak Ridge Research Reactor”, Proc. 9th Int. Mtg on Reduced Enrichment for Research and Test Reactors, Gatlinburg, 3–6 November 1986, Rep. ANL/RERTR/TM-9, Argonne Natl Lab., IL (1988) 211–221.

[126] KRUG, W., GROOS, E., SEFERIADIS, J., THAMM, G., “Final results of test-irradiations with LEU-plates at KFA Jülich”, Proc. 11th Int. Mtg on Reduced Enrichment for Research and Test Reactors, San Diego, 19–22 September 1988, Rep. ANL/RERTR/TM-13, Argonne Natl Lab., IL (1993) 155–181.

[127] MARAJOFSKY, A., KOHUT, C., HOFMAN, G.L., “Irradiation behavior of the CNEA’s experimental uranium silicide dispersion fuel plates”, Proc. 11th Int. Mtg on Reduced Enrichment for Research and Test Reactors, San Diego, 19–22 September 1988, Rep. ANL/RERTR/TM-13, Argonne Natl Lab., IL (1993) 182–205.

[128] SAKAI, H., et al., “Post-irradiation Examination of Low-Enrichment Uranium (LEU) Miniplates in the JMTR”, Proc. 9th Int. Mtg on Reduced Enrichment for Research and Test Reactors, Gatlinburg, 3–6 November 1986, Rep. ANL/RERTR/TM-9, Argonne Natl Lab., IL (1988) 185–200.

[129] SNELGROVE, J.L., “Overview of reduced enrichment fuels development, testing and specification”, Proc. Amer. Nucl. Soc. Winter Mtg Los Angeles, 1987, ANS, La Grange Park, IL (1987).

[130] SNELGROVE, J.L., et al., Evaluation of Existing Technology Base for Candidate Fuels for the HWR-NPR, Rep. ANL/NPR-93/002, Argonne Natl Lab., IL (1993).

[131] AMOUYAL, Y., SCHMITZ, G., Atom probe tomography — a cornerstone in materials characterization, MRS Bull. **41** (2016) 13–18.

[132] MIAO, Y., et al., “High-energy synchrotron study of in-pile-irradiated U–Mo fuels”, Proc. 36th Int. Mtg on Reduced Enrichment for Research and Test Reactors, Seoul, 11–14 October 2015, Argonne Natl Lab., IL (2015).

ABBREVIATIONS

AFIP	ATR Full sized plate In center flux trap Position
APT	atom probe tomography
ASTM	American Society for Testing and Materials
ATR	Advanced Test Reactor
BOL	beginning of life
BSE	backscattered electron
CEA	French Alternative Energies and Atomic Energy Commission
EBSD	electron backscatter diffraction
EDS	energy dispersive spectroscopy
ELAF	Extended Life Aluminide Fuel
EOL	end of life
EPMA	electron probe microanalysis
FIB	focused ion beam
HEU	high enriched uranium
HPGe	high purity germanium
INL	Idaho National Laboratory
LEU	low enriched uranium
LVDT	linear variable differential transformer
NDT	non-destructive testing
PIE	post-irradiation examination
PNNL	Pacific Northwest National Laboratory
RERTR	Reduced Enrichment for Research and Test Reactors
SCK•CEN	Studiecentrum voor Kernenergie — Centre d’étude de l’énergie nucléaire (Belgian Nuclear Research Centre)
SEM	scanning electron microscopy
SIMS	secondary ion mass spectrometry
TEM	transmission electron microscopy
TIMS	thermal ionization mass spectrometry
WDS	wavelength dispersive X ray spectroscopy

CONTRIBUTORS TO DRAFTING AND REVIEW

Agarwal, K.	International Atomic Energy Agency
Fuentes Solis, N.	International Atomic Energy Agency
Geupel, S.	International Atomic Energy Agency
Goncharenko, Y.	Research Institute of Atomic Reactors, Russian Federation
Jenssen, H.	Institute for Energy Technology, Norway
Keiser, D.	Idaho National Laboratory, United States of America
Leenaers, A.	Belgian Nuclear Research Centre, Belgium
Marshall, F.	International Atomic Energy Agency
Monaghan, B.	Consultant, Canada
Muhammad Nor, A.W.	International Atomic Energy Agency
Noirot, J.	French Alternative Energies and Atomic Energy Commission, France
Tiratay, X.	French Alternative Energies and Atomic Energy Commission, France
Van den Berghe, S.	Belgian Nuclear Research Centre, Belgium
Varjonen, H.	International Atomic Energy Agency

Consultants Meetings

Vienna, Austria: 9–11 December 2014, 28–30 October 2015, 15–16 June 2016,
14–15 December 2016, 8–9 October 2018

Structure of the IAEA Nuclear Energy Series*

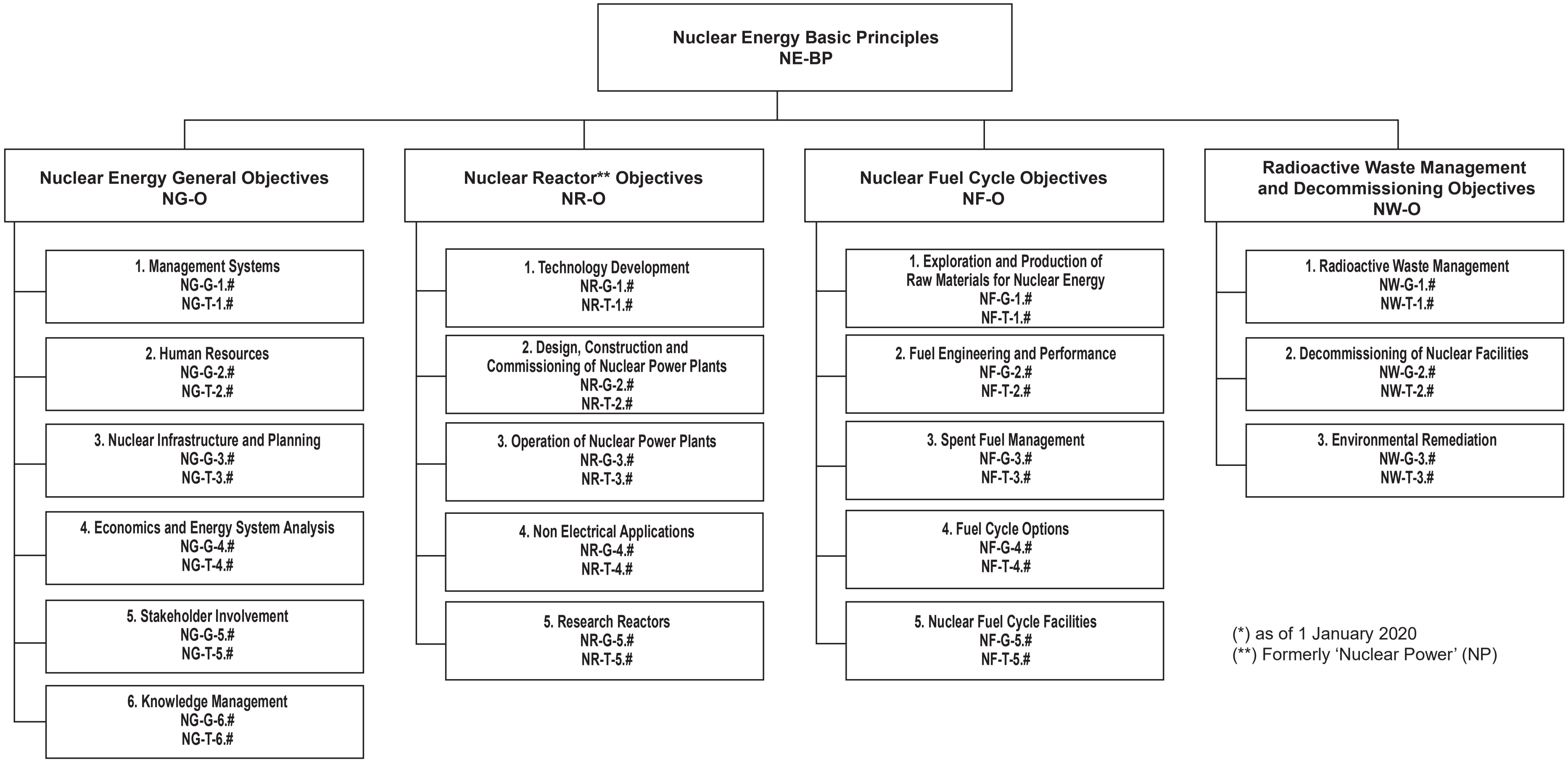

(*) as of 1 January 2020
(**) Formerly ‘Nuclear Power’ (NP)

Key

BP:	Basic Principles
O:	Objectives
G:	Guides and Methodologies
T:	Technical Reports
Nos 1–6:	Topic designations
#:	Guide or Report number

Examples

NG-G-3.1:	Nuclear Energy General (**NG**), Guides and Methodologies (**G**), Nuclear Infrastructure and Planning (topic **3**), **#1**
NR-T-5.4:	Nuclear Reactors (**NR**), Technical Report (**T**), Research Reactors (topic **5**), **#4**
NF-T-3.6:	Nuclear Fuel (**NF**), Technical Report (**T**), Spent Fuel Management (topic **3**), **#6**
NW-G-1.1:	Radioactive Waste Management and Decommissioning (**NW**), Guides and Methodologies (**G**), Radioactive Waste Management (topic **1**) **#1**

ORDERING LOCALLY

IAEA priced publications may be purchased from the sources listed below or from major local booksellers.

Orders for unpriced publications should be made directly to the IAEA. The contact details are given at the end of this list.

NORTH AMERICA

Bernan / Rowman & Littlefield
15250 NBN Way, Blue Ridge Summit, PA 17214, USA
Telephone: +1 800 462 6420 • Fax: +1 800 338 4550
Email: orders@rowman.com • Web site: www.rowman.com/bernan

REST OF WORLD

Please contact your preferred local supplier, or our lead distributor:

Eurospan Group
Gray’s Inn House
127 Clerkenwell Road
London EC1R 5DB
United Kingdom

Trade orders and enquiries:
Telephone: +44 (0)176 760 4972 • Fax: +44 (0)176 760 1640
Email: eurospan@turpin-distribution.com

Individual orders:
www.eurospanbookstore.com/iaea

For further information:
Telephone: +44 (0)207 240 0856 • Fax: +44 (0)207 379 0609
Email: info@eurospangroup.com • Web site: www.eurospangroup.com

Orders for both priced and unpriced publications may be addressed directly to:

Marketing and Sales Unit
International Atomic Energy Agency
Vienna International Centre, PO Box 100, 1400 Vienna, Austria
Telephone: +43 1 2600 22529 or 22530 • Fax: +43 1 26007 22529
Email: sales.publications@iaea.org • Web site: www.iaea.org/publications

INTERNATIONAL ATOMIC ENERGY AGENCY
VIENNA